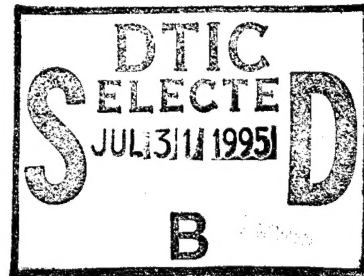


DEPARTMENT OF DEFENSE  
ELECTROMAGNETIC COMPATIBILITY ANALYSIS CENTER  
ANNAPOLIS, MARYLAND 21402-5064

**TIREM/SEM HANDBOOK**



HANDBOOK

Prepared by

David Eppink and Wolf Kuebler

IIT Research Institute  
Under Contract to  
Department of Defense

DTIC QUALITY INSPECTED 5

19950728 082

This Handbook (HDBK) supersedes ECAC-HDBK-86-076 dated September 1986. Approved for public release; distribution unlimited.

---

MARCH 1994

This report was prepared by the IIT Research Institute as part of AF Project 649E under Contract F-19628-90-C-0014 with the Electronic Systems Center of the Air Force Materiel Command in support of the DoD Electromagnetic Compatibility Analysis Center, Annapolis, Maryland.

This report has been reviewed and is approved for publication.

Reviewed by:

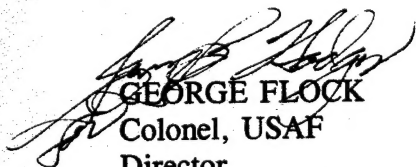


DAVID W. EPPINK  
Project Manager, IITRI

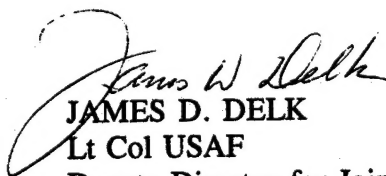


RICHARD H. MEIDENBAUER  
Director of Research  
Contractor Operations

Approved by:



GEORGE FLOCK  
Colonel, USAF  
Director



JAMES D. DELK  
Lt Col USAF  
Deputy Director for Joint and Technical  
Support

REPORT DOCUMENTATION PAGE				
1a. REPORT SECURITY CLASSIFICATION <b>UNCLASSIFIED</b>			1b. RESTRICTIVE MARKINGS	
2a. SECURITY CLASSIFICATION AUTHORITY			3. DISTRIBUTION/AVAILABILITY OF REPORT Approved for public release; distribution unlimited.	
2b. DECLASSIFICATION/DOWNGRADING SCHEDULE				
4. PERFORMING ORGANIZATION REPORT NUMBER(S) ECAC-HDBK-93-076			5. MONITORING REPORT NUMBER(S)	
6a. NAME OF PERFORMING ORGANIZATION  Electromagnetic Compatibility Analysis Center		6b. OFFICE SYMBOL (If applicable)  CJ	7a. NAME OF MONITORING ORGANIZATION	
6c. ADDRESS (City, State, and Zip Code) 120 Worthington Basin Annapolis, MD 21402-5064			7b. ADDRESS (City, State, and Zip Code)	
8a. NAME OF FUNDING/SPONSORING ORGANIZATION		8b. OFFICE SYMBOL (If applicable)	9. PROCUREMENT INSTRUMENT IDENTIFICATION NUMBER	
8c. ADDRESS (City, State, and Zip Code)			10. SOURCE OF FUNDING NOS.	
			PROGRAM ELEMENT NO.  P0813	PROJECT NO.  P0813
11. TITLE (Include Security Classification) TIREM/SEM Handbook (U)				
12. PERSONAL AUTHOR(S) David Eppink and Wolf Kuebler				
13a. TYPE OF REPORT HANDBOOK		13b. TIME COVERED FROM _____ TO _____	14. DATE OF REPORT (Yr., Mo., Day) 1994 MARCH	15. PAGE COUNT 134
16. SUPPLEMENTARY NOTATION				
17. COSATI CODES			18. SUBJECT TERMS (Continue on reverse if necessary and identify by block number)	
FIELD	GROUP	SUB. GR.	RADIO WAVE PROPAGATION, IRREGULAR TERRAIN, ROUGH-EARTH MODEL, SPHERICAL-EARTH MODEL, TIREM, SEM, BASIC MEDIAN PROPAGATION LOSS, LINE-OF-SIGHT, DIFFRACTION, TROPOSCATTER.	
19. ABSTRACT (Continue on reverse if necessary and identify by block number)  This document provides a description of the operation of the Terrain-Integrated Rough Earth Model (TIREM) and the Spherical Earth Model (SEM), including the engineering formulations on which the models are based. Both models are modular programs with many common subroutines that conform with ANSI Fortran standards. TIREM and SEM can be used as independent propagation models for rough-earth (with a known terrain profile) or smooth-earth applications, respectively. Both models consider the effects of free-space spreading, reflection, surface-wave propagation, diffraction, tropospheric-scatter propagation, and atmospheric absorption, as appropriate.				
20. DISTRIBUTION/AVAILABILITY OF ABSTRACT  UNCLASSIFIED/UNLIMITED <u>  X  </u> SAME AS RPT. <u>  </u> DTIC USERS <u>  </u>			21. ABSTRACT SECURITY CLASSIFICATION	
22a. NAME OF RESPONSIBLE INDIVIDUAL  R. Schneider			22b. TELEPHONE NUMBER (Include Area Code)  410-293-4956 DSN 281-4956	22c. OFFICE SYMBOL  CJ

## TABLE OF CONTENTS

<u>Paragraph</u>	<u>Page</u>
GLOSSARY .....	ix

## CHAPTER 1

### INTRODUCTION

1.1	BACKGROUND .....	1-1
1.1.1	Spherical-Earth Models .....	1-1
1.1.2	Rough-Earth Models .....	1-2
1.2	PURPOSE .....	1-5
1.3	OVERVIEW OF MODEL OPERATION .....	1-6
1.3.1	TIREM Overview .....	1-6
1.3.2	SEM Overview .....	1-8
1.4	CONVENTIONS .....	1-8
1.4.1	Unit of Measure Conventions .....	1-8
1.4.2	Software Version Conventions .....	1-9

## CHAPTER 2

### COMMON CONCEPTS AND TECHNIQUES

2.1	GENERAL .....	2-1
2.2	FREE-SPACE PROPAGATION .....	2-1
2.3	EFFECTIVE EARTH RADIUS .....	2-2
2.4	MOLECULAR ABSORPTION .....	2-5
2.5	TROPOSCATTER PROPAGATION .....	2-10
2.6	SPHERICAL-EARTH LOSS .....	2-12



## TABLE OF CONTENTS - Continued

<u>Paragraph</u>		<u>Page</u>
CHAPTER 3		
SPHERICAL-EARTH MODEL (SEM)		
3.1	GENERAL .....	3-1
3.2	SPACE-WAVE PROPAGATION .....	3-3
3.3	SURFACE-WAVE PROPAGATION .....	3-9
3.4	DIFFRACTED-WAVE PROPAGATION .....	3-10
3.5	SPLICE FUNCTIONS .....	3-12
3.6	SUMMARY OF SPHERICAL-EARTH PROPAGATION FORMULAS .....	3-14
CHAPTER 4		
TERRAIN-INTEGRATED ROUGH-EARTH MODEL (TIREM)		
4.1	GENERAL .....	4-1
4.2	DIGITAL TERRAIN DATA IN PROPAGATION MODELING .....	4-1
4.3	PROPAGATION OVER LAND .....	4-3
4.3.1	Line-of-Sight Region .....	4-3
4.3.2	Diffraction Region .....	4-9
4.3.3	Summary of Land Propagation Formulas .....	4-14
4.4	PROPAGATION OVER LAND/SEA .....	4-17
4.4.1	Weighting Factors .....	4-19
4.4.2	Propagation Formulas for Land/Sea Profiles .....	4-20

## TABLE OF CONTENTS - Continued

ParagraphPage

## CHAPTER 5

MODEL LIMITATIONS, STATISTICS, MEASUREMENT  
ERROR, AND REPEATABILITY STATISTICS

5.1	MODEL LIMITATIONS . . . . .	5-1
5.2	SEM MODEL STATISTICS . . . . .	5-2
5.3	TIREM MODEL STATISTICS . . . . .	5-2
5.4	ERROR ESTIMATES OF THE MEASUREMENTS . . . . .	5-5
5.5	STATISTICS CONCERNING REPEATED MEASUREMENTS . . . . .	5-6

## APPENDIX A INPUT PARAMETER RANGES

## APPENDIX B TROPOSPHERIC SCATTER

## APPENDIX C SEM CRITICAL DISTANCES

## APPENDIX D REFLECTION LOSS

Accession For	
NTIS GRA&I	<input checked="" type="checkbox"/>
DTIC TAB	<input type="checkbox"/>
Unannounced	<input type="checkbox"/>
Justification	
By	
Distribution/ Use	
Availability Codes	
DISC	Small sec/yr
A-1	Special

## LIST OF ILLUSTRATIONS

<u>Figure</u>		<u>Page</u>
1-1	Top-Level Block Diagram of TIREM and SEM . . . . .	1-7
2-1	Effective Earth Radius, $a_e$ . . . . .	2-3
2-2	Specific Attenuation of Oxygen and Water Vapor . . . . .	2-6
2-3	Propagation Paths for Different Modes (Showing $H(r)$ Determined From Path Geometry) . . . . .	2-9
2-4	Terrain-Dependent Geometrical Parameters . . . . .	2-11
3-1	Geometry for Spherical-Earth Calculations at Points Within LOS . . . . .	3-4
3-2	Numerical Example Showing the Interference of the Direct and the Reflected Ray ( $f = 100$ MHz, $h_1 = h_2 = 100$ m, $\epsilon = 10$ , $\sigma = 0.01$ S/m, Vertical Polarization) . . . . .	3-7
3-3	Example of the Splice Function Joining Either the Space-Wave or Surface-Wave Fields with the Diffracted-Wave Field . . . . .	3-13
4-1	Geometry of the First Fresnel Zone Spheroid . . . . .	4-5
4-2	Diffraction Over Two Knife Edges, Epstein-Peterson Construction . . . . .	4-9
4-3	Comparison of Millington's Method and Results Derived Using Weighting Factors With Measurements . . . . .	4-18
4-4	Line-of-Sight Land/Sea Path . . . . .	4-22
4-5	Land/Sea Path Diffracted Over Sea Only . . . . .	4-23
4-6	Land/Sea Path Segments . . . . .	4-26
4-7	Cascading of Subpath Segments . . . . .	4-29

## LIST OF TABLES

<u>Table</u>		<u>Page</u>
2-1	US Standard Atmosphere, 1962 . . . . .	2-7
3-1	Summary of Spherical-Earth Propagation Formulas . . . . .	3-15
4-1	Summary of Terrain-Dependent Propagation Formulas for LOS or Diffraction . . . . .	4-15
4-2	Land/Sea Definitions . . . . .	4-21
5-1	Summary of Terrain Characteristics . . . . .	5-3
5-2	TIREM Statistical Summary . . . . .	5-5
5-3	Results of Repeated Measurement Series . . . . .	5-6

## GLOSSARY

ANSI	American National Standards Institute
Atmospheric absorption	Attenuation caused by absorption of energy by molecules of oxygen and water vapor in the atmosphere
Basic median propagation loss	The propagation loss between loss-free isotropic antennas with polarization the same as that of the transmitted wave
BLOS	Beyond line of sight
CCIR	International Radio Consultative Committee
Conductivity	The effective conductivity (reciprocal of resistivity) of the earth along the path to a depth corresponding to the penetration depth appropriate for the frequency
CRPL	Central Radio Propagation Laboratory (now ITS, part of NTIA)
Diffacted wave	A wave that is bent into the shadow region beyond the horizon of an obstacle
Direct wave	A wave that travels outward from its source along a radial line without interaction with the earth (although it may be refracted by the atmosphere)
Divergence factor	The ratio of field strength from a source after reflection from a perfectly reflecting spherical surface to the incident field
DTED	Digital terrain elevation data
DoD	Department of Defense
ECAC	Electromagnetic Compatibility Analysis Center (DoD)
Effective earth radius	An earth radius used in place of the actual earth radius to correct for atmospheric refractivity in estimating clearances and horizon distances

# GLOSSARY - Continued

EFFSECC	ECAC Far-Field Smooth-Earth Coupling Code
Excess loss	Loss relative to free-space loss
First Fresnel zone	An ellipsoid of revolution about the direct path between antennas such that the sum of the distances from any point on the ellipsoid to each of the antennas is one-half wavelength longer than the direct path
Free-space loss	The loss that would occur between isotropic antennas in a homogeneous ideal dielectric medium at a given distance
Fresnel zone	The circular (annular) portion of a wave front, in a plane perpendicular to the line joining two antennas, such that the n-th zone includes all paths whose lengths exceed the direct line path by $n - 1$ to $n$ half wavelengths
Ground wave	A wave that consists of three components: the direct wave, the reflected wave, and the surface wave
GTD	Geometric theory of diffraction
IPS	Integrated Propagation System
Isotropic antenna	A theoretical antenna that radiates uniformly in all directions with a directivity of unity
ITS	Institute for Telecommunication Sciences
LOS	Line of sight
MMWPROP	Millimeter-Wave Propagation model
MSL	Mean sea level - A reference level for measurement of elevations (heights)
NBS	National Bureau of Standards (now NIST)

## GLOSSARY - Continued

NIST	National Institute of Standards and Technology (formerly National Bureau of Standards)
NLAMBDA	A spherical-earth propagation model for theoretically accurate ground wave predictions
NTIA	National Telecommunications and Information Administration
Path loss	Basic median propagation loss
PE	Parabolic equation approximation for the solution of the wave equation
Permittivity	The effective relative permittivity (dielectric constant) of the earth along the path to a depth corresponding to the penetration depth appropriate for the frequency
Phase factor	The angular phase difference between the lengths of the direct and earth-reflected paths ( $2\pi \times$ path length difference in wavelengths)
Reflected wave	A wave that has been reflected by the surface of the earth
Refractivity	A measure of the index of refraction of the atmosphere that depends on barometric pressure, temperature, and humidity
RMS	Root mean squared
Rough-earth model	A propagation model that considers the terrain elevations along the path
SCSE	Smooth Curve Smooth Earth propagation model
SEM	ECAC Spherical-Earth Model
Space wave	That part of the ground wave that consists of the direct and reflected waves

GLOSSARY - Continued

Spherical-earth model	A ground-wave propagation prediction model that regards the earth as a smooth sphere with known electrical characteristics (conductivity and relative permittivity)
Splice function	A mathematical function that serves to join two equations with different domains of applicability
Surface wave	A guided wave along the surface of the earth that is generated and sustained by ground currents induced by the refracted energy that enters the ground
TIREM	Terrain-Integrated Rough-Earth Model
Troposcatter propagation	Tropospheric forward scatter propagation of radio waves through the atmosphere by scattering from inhomogeneities in the refractive index of the troposphere



# CHAPTER 1

## INTRODUCTION

### 1.1 BACKGROUND

The Electromagnetic Compatibility Analysis Center (ECAC) is responsible for developing capabilities for analyzing the compatibility of communications and electronic equipment that make use of the electromagnetic spectrum. This responsibility includes the development of mathematical models of propagation phenomena for a wide range of applications. Some of the earliest computer-automated models developed at ECAC were purely theoretical techniques for calculating radio-wave propagation loss between antennas above an imperfectly-conducting spherical earth. Later, a model was developed that required a point-by-point representation of the terrain elevations at intervals along the irregular profile of the earth in the great-circle plane between the antennas. Both types of models, whether for use over smooth spherical earth or over rough earth, must evaluate the geometry of the path, determine the appropriate mode(s) of propagation, and apply suitable algorithms to calculate the path loss for the dominant mode.

#### 1.1.1 Spherical-Earth Models

In a spherical-earth model, the terrain profile is represented as the arc of a circle whose radius may depend on the gradient of atmospheric refractivity. Such a model is valid for propagation over a smooth sea or lake or even over a relatively smooth plain if the frequency is low enough that the wavelength is long compared with the dimensions of the terrain irregularities. One of the earliest ECAC spherical-earth models is the Smooth Curve Smooth Earth (SCSE) model. Later, a simplified spherical-earth model, intended for lower frequencies and antenna heights, and a modification of a simple method for predicting tropospheric scatter propagation loss were combined with SCSE in the Integrated Propagation System (IPS).<sup>1-1</sup> At about the same time a theoretical ground-wave model called NLAMBDA, capable of accommodating antennas many wavelengths in

---

<sup>1-1</sup>Meidenbauer, R., Chang, S., and Duncan, M., A Status Report on the Integrated Propagation System (IPS), ECAC-TN-78-023, DoD ECAC, Annapolis, MD, October 1978.

height, was developed.<sup>1-2</sup> Later, the NLAMBDA capability for calculation of path loss was used as the foundation for the current ECAC standard for spherical-earth models, the ECAC Far-Field Smooth-Earth Coupling Code (EFFSECC).<sup>1-3</sup> EFFSECC combines the theoretical path-loss calculation for an ideal spherical earth with the gain and radiation characteristics for a package of commonly used linear antennas.

NLAMBDA and EFFSECC provide accurate theoretical predictions of ground-wave loss or electric field strength between antennas on a spherical earth. However, for many applications involving the analysis of large environments of equipment and the estimation of the necessary separation distance required to prevent interference between systems, the IPS was used. The IPS yields acceptable accuracy in situations requiring conservation of computation time.

In 1990, the Spherical-Earth Model (SEM) was designed to replace the IPS for calculation of propagation loss over smooth homogeneous terrain. The model design is considerably more compact than IPS (line count is reduced by 80 percent), yet the program is thoroughly commented (annotated with explanatory comments) for easy integration into analysis programs. The modular construction of the model makes it possible to select subroutines for specific applications. Many of the modular SEM subroutines were specifically designed for both SEM and the rough-earth model described below in paragraph 1.1.2.

### **1.1.2 Rough-Earth Models**

Rough-earth models take into account the effects of the irregular terrain along the propagation path and in the vicinity of the antennas. Thus, rough-earth models require information regarding terrain elevations in the region of interest. The development of rough-earth models began in the early 1960s with the formulation of techniques for extracting the necessary parameters for evaluation of the path from great-circle terrain profiles, selection of the appropriate mode of propagation, and

---

<sup>1-2</sup>Maiuzzo, M. A. and Frazier, W. E., A Theoretical Ground Wave Propagation Model - NLAMBDA Model, ESD-TR-68-315, DoD ECAC, Annapolis, MD, December 1968.

<sup>1-3</sup>Marcus, S., Description of the ECAC Far-Field Smooth-Earth Coupling Code (EFFSECC), ECAC-TN-80-014, DoD ECAC, Annapolis, MD, August 1980.

calculation of the loss. Many of the concepts and algorithms employed in the rough-earth model known as the Terrain-Integrated Rough-Earth Model (TIREM) were based on work done at the Central Radio Propagation Laboratory (CRPL) of the National Bureau of Standards (NBS).<sup>1-4</sup> CRPL has since become the Institute for Telecommunication Sciences (ITS) of the National Telecommunications and Information Administration (NTIA).

TIREM provided the first means for determining terrain-dependent propagation path loss entirely by automated computer processes. Early TIREM versions included three line-of-sight (LOS) modes (including free space) and three beyond LOS (BLOS) modes. There was also a spherical-earth mode which served as a recovery model when rough-earth engineering models were not applicable.

Over the ensuing years, the TIREM modeling was revised with new capabilities and features. By 1983, the model recognized unique path geometry situations requiring loss algorithms for three LOS modes, five diffraction modes, and five combination modes involving tropospheric scatter or diffraction. This TIREM version could calculate the basic transmission loss over irregular terrain for frequencies between 40 and 20,000 MHz. Comparisons with propagation loss measurements made by ITS showed root mean squared (RMS) prediction errors for various measurement regions of 10 to 43 dB. Later in 1983, TIREM was modified to allow a low frequency limit of 20 MHz and a low antenna height limit of 0.5 m.

In response to observations that several of the prediction modes for the region BLOS were inaccurate, an investigation of the beyond LOS methods was performed. The BLOS calculations were improved by combining the diffraction calculations into a single unified mode based on diffraction over multiple knife edges. Also, in the transition region between propagation by diffraction and propagation by troposcatter, a single new mode was added in place of several transition modes. A comparison of propagation predictions of the revised version of TIREM with measured propagation data showed that it significantly outperformed the existing version of TIREM.

---

<sup>1-4</sup>Rice, P. L., Longley, A. G., Norton, K. A., and Barsis, A. P., Transmission Loss Predictions For Tropospheric Communication Circuits, Volumes 1 and 2, NBS Technical Note 101, CRPL, NBS, Boulder, CO, May 1965, Revised January 1967.

This revised TIREM version became ECAC TIREM Version 1.0 and was described in the first TIREM Handbook.<sup>1-5</sup>

TIREM version 1.0 sometimes exhibited an unexpected decrease of loss with increasing distance for paths over smooth water. This discontinuity was caused by mode switching between LOS and rough-earth diffraction modes when the diffraction occurred on a smooth water surface. TIREM Version 2.0 added a smooth spherical-earth propagation mode for path segments over smooth water surfaces. Losses for water segments are combined with multiple knife-edge diffraction losses for land segments, weighting each by the proportionate distances of water and land in the entire path. These measures assure that a correct loss calculation is made for diffraction over the surface of a smooth earth and that a smooth transition occurs.

In order to facilitate integration into analysis programs, TIREM Version 2.0 was completely rewritten as a callable subroutine in standard ANSI FORTRAN 77 and became TIREM Version 3.0.<sup>1-6</sup> The engineering design of some of the algorithms was also revised to simplify the calculations and preserve the model accuracy. For example, the smooth spherical-earth mode calculations were improved and validated with propagation measurements. This allowed the lower frequency limit to be extended to 1 MHz. Version 3.0 also simplifies the LOS calculations.

Recent efforts to improve TIREM have concentrated on simplification and reduction of the computation time. Thus, the model is more suitable for application programs requiring many loss calculations such as the analysis of large environments of equipment or the plotting of propagation-related performance contours. Although past efforts have produced a model with a near-zero mean prediction error, the standard deviation is 11 dB, a figure that may be unacceptable for some applications. Further improvement of the error statistics of TIREM has proven to be difficult using elementary yet expedient algorithms. ECAC continues to investigate other more sophisticated techniques for propagation prediction such as the geometric theory of diffraction (GTD), integral

---

<sup>1-5</sup>Benoit, G., Terrain-Integrated Rough-Earth Model (TIREM) Handbook, ECAC-HDBK-86-076, DoD ECAC, Annapolis, MD, September 1986.

<sup>1-6</sup>Sciandra, R. M., TIREM/SEM Programmer's Reference Manual, ECAC-CR-90-039, DoD ECAC, Annapolis, MD, July 1990.

equation methods, and methods based on the parabolic equation (PE) approximation to the solution of the Helmholtz equation for electromagnetic propagation. Some of these methods have the potential not only to account for the effects of an inhomogeneous atmosphere, but also to account for three-dimensional terrain effects outside the great-circle plane.

## 1.2 PURPOSE

The purpose of this Handbook is to provide a description of the current versions of TIREM and SEM, including the engineering formulations on which the models are based. Both TIREM and SEM are modular programs with many common subroutines that conform with ANSI FORTRAN 77 standards. The two programs are designed for easy integration into other programs. Both models have been, and continue to be, incorporated into performance evaluation programs as replacements for earlier versions of rough-earth and smooth-earth propagation models.

SEM is considerably faster than TIREM because it does not require the extraction of a terrain profile from elevation data. However, it is theoretically valid only when used for propagation over a smooth, spherical earth. It is commonly used when approximate loss predictions are required or when terrain elevation data are unavailable.

TIREM and SEM can be used as independent propagation models for rough-earth or smooth-earth applications, respectively. However, subroutines from SEM are extensively used in TIREM. Therefore, the engineering theory of TIREM and SEM are described together in this Handbook. The models are modular and contain 26 common subroutines. Both models conform with ANSI FORTRAN 77 and use argument lists rather than common blocks whenever possible. The models described in this Handbook are TIREM Version 3.09 and SEM Version 1.07, and reflect corrections and enhancements to the original models.

### 1.3 OVERVIEW OF MODEL OPERATION

Figure 1-1 is a top-level block diagram of TIREM and SEM; detailed flowcharts are presented in Reference 1-6. Both models provide estimates of the propagation loss over an imperfectly conducting earth. Both models consider the effects of free-space spreading, reflection, surface-wave propagation, diffraction, tropospheric-scatter propagation, and atmospheric absorption, as appropriate. Only TIREM evaluates the effects of irregular terrain along the great circle path. SEM regards the surface of the earth as a perfectly smooth, imperfectly conducting sphere. Neither model considers ducting phenomena, fading, or ionospheric (skywave) propagation. Calculations of performance improvement that would result from angle, space, or frequency diversity are not performed. Lastly, neither model explicitly addresses attenuation due to rain, foliage, or man-made obstacles. However, if the terrain elevation profile supplied to TIREM has been adjusted by adding the height of known man made obstacles or trees, their effect on diffraction will be included in the predicted path loss.

#### 1.3.1 TIREM Overview

TIREM is designed to calculate basic median propagation loss (hereafter referred to as path loss) over irregular terrain for frequencies between 1 and 20,000 MHz. Because it can consider the terrain elevations along the path, TIREM is one of the most frequently used propagation models at ECAC. TIREM uses as input a terrain profile described by a number of discrete points, the position of which is specified by a distance from the transmitter and an elevation above mean sea level. Also required is information on the transmitter (antenna height, frequency, and antenna polarization), the receiver (antenna height), atmospheric constants (surface refractivity and humidity) and ground constants (relative permittivity and conductivity). There is also a profile indicator flag to save time when a profile is an extension of the existing profile. A description of TIREM parameters and their valid ranges is presented in Appendix A.

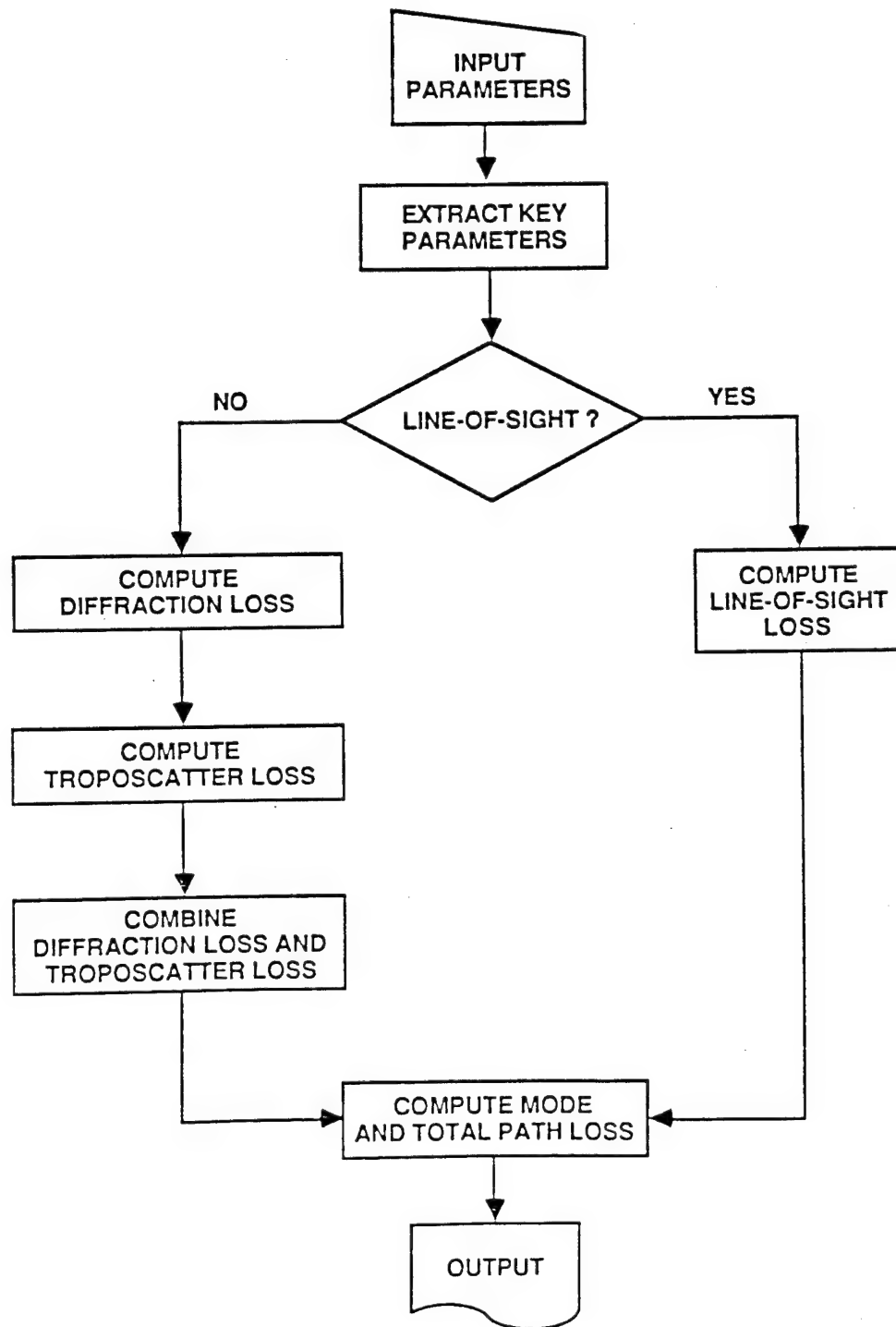


Figure 1-1. Top-Level Block Diagram of TIREM and SEM

### **1.3.2 SEM Overview**

SEM is a stand-alone spherical-earth model that disregards the effects of terrain features. The basis of SEM is the spherical earth propagation module contained in the subroutine SEARTH and its ancillary subroutines. SEARTH is a callable subroutine useful for spherical-earth propagation prediction. SEARTH is also used by TIREM to calculate propagation loss over sea or smooth earth. In the stand-alone application, SEM inputs are the distance between transmitter and receiver and information concerning the transmitter (antenna height, frequency, and antenna polarization), the receiver (antenna height), atmospheric constants (surface refractivity and humidity) and ground constants (permittivity and conductivity). SEM calculates and provides as output the basic propagation loss for antenna terminals located on a smooth spherical earth.

For a path within LOS, the LOS loss relative to free space is the smaller of the space-wave loss or the surface wave loss. For a path extending well into the diffracted region, the loss is the smaller of the diffraction loss or the troposcatter loss. Within a region that spans the horizon, where neither the LOS loss nor the diffracted wave loss is entirely valid, the loss is obtained by an empirical splice function.

If the path is BLOS, the total diffraction loss is the sum of the free-space loss, the loss relative to free space, and, if the frequency exceeds 10 GHz, the loss due to atmospheric absorption. The total path loss is set to the smaller of the total diffraction loss and the total tropospheric scatter loss.

## **1.4 CONVENTIONS**

### **1.4.1 Unit of Measure Conventions**

Throughout this document, metric units of measurement are used. Distances and heights are in meters, unless indicated otherwise. All angles are in radians. Frequency is in MHz. Propagation loss (or path loss) is the loss between loss-free isotropic antennas whose polarization is the same as the transmitted wave and is expressed in decibels.



### 1.4.2 Software Version Conventions

Each computer output carries the version number of the model. With each minor change, the decimal will be raised (i.e., in TIREM, 3.00, 3.01, 3.02, etc., and in SEM, 1.00, 1.01, 1.02, etc.) and with each major change the number will be reset to the next larger whole number (i.e., in TIREM, 4.00, 5.00, etc., and in SEM, 2.00, 3.00, etc.).

## CHAPTER 2

# COMMON CONCEPTS AND TECHNIQUES

### 2.1 GENERAL

Within TIREM and SEM, there are a number of concepts and techniques that are identical in both programs. Some components common to both programs are free-space propagation, effective earth radius, molecular absorption, and tropospheric scatter propagation. These concepts and techniques are discussed in this chapter. Because the spherical-earth calculations that are integral to SEM are also part of TIREM, these algorithms are also common to both. However, the methodology for calculation of propagation over spherical earth is fundamental to SEM and it is discussed in Chapter 3.

### 2.2 FREE-SPACE PROPAGATION

The fundamental concept in propagation formulations is propagation in free space, that is, in a region free of all objects that might absorb or reflect electromagnetic energy. For an ideal isotropic antenna, which radiates uniformly in all directions, the emitted power  $P_t$  is distributed uniformly over spheres of increasing radius. The power density  $S$  at a distance  $d$  is:

$$S = \frac{P_t}{4\pi d^2} \quad (2-1)$$

With  $\lambda$  the wavelength, the power  $P_r$  available to an isotropic receiving antenna having an effective aperture of  $\lambda^2/4\pi$  is:

$$P_r = S \frac{\lambda^2}{4\pi} \quad (2-2)$$

From Equations 2-1 and 2-2, the free-space transmission ratio is therefore:

$$\frac{P_r}{P_t} = \left( \frac{\lambda}{4\pi d} \right)^2 \quad (2-3)$$

and the free-space propagation loss  $L_{FS}$  between isotropic antennas is:

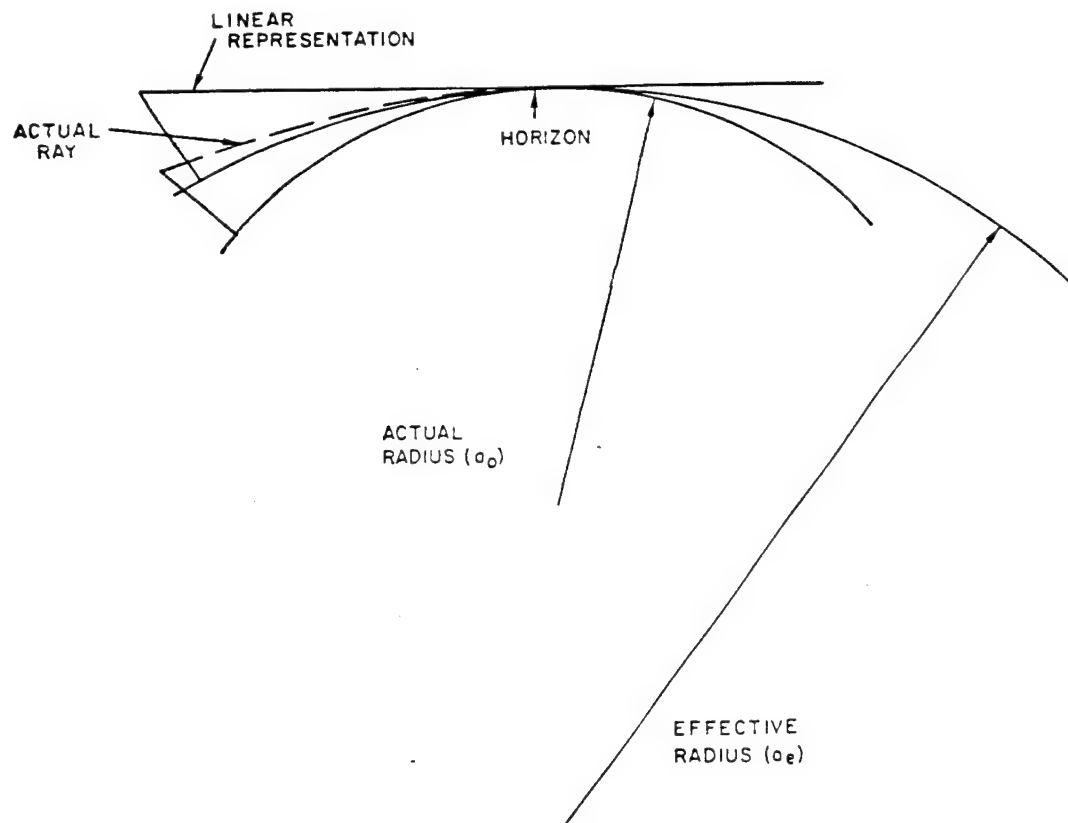
$$L_{FS} = 10 \log \left( \frac{P_t}{P_r} \right) = 20 \log \left( \frac{4\pi d}{\lambda} \right) \quad (2-4)$$

All formulas in subsequent sections that calculate the electric field strength are normalized to the free-space electric field strength,  $E_o$ , at the same point. In all cases, however, the final quantity required is the propagation loss between antennas, rather than the value of the electric field strength at a point. This loss is expressed as the sum of the free-space loss from Equation 2-4 and the excess loss relative to free space.

### 2.3 EFFECTIVE EARTH RADIUS

The properties of the atmosphere vary with elevation. The atmospheric property of concern in this subsection is the variation of refraction index with elevation. In a well mixed atmosphere, the refractivity diminishes with elevation and this gradient causes the radio rays to bend. However, the curvature of the ray path can be modified by a simple geometrical transformation to a change in the curvature of the earth, so the propagation of rectilinear rays is effectively restored. This is the effective-earth radius concept used in tropospheric wave propagation (see Figure 2-1). The transformation is accomplished by substituting an effective earth radius  $a_e$  for the actual earth radius  $a_o$  in path geometry calculations:

$$a_e = ka_o \quad (2-5)$$

Figure 2-1. Effective Earth Radius,  $a_e$ 

The distance  $a_0$  is the actual earth radius ( $= 6.372 \times 10^6$  meters) and  $k$  is the effective earth radius factor. Within approximately 3200 m of the surface of the earth, the gradient of atmospheric refractivity normally decreases at a rate that is linear with height. The slope tends to be correlated with the value of refractivity measured at the surface. At higher altitudes, the gradient decreases exponentially with height. Thus, TIREM and SEM employ either of two forms for the effective earth radius  $k$  factor, one for antennas below 3200 m in the linear portion of the atmosphere, and one for use if either antenna extends into the exponential atmosphere. Thus,  $k$  is defined as:

$$k = \begin{cases} k_{\text{lin}} = \left[ 1 - \frac{0.04665 \exp(0.005577 N_s)}{1 + 10^{-6} N_s} \right]^{-1} & h_1, h_2 \leq 3200 \text{ m} \\ k_{\text{exp}} = 4/3 \left[ 1 - \frac{\Delta h_1}{h_1 + \sqrt{h_1 h_2}} - \frac{\Delta h_2}{h_2 + \sqrt{h_1 h_2}} \right] & \max(h_1, h_2) > 3200 \text{ m} \end{cases} \quad (2-6)$$

where the variables are defined in the next two paragraphs.

The factor  $k_{lin}$  is determined by the nearly constant gradient of refractivity near the surface of the earth for heights of less than 3200 m.  $N_s$  is the surface value of refractivity at the lower of the antenna elevations;  $h_1$  and  $h_2$  are the structural antenna heights at those elevations.

The factor  $k_{exp}$  is derived from the CRPL Exponential Atmosphere<sup>2-1</sup> as follows. In Reference 2-1, the horizon distance  $d_H$  for a given (antenna) height  $h$  is tabulated for a set of  $N_s$  values. Also tabulated is the incremental height  $\Delta h$  required to produce the same horizon distance that would result for a  $k = 4/3$  earth-radius factor, so that:

$$d_H = \sqrt{2(4/3)a_0(h-\Delta h)} = \sqrt{2k_{exp}a_0h} \quad (2-7)$$

and hence

$$k_{exp} = 4/3 (1 - \Delta h/h) \quad (2-8)$$

This is the effective earth radius factor for one antenna height. For two antennas  $h_i$ ,  $i = 1, 2$ , each earth radius factor  $k_{exp,i}$  is weighted by the ratio of its horizon distance  $d_{H,i}$  to the total horizon distance  $d_{H,1} + d_{H,2}$  as follows:

$$k_{exp,i} = 4/3 (1 - \Delta h_i/h_i) \frac{d_{H,i}}{d_{H,1} + d_{H,2}} \quad (2-9)$$

so that

$$k_{exp} = k_{exp,1} + k_{exp,2} = 4/3 \left[ 1 - \frac{\Delta h_1}{h_1 + \sqrt{h_1 h_2}} - \frac{\Delta h_2}{h_2 + \sqrt{h_1 h_2}} \right] \quad (2-10)$$

<sup>2-1</sup>Bean, B. R. and Thayer, G. D., CRPL Exponential Reference Atmosphere, US Dept. of Commerce, National Bureau of Standards, NBS Monograph 4, October 1959.

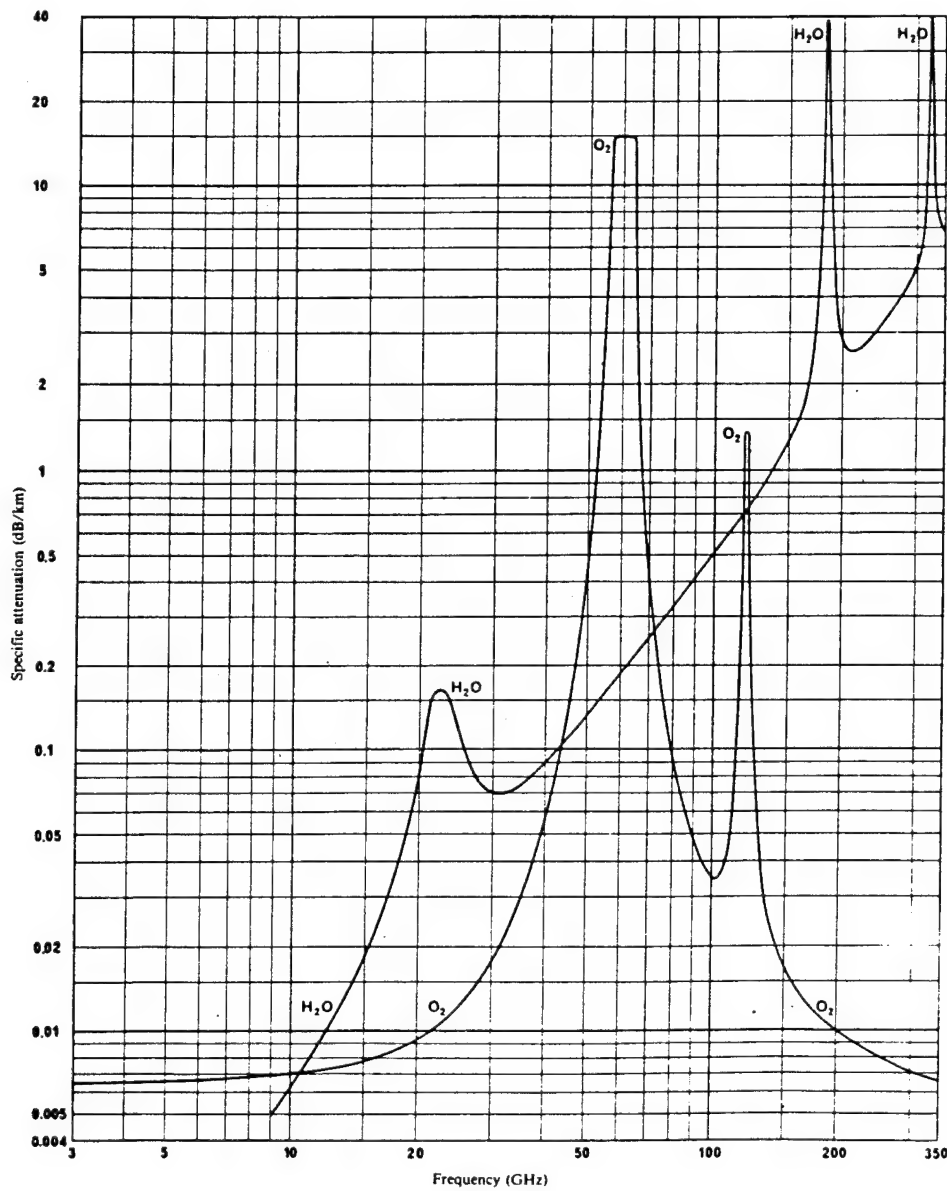
The transition height of 3200 m in Equation 2-6 is selected such that at that height  $k_{\text{lin}} \approx k_{\text{exp}}$  for all values of  $N_s$ .

The subroutine FAKTOR has stored a subset of the tabulated  $\Delta h$  data of Reference 2-1 (for initial angle  $\theta = 0$ , corresponding to the horizon distance) for  $N_s = 200.0, 252.9, 289.0, 313.0, 344.5, 377.2, 404.8, 450.0$ , and for incremental heights up to 475,000 m. For intermediate values of height and refractivity,  $\Delta h$  is derived by linear interpolation. The  $k$  factor given in Equation 2-6 is implemented in subroutine RFC2AK.

## 2.4 MOLECULAR ABSORPTION

In a clear atmosphere, oxygen and water vapor absorb microwaves. Oxygen has a magnetic interaction with the incident radiation because the  $O_2$  molecule is normally in a paramagnetic state, and water vapor contributes because of the electric polarity of the  $H_2O$  molecule. There are certain frequency regions where the absorption for both oxygen and water vapor is abnormally large because of resonance. Figure 2-2 gives an example of the specific attenuation in dB/km of  $H_2O$  and  $O_2$  versus frequency. The plots are for the average atmospheric conditions at sea level in temperate latitudes in summer.

At higher altitudes, the specific attenuation typically decreases at a rate that is dependent on the absolute temperature  $T(H)$ , the pressure  $P(H)$ , and on the density  $\rho(H)$  of the water vapor at a height  $H$  (km above mean sea level). Consequently, molecular absorption varies as a function of height and its calculation is dependent upon the selection of an atmospheric molecular model.



PRESSURE: 1 ATMOSPHERE  
TEMPERATURE: 20°C  
WATER VAPOR: 7.5 G/M<sup>3</sup>

Figure 2-2. Specific Attenuation of Oxygen and Water Vapor

A particular molecular model used in the meteorological and atmospheric physics community is the US Standard Atmosphere, 1962<sup>2-2</sup> as partially reproduced in Table 2-1, where  $P_s$ ,  $T_s$  and  $\rho_s$  are tabulated with height  $H$  as a parameter. This molecular model is used to derive the combined  $H_2O$  and  $O_2$  specific attenuation (absorption coefficient)  $\gamma$  which is the molecular absorption per unit path length at the height  $H$ . The coefficients  $\gamma$  used in TIREM and SEM were generated using the Millimeter Wave Propagation Prediction Model (MMWPROP)<sup>2-3,2-4</sup> and stored in data arrays in subroutine GAMMAR. Absorption coefficients are stored for discrete values of frequency ( $f = 1, 5, 10, 15, 20$  GHz), height ( $H = 0, 2, 4, 6, 8, 10, 15, 20, 25, 30$  km) and humidity at sea level ( $\rho(0) = 0, 10, 30, 50, 110$  g/m<sup>3</sup>). Intermediate values are linearly interpolated from these tabulations.

Table 2-1. US Standard Atmosphere, 1962 (from Reference 2-2)

Height $H$ (km)	Pressure $P_s$ (mbar)	Temperature $T_s$ (K)	Water Vapor $\rho_s$ (g/m <sup>3</sup> )
0	1.013E+03	288.1	5.9E+00
1	8.986E+02	281.6	4.2E+00
2	7.950E+02	275.1	2.9E+00
3	7.012E+02	268.7	1.8E+00
4	6.166E+02	262.2	1.1E+00
5	5.405E+02	255.7	6.4E-01
6	4.722E+02	249.2	3.8E-01
7	4.111E+02	242.7	2.1E-01
8	3.565E+02	236.2	1.2E-01
9	3.080E+02	229.7	4.6E-02
10	2.650E+02	223.2	1.8E-02

<sup>2-2</sup>McClatchy, R. A., et al, Optical Properties of the Atmosphere (Third Edition), AFCRL-72-0497, Air Force Cambridge Research Laboratories, August 1972.

<sup>2-3</sup>Meidenbauer, R., A Millimeter Wave Propagation Prediction Model--MMWPROP, ECAC-TN-81-046, DoD ECAC, Annapolis, MD, September 1981.

<sup>2-4</sup>Liebe, H. J., "An Updated Model for Millimeter Wave Propagation in Moist Air," Radio Science, Vol. 20, No. 5, 1985, pp. 1069-1089.



The humidity at sea level  $\rho(0)$  is obtained from the local absolute humidity  $\rho_{\text{LOCAL}}$  (in g/m<sup>3</sup>, required as input) from:

$$\rho(0) = \frac{1.7 \times 10^3}{T_s} \frac{\rho_{\text{LOCAL}}}{\rho_s} \quad (2-11)$$

where the temperature  $T_s$  and the vapor density  $\rho_s$  are again dependent upon the height  $H$  as tabulated in Table 2-1.  $T_s$  and  $\rho_s$  are approximated from the tabulated values by:

$$T_s = -6.48 H + 288.1 \quad (2-12)$$

and

$$\rho_s = \begin{cases} 5.9 (0.7011)^H & 0 \leq H \leq 2 \\ 7.6455 (0.6159)^H & H > 2 \end{cases} \quad (2-13)$$

Because the molecular absorption coefficient varies with height along the radio ray path due to variations in atmospheric temperature, pressure, and water vapor content, the total atmospheric absorption is obtained by integration along the entire path. Since the height is, for a particular path, a function of the distance  $r$ , the total atmospheric absorption for a path segment of length  $d$ , is formally given by:

$$A_{\text{ABSORB}} = \int_0^d \gamma[H(r)] dr \quad (2-14)$$

The numerical integration of Equation 2-14 is performed in subroutine ABSORB. For LOS paths and for troposcatter paths, the integration is by Simpson's  $\frac{1}{3}$  rule with  $H(r)$  and therefore  $\gamma(H)$  determined in 2-km intervals along the slant path  $r$  (see Figure 2-3). For a diffracted path, the integration in Equation 2-14 for the two paths  $r_1$  and  $r_3$  within the horizons of the transmitter and receiver is obtained in the same manner. In the diffracted path region  $r_2$ , the two horizon elevations  $h_1$  and  $h_2$  are averaged and the integration consists simply of the multiplication of the value  $\gamma$  for this averaged elevation by the distance between the two horizons. The absorption for diffracted paths is then the sum of the three absorption parts.

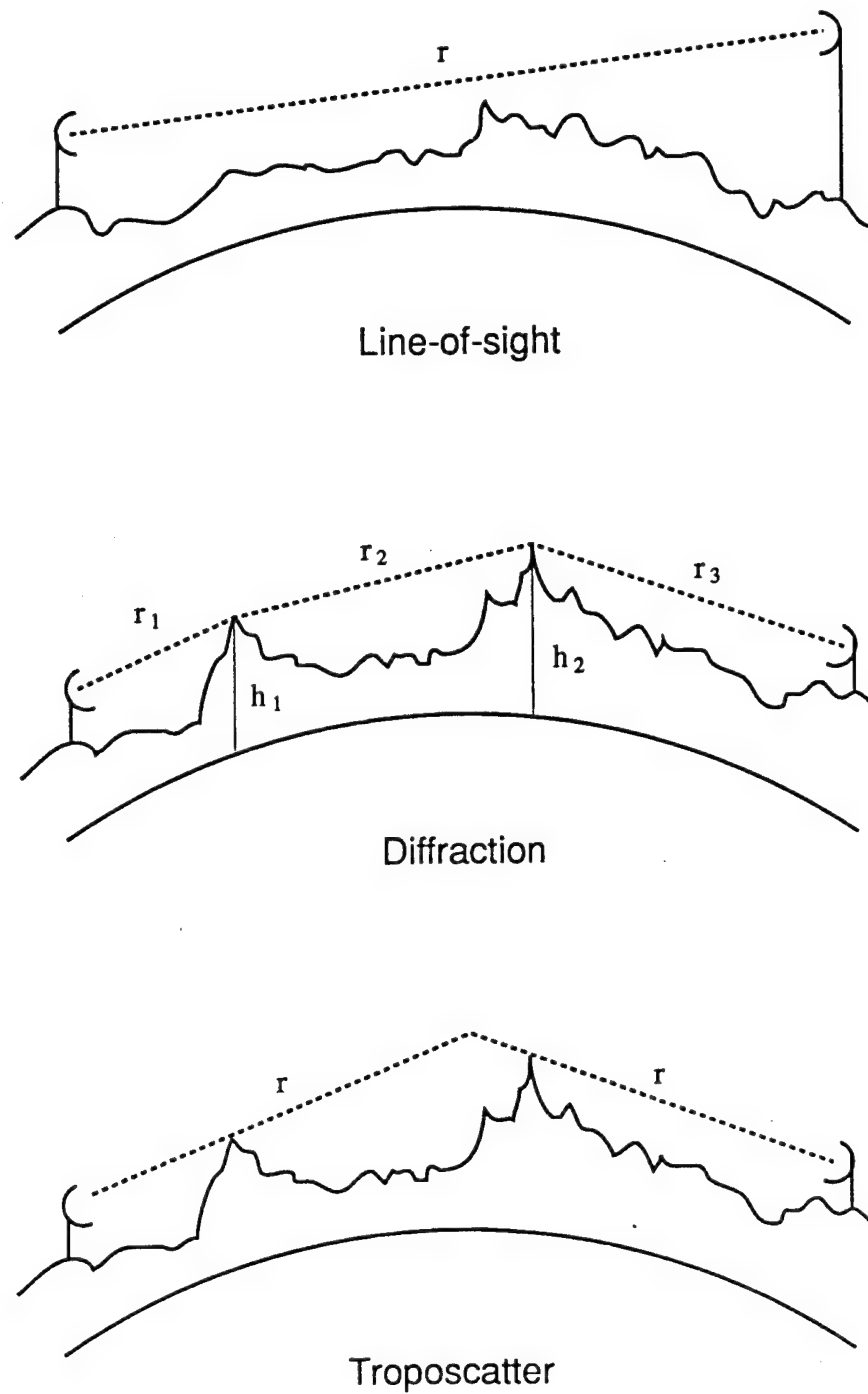


Figure 2-3. Propagation Paths for Different Modes  
(Showing  $H(r)$  Determined From Path Geometry)

## 2.5 TROPOSCATTER PROPAGATION

The transmission of electromagnetic energy beyond the radio horizon occurs by tropospheric forward scatter as well as by diffraction. In this section, the modeling of the median basic propagation loss resulting from tropospheric forward scatter  $L_{TRO}$  is discussed.  $L_{TRO}$  is given by an empirical formula:<sup>2-5</sup>

$$L_{TRO} = \max \{ [30 \log f - 20 \log D + 20 \log (r_o/D) + F(D\theta)], L_{FS} \} + H_o - F_o \quad (2-15)$$

where, with all losses in dB

- $L_{FS}$  = free-space loss
- $F(D\theta)$  = attenuation function
- $F_o$  = scattering efficiency correction
- $H_o$  = frequency gain function
- $r_o$  =  $\max(\bar{D}, D)$  (see Figure 2-4), in km
- $f$  = frequency, in MHz
- $D$  = great-circle distance between transmitter and receiver, in km
- $\theta$  = great-circle arc distance between transmitter and receiver, in radians.

$F(D\theta)$ ,  $F_o$ , and  $H_o$  are empirical functions that depend on angles and distances derived from the terrain intervening between transmitter and receiver. These functions are discussed in Appendix B.

The tropospheric forward scatter loss is implemented in subroutine TROPSC.

---

<sup>2-5</sup>International Radio Consultative Committee (CCIR), Tropospheric Wave Transmission Loss Prediction, CCIR, Doc. V/23-E, March 1962.

The scatter angle  $\theta_o$  is calculated from the terrain-dependent geometrical parameters (see Figure 2-4) as follows:

$$\theta_o = \alpha_1 + \alpha_2 \quad (2-16)$$

where

$$\tan \alpha_1 = \frac{D}{2a_e} + \theta_{e,1} + \frac{h_{s,1} - h_{s,2}}{D} \quad (2-17)$$

$$\tan \alpha_2 = \frac{D}{2a_e} + \theta_{e,2} - \frac{h_{s,1} - h_{s,2}}{D} \quad (2-18)$$

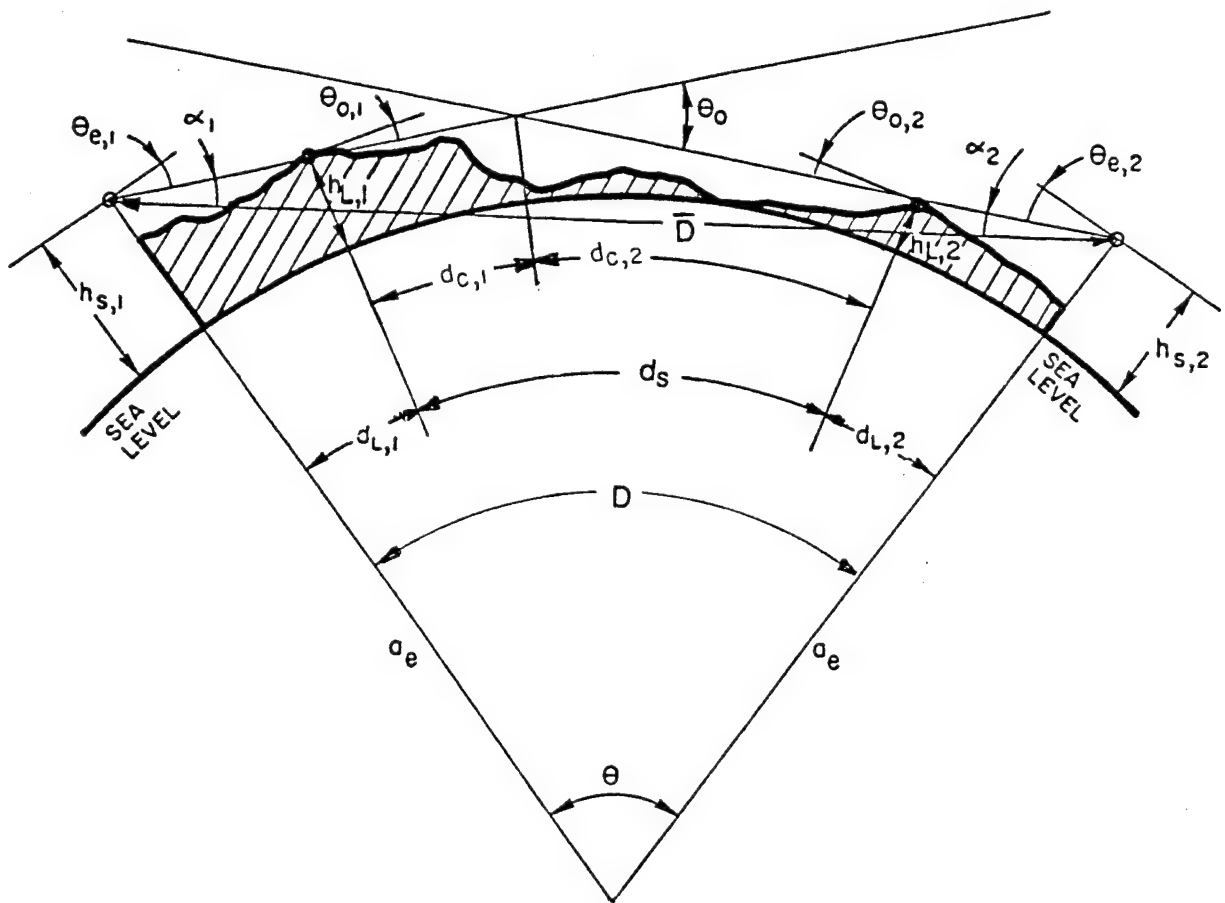


Figure 2-4. Terrain-Dependent Geometrical Parameters

In Equations 2-17 and 2-18,  $\theta_{e,i}$  are the elevation angles (above the horizontal) of the horizon obstacle at the transmitter ( $i = 1$ ) and at the receiver ( $i = 2$ ). These are:

$$\tan \theta_{e,i} = \frac{h_{L,i} - h_{s,i}}{d_{L,i}} - \frac{d_{L,i}}{2a_e} \quad i = 1,2 \quad (2-19)$$

where

- $h_{L,i}$  = height of the obstacle that produced the radio horizon above MSL
- $h_{s,i}$  = structural antenna height, plus the site elevation above MSL
- $d_{L,i}$  = distance from the antenna to the radio horizon
- $a_e$  = effective earth radius.

Angular elevation  $\theta_{o,i}$  of horizon rays at horizon location is:

$$\theta_{o,i} = \theta_{e,i} + d_{L,i}/a_e \quad (2-20)$$

Horizon obstacle to crossover distances,  $d_{c,i}$ , are:

$$d_{c,1} = D\alpha_2/\theta_o - d_{L,1} \quad (2-21)$$

$$d_{c,2} = D\alpha_1/\theta_o - d_{L,2} \quad (2-22)$$

## 2.6 SPHERICAL-EARTH LOSS

Another common modeling technique used in both TIREM and SEM is the method for calculating and combining the space-wave, surface-wave, and diffracted-wave losses over a smooth spherical earth. This process is programmed in subroutine SEARTH (and its ancillary subroutines). Since SEARTH is the fundamental basis of the SEM program, its theory and methodology are described in the next section.

## CHAPTER 3

### SPHERICAL-EARTH MODEL (SEM)

#### 3.1 GENERAL

In 1941, Norton<sup>3-1</sup> published a systematic method for calculating the ground-wave field for both vertically and horizontally polarized waves emitted by a Hertzian dipole and propagating over a spherical earth. Norton summarized the results of a number of classical papers dealing with the calculation of ground-wave field strength. He then presented a method, involving a combination of simple equations and graphs, for practical calculation of ground-wave field strength. The method is automated for use in TIREM and SEM by substituting simple equations for the graphical techniques of Norton. Essentially, the method consists of calculating the space wave and the surface wave, each to a certain distance, and the diffracted wave beyond a critical distance by the first term of the residue series.<sup>3-2</sup> By making a plot of the field versus the distance, the intermediate region between the two distance limits can then be traced in quite easily. The formulation given here and implemented in the subroutine SEARTH (and those called by SEARTH) is virtually the same as that in Norton's paper with the following exceptions:

- the Hertzian dipole is replaced by a uniformly radiating source
- the tracing is replaced by a splice function
- the fields are referenced to a free-space field.

This chapter provides the propagation formulas of subroutine SEARTH in four sections for (1) the space wave, (2) the surface wave, (3) the diffracted wave, and (4) the splice functions. All field formulas are normalized to the free-space field  $E_0$ , that is, the field identified with the direct wave.

---

<sup>3-1</sup>Norton, K. A., "The Calculation of Ground-Wave Field Intensity Over A Finitely Conducting Spherical Earth," Proc. I.R.E., Vol. 29, No. 12, December 1941, pp. 623-639.

<sup>3-2</sup>Bremmer, H., Terrestrial Radio Waves, Elsevier Publishing Co., Amsterdam, 1949.

Before presenting the formulas, it may be well to add a short historical note. The problem of dipole radiation in the presence of a dissipative half-space dates back to Sommerfeld's classical paper<sup>3-3</sup> and, for practical purposes, efforts to define a solution continued into the 1960s. There are numerous references covering the subject. As a starting point, the interested reader should consult the books authored by King,<sup>3-4</sup> Bremmer (Reference 3-2), Banos,<sup>3-5</sup> and Wait.<sup>3-6</sup> Bremmer also presented an interesting historical survey paper,<sup>3-7</sup> and in the same publication King and Wait<sup>3-8</sup> provided a consolidated treatment of ground-wave propagation.

It is noted here that the propagation formulas in ECAC's EFFSECC model (Reference 1-3) are essentially the formulas of Reference 3-2. In the diffracting region, a great number of the terms in the residue series are retained and consequently the propagation subroutines of EFFSECC require considerable computer time. Because of a requirement for a fast and efficient spherical-earth model, the SEM model was implemented based on Norton's paper (Reference 3-1). A statistical comparison between SEM and EFFSECC is given in Chapter 5.

---

<sup>3-3</sup>Sommerfeld, A., "Über die Ausbreitung der Wellen in der Drahtlosen Telegraphie," Ann. Physics, 28, 1909, pp. 667-737.

<sup>3-4</sup>King, R. W. P. and Prasad, S., Fundamental Electromagnetic Theory and Applications, Prentice-Hall, Inc., Englewood Cliffs, NJ, 1986.

<sup>3-5</sup>Banos, A., Dipole Radiation in the Presence of a Conducting Half Space, Pergamon Press, Oxford, 1966.

<sup>3-6</sup>Wait, J. R., Electromagnetic Waves in Stratified Media, Pergamon Press, Oxford, 1962.

<sup>3-7</sup>Bremmer, H., "A Historical Survey of the Mathematical Theories of Radio Wave Propagation," Symposia Matematica (Istituto Nazionale Di Alta Matematica, Bologna, Italy) Vol. 18, 1976, pp. 57-83.

<sup>3-8</sup>King, R. J. and Wait, J. R., "Electromagnetic Ground Wave Propagation, Theory and Experiment," Symposia Matematica (Istituto Nazionale Di Alta Matematica, Bologna, Italy) Vol. 18, 1976, pp. 107-208.

### 3.2 SPACE-WAVE PROPAGATION

The geometry for spherical-earth calculations at points within LOS is shown in Figure 3-1. Constructive or destructive interference will occur between the direct and reflected waves at the receiving antenna because the reflected ray path is electrically longer than that of the direct ray. The electrical length of the reflected ray path is greater because the physical path length is longer and because of the phase delay that occurs at the point of reflection. Also, the magnitude of the reflected wave will be smaller than that of the direct wave because it is proportional to the magnitude of the reflection coefficient and the divergence factor. The space wave is formed by the vector addition of the direct and reflected waves. For vertical and horizontal polarization, the space-wave electric field  $E_{SPW}$ , normalized to the direct (or free space) field  $E_o$  at the field point, is expressed by:

$$|E_{SPW}/E_o| = |1 + (r_1'/r_2') D_c R e^{j\Delta}| \quad D \leq d_{SPW} \quad (3-1)$$

where

$$r_1' = \sqrt{D^2 + (h_1' - h_2')^2} \quad (3-2)$$

$$r_2' = \sqrt{D^2 + (h_1' + h_2')^2} \quad (3-3)$$

are the path distances traversed by the direct and reflected waves, respectively.

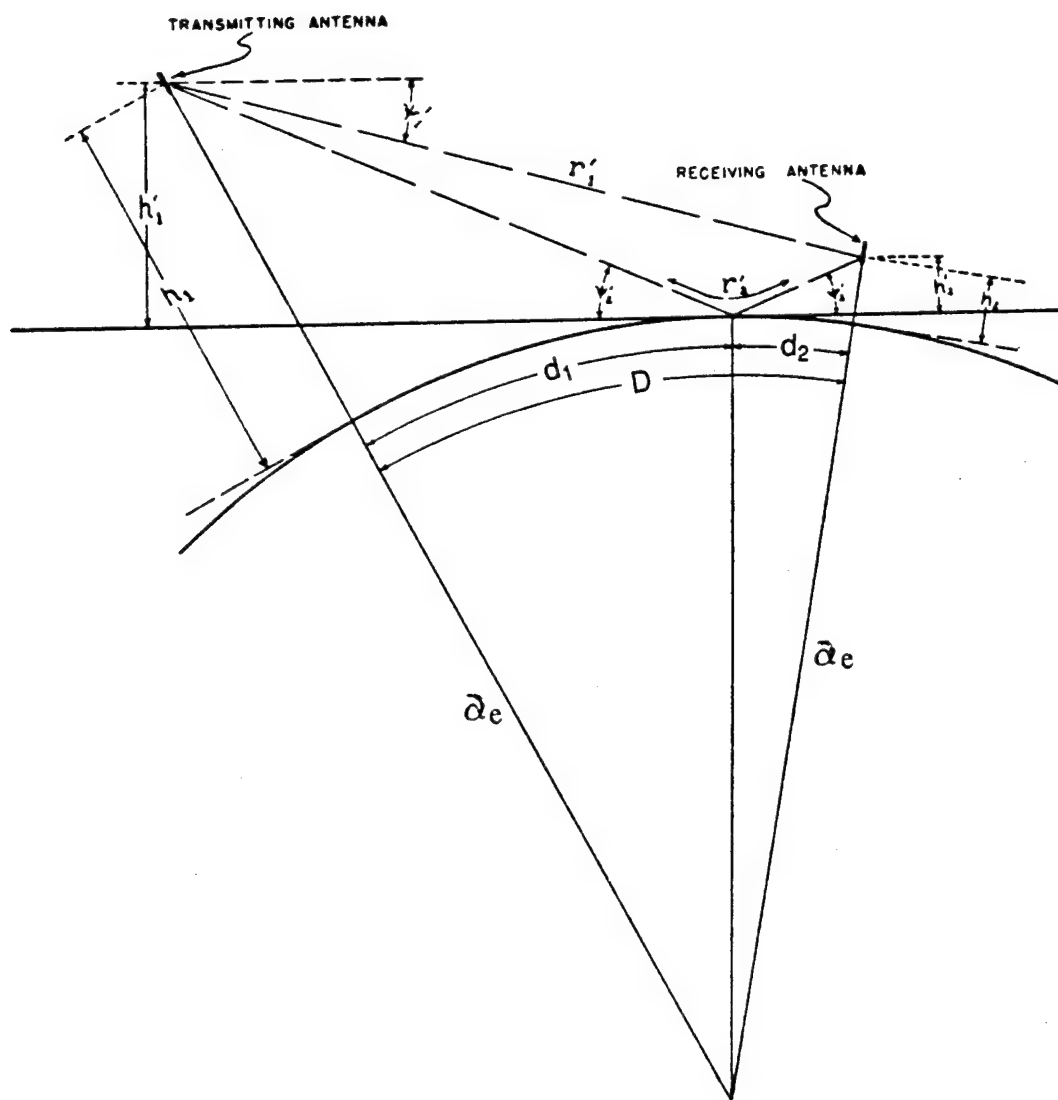
The phase factor  $\Delta$  and the divergence coefficient  $D_c$  are:

$$\Delta = \frac{2\pi}{\lambda} (r_2' - r_1') \quad (3-4)$$

$$D_c = \left[ 1 + \frac{2d_1 d_2}{a_e (h_1' + h_2')} \right]^{-\frac{1}{2}} \quad (3-5)$$

and are independent of polarization.





(FROM REFERENCE 3-1)

Figure 3-1. Geometry for Spherical-Earth Calculations at Points Within LOS

The divergence factor is the ratio of field strength after reflection from a perfectly reflecting spherical surface to the incident field. It is necessary because the beam reflected from a spherical surface diverges at a greater rate than it would if reflected from a plane surface.

The heights  $h_1'$  and  $h_2'$  are the antenna heights measured from the tangent plane:

$$h_1' = h_1 - \frac{d_1^2}{2 a_e} \quad (3-6)$$

$$h_2' = h_2 - \frac{d_2^2}{2 a_e} = h_2 - \frac{(D - d_1)^2}{2 a_e} \quad (3-7)$$

where  $h_1$  and  $h_2$  are the structural antenna heights. The distance  $d_1$  to the reflection point is:

$$d_1 = \frac{D}{2} + \frac{2}{\sqrt{3}} \cos(\phi/3 + \pi/3) \sqrt{a_e (h_1 + h_2) + (D/2)^2} \quad (3-8)$$

which is the trigonometric solution of a cubic equation with:

$$\cos \phi = \frac{3^{\frac{3}{2}} a_e (h_1 - h_2) D}{4 [a_e (h_1 + h_2) + (D/2)^2]^{\frac{3}{2}}} \quad (3-9)$$

The reflection coefficient R is dependent on the polarization as follows:

For Vertical Polarization

$$R = \frac{N^2 \sin \psi_2' - \sqrt{N^2 - \cos^2 \psi_2'}}{N^2 \sin \psi_2' + \sqrt{N^2 - \cos^2 \psi_2'}} \quad (3-10)$$

For Horizontal Polarization

$$R = \frac{\sin \psi_2' - \sqrt{N^2 - \cos^2 \psi_2'}}{\sin \psi_2' + \sqrt{N^2 - \cos^2 \psi_2'}} \quad (3-11)$$

with

$$\cos \psi_2' = D/r_2' \quad (3-12)$$

The square of the complex index of refraction is:

$$N^2 = \epsilon_r + j \ 60 \ \sigma \lambda \quad (3-13)$$

where

$\epsilon_r$  = relative dielectric constant of earth

$\sigma$  = earth conductivity, in S/m.

The normalized space-wave (geometric-optical) field, given in Equation 3-1, oscillates with distance due to the interference of the direct and the reflected waves. The phenomenon is depicted in Figure 3-2. The envelope of the maximum ( $C_1$  in Figure 3-2) is:

$$|E_{MAX}/E_o| = \begin{cases} 1 + \frac{r_1'}{r_2'} D_c |R| & D \leq d_{MAX} \\ |E_{SPW}/E_o| & d_{MAX} < D \leq d_{SPW} \end{cases} \quad (3-14)$$

and the envelope of the minimum ( $C_2$  in Figure 3-2) is:

$$|E_{MIN}/E_o| = \begin{cases} 1 - \frac{r_1'}{r_2'} D_c |R| & D \leq d_{MIN} \\ |E_{SPW}/E_o| & d_{MIN} < D \leq d_{SPW} \end{cases} \quad (3-15)$$

where

$$|E_{SPW}/E_o| = \left| 1 + \frac{r_1'}{r_2'} D_c R \exp \left[ \frac{j2\pi}{\lambda} (r_2' - r_1') \right] \right| \quad (3-16)$$

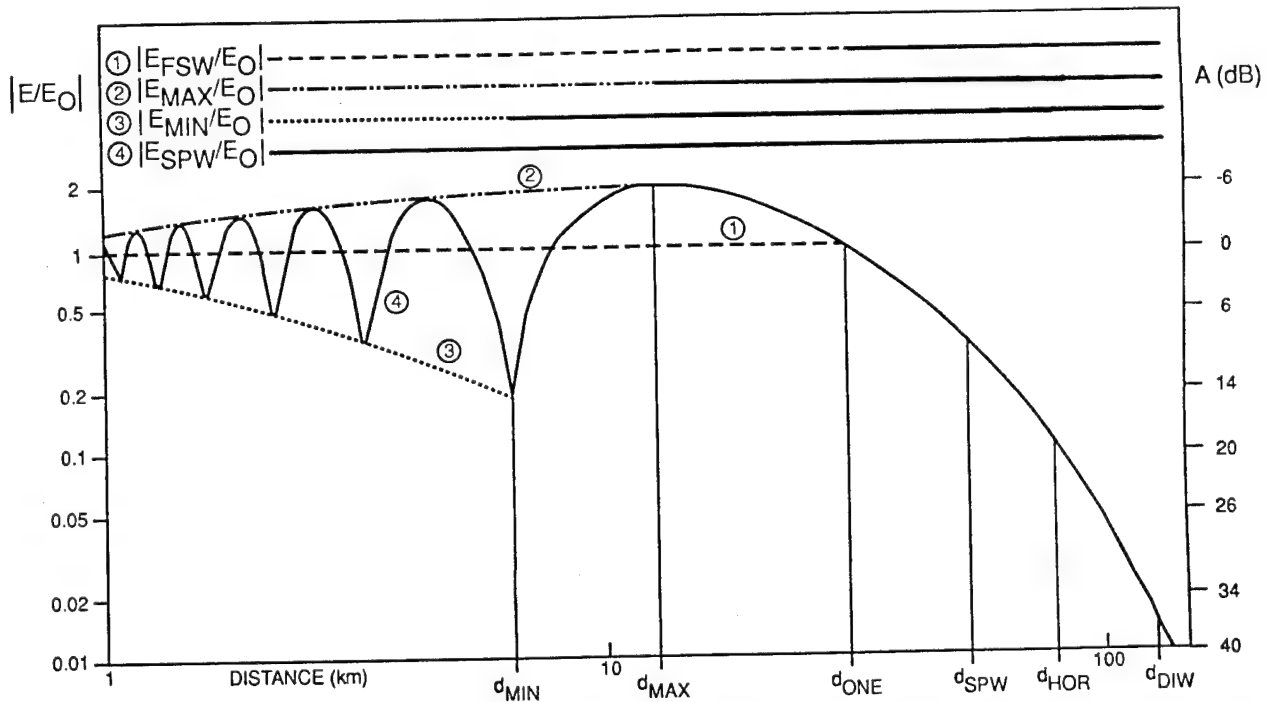


Figure 3-2. Numerical Example Showing the Interference of the Direct and the Reflected Ray ( $f = 100$  MHz,  $h_1 = h_2 = 100$  m,  $\epsilon = 10$ ,  $\sigma = 0.01$  S/m, Vertical Polarization)

The distance to the last maximum of the oscillations  $d_{MAX}$  and the distance to the last minimum  $d_{MIN}$  are found by the methods in Appendix C. The distance  $d_{SPW}$  limiting the range of applicability of Equations 3-1, 3-14, and 3-15 lies between the distance of the last maximum  $d_{MAX}$ , and the radio horizon distance  $d_{HOR}$ , where the geometric-optical equations fail, and is given by:

$$d_{SPW} = d_{MAX} + w_1 (d_{HOR} - d_{MAX}) \quad (3-17)$$

The factor  $w_1 = 0.6$  is empirically determined from comparison with results derived with the residue series. The radio horizon distance  $d_{HOR}$  is:

$$d_{HOR} = \sqrt{2a_e h_1} + \sqrt{2a_e h_2} \quad (3-18)$$

In many applications it is preferable to replace the normalized field in the oscillating region (Equation 3-1) by the free-space value ( $C_0$  in Figure 3-2), so that for  $D < d_{SPW}$ :

$$|E_{FSW}/E_o| = \min \{1, |E_{MAX}/E_o|\} \quad (3-19)$$

where the subscript SPW in  $E_{SPW}$  has been replaced by FSW to distinguish Equation 3-19 from Equation 3-1.

When the free-space wave option is selected, the predicted field relative to free space is given by the horizontal line  $C_0$  (see Figure 3-2) for LOS distances in the oscillating region. At distances beyond the intersection of  $C_0$  and  $C_1$ , the field is given by the curve  $C_1$ . One application where the free-space replacement of the space wave is required is in TIREM. The use of a geometric-optical field based on smooth-earth geometry for a distance less than  $d_{MAX}$  would be unsuitable in a rough-earth model and would lead to large prediction errors.

### 3.3 SURFACE-WAVE PROPAGATION

The ground wave consists of three components: the direct wave, the reflected wave, and the surface wave. The direct and reflected waves constitute the space wave. For high antennas at LOS distances, the direct and reflected waves may combine alternately in-phase or out-of-phase as distance increases causing signal peaks and nulls. If the distance continues to increase until the receiving antenna approaches the horizon, the lengths of the direct and reflected paths become nearly the same, and because of a phase reversal of the reflected wave, the direct and reflected waves nearly cancel leaving only the surface wave. The surface wave is of primary importance when both antennas are within a few wavelengths of the ground. For low antennas, less than about a wavelength, the surface wave can be significant compared to the space wave at short LOS distances. The surface-wave field intensity  $E_{\text{SUW}}$ , normalized to the free-space intensity is:

$$E_{\text{SUW}}/E_o = \begin{cases} |(1-R)|(r_1'/r_2') f(p) & p < 0.729 \\ |(1-R)| \min \{(r_1'/r_2') F_{\text{SUW},1} F_{\text{SUW},2} f(p), 0.5\} & p \geq 0.729 \end{cases} \quad (3-20)$$

where  $f(p)$  is the Sommerfeld reduction factor and  $F_{1,2}$  are functions described below. The ratio  $f(p)/p$  is plotted in Figure 2 of Reference 3-1. The Sommerfeld reduction factor  $f(p)$  is approximated here by the empirical relation:

$$f(p) = \frac{1 + 3p}{1 + 3p + 6p^2} \quad (3-21)$$

The parameter  $p$  is the Sommerfeld numerical distance and is:

$$p = \frac{\pi \sqrt{D^2 + (h_1 + h_2)^2}}{\lambda |N^2|^y} \quad (3-22)$$

where,  $y = 1/2$  for vertical polarization and  $y = -1/2$  for horizontal polarization.

The function

$$F_{\text{SUW},i} = \sqrt{1 + \left( \frac{2\pi h_i}{\lambda |N^2|^y} \right)^2} \quad (3-23)$$

is a height-gain function for a surface wave area over a plane earth.

The distance  $d_{\text{SUW}}$ , limiting the range of applicability of the surface wave formulas, is generally taken to be:

$$d_{\text{SUW}} = 12000 \lambda^{\frac{1}{3}} \quad (3-24)$$

### 3.4 DIFFRACTED-WAVE PROPAGATION

For low antennas at a short distance, the direct and ground reflected waves cancel leaving only the surface wave. The surface wave at large distances is a diffracted wave. The curvature of the earth prevents the waves from passing directly into a shadow region. They must reach this shadow region by a process of bending around the curved surface of the earth. This process is called diffraction.

For distances  $D \geq d_{\text{DIW}}$ , the diffracted field intensity  $E_{\text{DIW}}$  normalized to the free-space field is given as the first term of the residue series:

$$|E_{\text{DIW}}/E_o| = 113 F_1 F_2 \frac{\gamma}{\beta} \sqrt{\eta'} \exp[-(2\pi)^{1/3} \eta'] \quad (3-25)$$

where

$$\eta' = \beta \eta D \quad (3-26)$$

$$\eta = (a_e^2 \lambda)^{-1/3} \quad (3-27)$$

$$\gamma = \min \{0.03, 0.08 K^2\} \quad (3-28)$$

$\gamma$  is an approximation to the plot of Figure 6 of Reference 3-1.

The height-gain functions  $F_i$  in Equation 3-25 (for  $i = 1, 2$ ) are:

$$F_i = \begin{cases} \max \{F_{SUW,i}, F_{DIW,i}\} & , \bar{h}_i \geq 1 \\ F_{SUW,i} & , \bar{h}_i < 1 \end{cases} \quad (3-29)$$

The height-gain function for elevated antennas BLOS is:

$$F_{DIW,i} = \delta f_1(\bar{h}_i) \quad (3-30)$$

where  $f_1(\bar{h}_i)$  is a polynomial approximation to Figure 11 in Reference 3-1.

The parameters  $\bar{h}_i$  and  $\delta$  are defined as:

$$\bar{h}_i = \frac{\beta^2}{(a_e^2 \lambda^2)^{1/3}} h_i \quad (3-31)$$

$$\delta = \max (0.328776/K, 0.357945) \quad (3-32)$$



The parameter  $\beta$  in Equations 3-25 and 3-26 is:

$$\beta = 0.9[e^{-3.26K^2} + 0.78] \quad (3-33)$$

where

$$K = (2\pi a/\lambda)^{-1/3} |N^2|^y \quad (3-34)$$

$F_{DIW,i}$  is Equation 20 of Reference 3-1 and  $\delta$  and  $\beta$  are approximations to the plots of Figures 10 and 5, respectively of Reference 3-1. The distance  $d_{DIW}$  is:

$$d_{DIW} = d_{HOR} + \frac{1.5}{\beta\eta} \quad (3-35)$$

### 3.5 SPLICE FUNCTIONS

For situations where the minimum distance  $d_{DIW}$ , beyond which the diffraction calculation applies, is greater than the maximum distances  $d_{SPW}$  or  $d_{SUW}$ , where either the space wave or surface wave calculations apply, it is necessary to estimate the normalized field by using a splice function. This function is equivalent to Norton's graphical method (Reference 3-1, p. 632) in which he suggests that "a smooth transition curve may be drawn." The splice function  $|E_{SPLICE}/E_o|$  developed for this purpose simulates the normalized field between these limits.

The technique is illustrated in Figure 3-3. The figure is divided into three regions. In the leftmost region, the normalized field is represented by  $|E_s/E_o|(D)$  and can be either  $|E_{SPW}/E_o|$  or  $|E_{SUW}/E_o|$  depending on which is dominant. This region ends at a distance of either  $d_{SPW}$  or  $d_{SUW}$ , given generically as  $D_s$ . The rightmost region is the diffraction region where the field is represented by  $|E_{DIW}/E_o|(D)$ . This region begins at  $D_D = d_{DIW}$ . The splice function in the middle region serves to connect  $|E_s/E_o|(D)$  to  $|E_{DIW}/E_o|(D)$ .

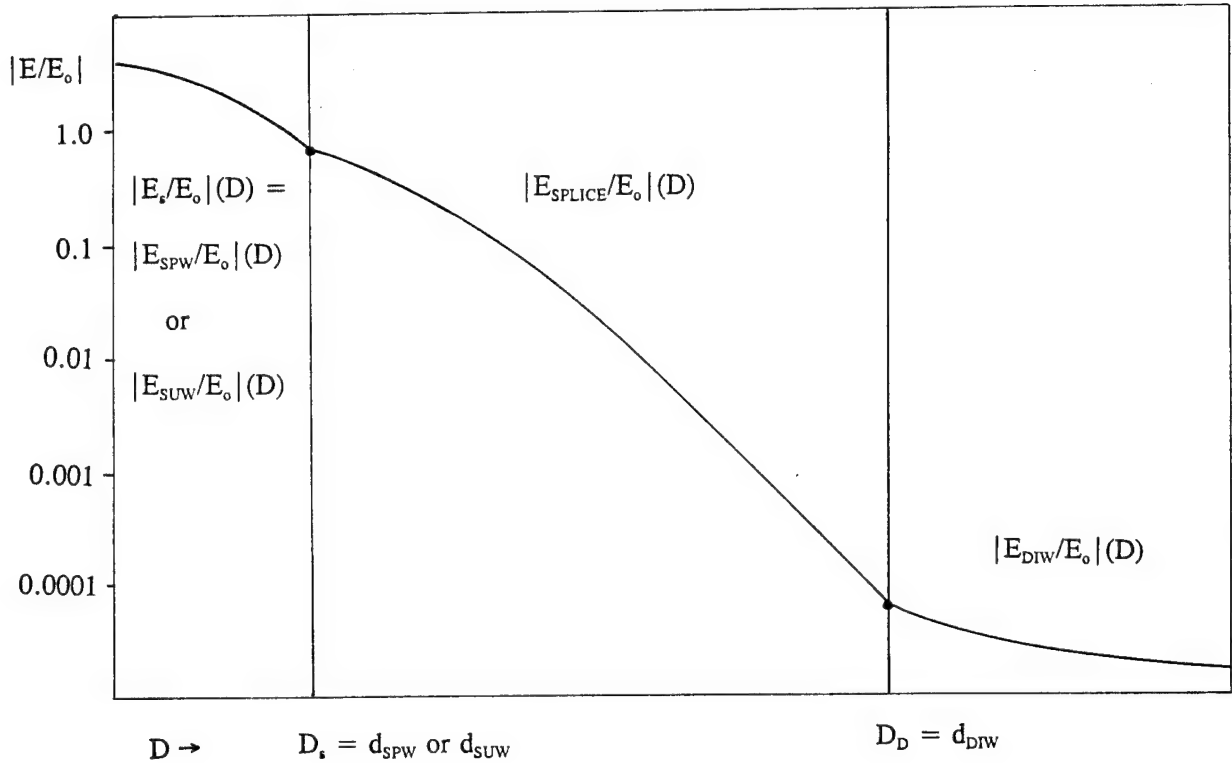


Figure 3-3. Example of the Splice Function Joining Either the Space-Wave or Surface-Wave Fields with the Diffracted-Wave Field

The splice function is of the form

$$|E_{\text{SPLICE}}/E_o|(D) = |E_s/E_o|(D_s) e^{\beta_s(D_s^2 - D^2)} \quad (3-36)$$

where  $|E_s/E_o|(D_s)$ ,  $D_s$ , and  $\beta_s$  are determined such that the normalized field is continuous at the pair of limiting distances  $D_s = d_{\text{SPW}}$  or  $d_{\text{SUW}}$ , as appropriate, and  $D_D = d_{\text{DIW}}$ .

The parameter  $\beta_s$  is:

$$\beta_s = \frac{1}{d_{\text{DIW}}^2 - d_s^2} \ln \left[ \frac{|E_s/E_o|(D_s)}{|E_{\text{DIW}}/E_o|(D_D)} \right] \quad (3-37)$$

Equation 3-36 is the general form for the splice function. The coefficient  $|E_s/E_o|(D_s)$  is either the normalized space-wave field at  $D_s = d_{SPW}$  or the normalized surface wave field at  $D_s = d_{SUW}$ , as appropriate. In Equation 3-37,  $|E_{DIW}/E_o|(D_D)$  is the normalized diffracted wave field evaluated at the limiting distance  $D_D = d_{DIW}$ . The splice function makes the field strength continuous at the transition points. However, the first derivative of the field strength is discontinuous at the transition points.

### 3.6 SUMMARY OF SPHERICAL-EARTH PROPAGATION FORMULAS

The excess propagation loss is calculated by multiplying the logarithm of the normalized field by -20. The excess propagation loss for the space wave, free space, surface wave, splice function, and diffracted waves are designated as  $A_{SPW}$ ,  $A_{FSW}$ ,  $A_{SUW}$ ,  $A_{SPLICE}$ , and  $A_{DIW}$ , respectively. Table 3-1 contains a summary of the excess loss calculations, the range of applicability, and a cross reference to the equation in the text. The SEM excess loss  $A_{SEM}$  is the excess loss for the appropriate wave type depending on distance. At distances less than  $d_{DIW}$ , it is possible that the formulations for both the space wave and the surface wave are applicable. In such a case, the appropriate loss is the smaller of  $A_{SPW}$  or  $A_{SUW}$ . The total spherical-earth propagation loss calculated by SEM is:

$$L_{SEM} = \begin{cases} L_{FS} + A_{SEM} + A_{ABSORB} & \text{LOS paths} \\ \min [L_{FS} + A_{SEM} + A_{ABSORB}, L_{TRO}] & \text{Beyond LOS paths} \end{cases} \quad (3-38)$$

TIREM also requires the calculation of a spherical-earth propagation loss relative to free space  $A_{SELOSS}$ .  $A_{SELOSS}$  is the appropriate loss of the following subset from Table 3-1:  $A_{FSW}$ ,  $A_{SUW}$ ,  $A_{SPLICE}$ , and  $A_{DIW}$ . Use of the theoretical space wave  $A_{SPW}$ , calculated for a smooth earth, or its upper or lower envelopes,  $A_{MAX}$  or  $A_{MIN}$ , would be inappropriate for a rough-earth model and would contribute to excessive prediction errors for LOS paths. These optional modes are therefore not used in TIREM.

Table 3-1. Summary of Spherical-Earth Propagation Formulas

Wave Type	Excess Propagation Loss	Region of Applicability	Equation in Text
Space Wave	$A_{SPW} = -20 \log   E_{SPW}/E_0  $	$D \leq d_{SPW}$	3-1
Envelope of Space Wave	$A_{MAX} = -20 \log   E_{MAX}/E_0  $ $A_{MIN} = -20 \log   E_{MIN}/E_0  $	$D \leq d_{MAX}$ $D \leq d_{MIN}$	3-14 3-15
Space Wave Approximation	$A_{FSW} = -20 \log   E_{FSW}/E_0  $	$D \leq d_{SPW}$	3-19
Surface Wave	$A_{SUW} = -20 \log   E_{SUW}/E_0  $	$D \leq d_{SUW}$	3-20
Space/Diffracted Wave Splice	$A_{SPLICE} = -20 \log   E_{SPLICE}/E_0  $	$d_{SPW} < D < d_{DIW}$	3-36
Surface/Diffracted Wave Splice		$d_{SUW} < D < d_{DIW}$	
Diffracted Wave	$A_{DIW} = -20 \log   E_{DIW}/E_0  $	$D \geq d_{DIW}$	3-25
The equations defining the distances are as follows: $d_{SPW}$ , (Equation 3-17); $d_{SUW}$ , (Equation 3-24); $d_{DIW}$ , (Equation 3-35).			

## **CHAPTER 4**

# **TERRAIN-INTEGRATED ROUGH-EARTH MODEL (TIREM)**

### **4.1 GENERAL**

The Terrain-Integrated Rough-Earth Model (TIREM) is designed for calculation of the reference basic median propagation loss (path loss) using digital terrain-elevation data (DTED) to construct the terrain profile along the great-circle path between two antennas. A combination of theoretical techniques and empirically-derived equations is used in TIREM to produce acceptable estimates of path loss over irregular terrain for most purposes. These methods are integrated formally into a TIREM module, which has been validated by comparison with measured propagation data. Statistical comparisons of predicted propagation losses with corresponding measured losses are provided in Chapter 5.

### **4.2 DIGITAL TERRAIN DATA IN PROPAGATION MODELING**

The modeling of propagation in TIREM depends on terrain-elevation information. TIREM requires a terrain profile described by a set of discrete points, the position of which is specified by a distance from the transmitter and an elevation above mean sea level. TIREM evaluates each such profile to determine whether propagation takes place over land or sea or a combination of the two. TIREM differentiates land from sea by noting that profile elevations for land are not equal to 0 while elevations for sea are equal to 0. The user-specified earth conductivity and relative permittivity are used if the path is over land and the corresponding characteristics for sea water are used if the path is over sea. These electrical characteristics for land and sea differ significantly and greatly influence the predicted propagation loss for smooth or nearly smooth surfaces.

Using effective earth radius geometry and the terrain profile, TIREM then determines whether the antenna terminals are within LOS or BLOS. This is done by calculating the slope (tangent of the elevation angle) to each profile point as measured at the transmitting antenna. The calculation is done in subroutine SLTANG, using Equation 2-19.

The process begins by assuming that the maximum slope is that of the receiving antenna (i.e., that the path is LOS). Then, the slope to each profile point between the antennas is calculated beginning at the receiver and working back to the transmitter. If the slope to the receiving antenna is greater than that to all other profile points, the path is LOS, otherwise it is BLOS.

If the path is BLOS, the profile point forming the steepest slope is recognized as the transmitter horizon. That point then becomes a beginning point of observation for the measurement of slopes to subsequent profile points. If that observation point is within LOS of the receiving antenna, the transmitter and receiver have a common horizon. If not, subsequent points with the highest elevation angles become successive points of observation (and are also identified as diffraction knife edges) until an observation point is found that is within LOS of the receiving antenna. That point is then the receiver horizon.

In the majority of cases, the required terrain information is taken from extensive coverage of level 1 digital terrain-elevation data generated by the Defense Mapping Agency (DMA).<sup>4-1</sup> DMA provides Digital Terrain-Elevation Data (DTED). The DTED level 1 format is a uniform matrix of terrain-elevation values spaced at 3 arc-second (approximately 100 m) intervals to approximate the vertical resolution of 1:250,000 scale elevation contour maps. The terrain-elevation values are not exact. The linear error in the elevation of a point with respect to mean sea level is  $\pm 30$  m; the circular error of a point in the horizontal position with respect to the World Geodetic System is 50 m (both errors are at 90-percent confidence level).

---

<sup>4-1</sup>Military Specification For Digital Terrain Elevation Data (DTED) Level 1 (1CD), MIL-D-89000, Defense Mapping Agency, Fairfax, VA, 26 February 1990.

Studies conducted at ECAC established that for the purpose of propagation modeling, thinning the data by a factor of 5 to a resolution of 15 arc seconds did not degrade any of the performance measurements considered.<sup>4-2</sup> With this 15 arc-second grid spacing, the storage requirement for the Level 1 DTED is reduced by a factor of 25 over that required for archiving the 3 arc-second resolution data provided by DMA. A further reduction of storage space by a factor of about 3:1 is effected by quantization of the elevation into 3-meter (10-foot) increments rather than the 1-meter increments of the raw Level 1 DTED. ECAC studies have shown that using the 3-meter elevation quantum does not degrade TIREM error statistics when comparing model predictions with measurements. The ECAC operational topographic data system therefore uses a 3-meter elevation quantum and a 15 arc-second spatial resolution for archiving the Level 1 DTED.

### 4.3 PROPAGATION OVER LAND

#### 4.3.1 Line-of-Sight Region

For propagation over irregular earth in the LOS region, there is coupling between the antennas because of the direct free-space wave. Also, there is a coupling path via an earth-reflected wave; however, this path may or may not be important. Unlike the LOS case discussed in the previous section for propagation over a smooth spherical earth, there generally is no broad expanse of level terrain to provide a single significant reflected wave at the receiver. Instead, the earth resembles a multi-faceted solid composed of reflecting planes of many sizes, shapes, and orientations. It is, of course, impractical to represent such an earth by a terrain profile confined to the great-circle plane, as TIREM attempts to do. For this reason, at frequencies above 20 MHz, TIREM does not attempt to predict ground-wave propagation in the manner of SEM. Instead, TIREM predicts a free-space loss unless it determines that terrain protrudes into the first Fresnel zone.

---

<sup>4-2</sup>Cameron, S. and Kuebler, W., "Digital Terrain Data in Radio Wave Propagation Predictions: An Assessment," Proc. DMA Symposium 89, DMA Systems Center, Reston, VA, 15-17 May 1989.

The first Fresnel zone is defined as the spheroid of revolution about the line joining the antennas (the direct path) such that the sum of the distances from any point on its surface to each of the antennas exceeds the direct path by exactly one-half wavelength. If sufficient penetration into the Fresnel zone region occurs, an additional space-wave reflection loss is added to the free-space loss.

Because of the requirement that the reflection point be within the first Fresnel zone, it is possible to make small grazing angle approximations without loss of validity. It is also possible to assume that the antenna gains associated with the direct and reflected field contributions within the first Fresnel zone are virtually the same. It is this concept that makes possible the calculation of the so-called basic propagation loss between isotropic antennas.

In the LOS region, the terrain intercepts a portion of the radiation emitted by a source, and part of the intercepted energy is reflected in a direction leading to a receiving point as shown in Figure 4-1. Interference then takes place between the radiation arriving via the direct ray and that arriving via the reflected ray. The space wave  $E_{SPW}$  normalized to the direct wave  $E_o$  for an irregular surface is given by:

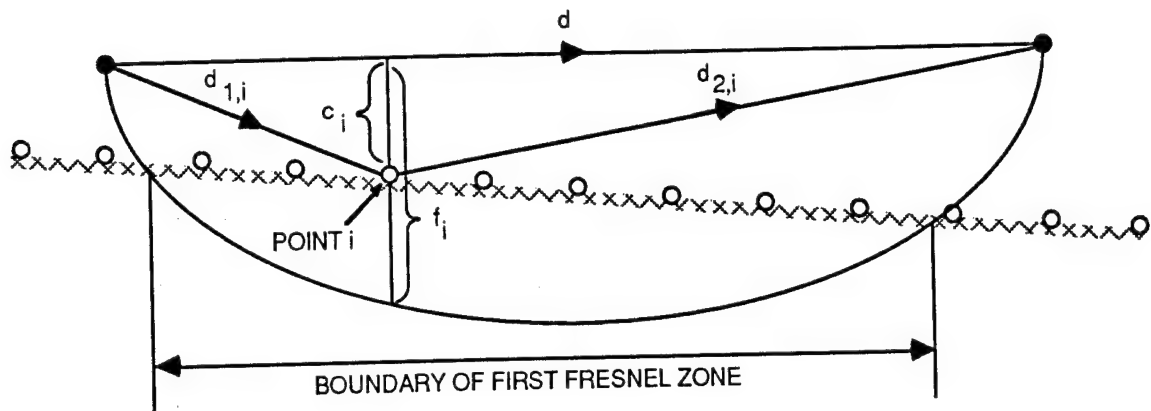
$$|E_{SPW}/E_o| = |1 + \rho_o R e^{j\Delta}| \quad (4-1)$$

This equation is the same as Equation 3-1 for the special case of  $r_1' \approx r_2'$  (when both antennas are near the ground) except that the divergence coefficient is replaced by the scattering coefficient  $\rho_o$ . This equation applies for reflection from a rough planar surface that approximates the dominant reflecting surface in irregular terrain.<sup>4-3</sup>

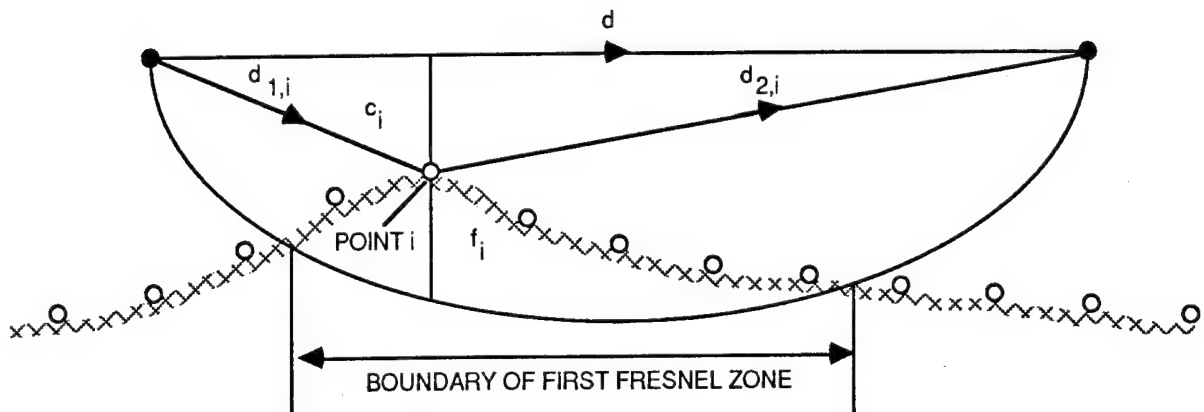
---

<sup>4-3</sup>Schelleng, J., Burrows, C., and Ferrell, E., "Ultra-Short-Wave Propagation," Proc. I.R.E., Vol. 21, No. 3., March 1933, pp 427-463.





(EXAMPLE A) INTERCEPTED BY A FLAT TERRAIN PLANE



(EXAMPLE B) INTERCEPTED BY UNDULATING TERRAIN

Figure 4-1. Geometry of the First Fresnel Zone Spheroid

In the modeling, Equation 4-1 is approximated by a first-order expansion of  $\cos \Delta$ , so that:

$$|E_{\text{SPW}}/E_o| = \sqrt{1 + \rho_o^2 - 2 \rho_o \cos \Delta} \quad (4-2a)$$

$$\approx \sqrt{(1 - \rho_o)^2 + \rho_o \Delta^2} \quad (4-2b)$$

These formulas are based on the ray representation implying that the principal part of the specularly reflected energy arises from an area near the point of reflection of the maximum terrain intrusion into the first Fresnel zone. The total reflection area, in fact, extends to an area of approximately half the area formed by the intersection of the first Fresnel zone spheroid with the terrain. Equations 4-2 are correct only for flat terrain. For undulating terrain, they must be considered as approximations. Note, however, that the space-wave formulation does not depend on the polarization of the source nor on the dielectric constant or conductivity of the terrain. The approximation given in Equation 4-2b is actually used in TIREM.

The phase factor  $\Delta$  for terrain points  $i = 1, 2, \dots$  is, as shown in Appendix D, expressed in terms of the clearance  $c_i$  and the width of the first Fresnel zone  $f_i$  as:

$$\Delta = \pi \min \left\{ (c_i/f_i)^2, \frac{1}{3} \right\} \quad (4-3a)$$

$$\approx \pi \min \left\{ (c_i/f_i)^2, \frac{1}{\pi} \right\} \quad (4-3b)$$

The approximation given in Equation 4-3b corresponds to the approximation of Equation 4-2b and is used in TIREM. The clearance  $c_i$  is the distance of the direct ray above the  $i$ -th terrain-elevation point (see Figure 4-1) and  $f_i$  is given by:

$$f_i = \sqrt{\lambda \left( \frac{1}{d_{1,i}} + \frac{1}{d_{2,i}} \right)} \quad (4-4)$$

where  $d_{1,i}$  and  $d_{2,i}$  are the direct ray distances from the  $i$ -th terrain point to the transmitter and receiver, respectively. Use of the factor  $1/\pi$  in Equation 4-3b restricts the phase factor to  $\Delta \leq 1$  so that  $E_{SPW}/E_o \leq 1$  and Equation 4-2b applies only if  $(c_i/f_i)^2 \leq 1/\pi$ . For larger clearance ratios, the substitution  $\Delta = 1$  so that  $E_{SPW}/E_o = 1$  is made, thereby replacing the oscillating lobe structure of the normalized field, Equation 4-1, by the free-space value. Refer to Appendix D and Figure D-2 for a complete explanation and an illustration of this substitution. Although the oscillating structure of the field is observed in practice when the terrain is relatively flat, modeling of the field oscillations is not advisable. The predicted oscillations are nearly always shifted with respect to the observed field and thus result in large modeling errors despite the fact that the oscillating characteristic of the field is preserved. Consequently, it proved both practical and expedient in modeling to eliminate the oscillation. Equation 4-3b also implies that the clearance  $c_i = f_i/\sqrt{\pi} \approx 0.56 f_i$  (the terrain effects on the propagating wave are restricted to clearances well within the first Fresnel zone).

The reflection coefficient  $R$  (given by Equations 3-10 and 3-11) is very nearly -1 regardless of polarization when the angle between the reflected ray and the ground is small, such as is the case when the reflecting terrain points are well within the first Fresnel zone. The scattering coefficient  $\rho_o$  represents the effects of the irregularities of the ground, and a mean value has been established empirically from measured propagation data and depends upon the wavelength  $\lambda$  as:

$$\rho_o = e^{-\lambda_o/\lambda}, \quad (4-5)$$

with  $\lambda_o \approx 0.02$  meters.

The loss relative to free space due to the reflected ray  $A_{\text{REF}}$  is evaluated in subroutine RFLECT and is:

$$\begin{aligned} A_{\text{REF}} &= -20 \log(|E_{\text{SPW}}/E_o|) \\ &= -10 \log [(1 - \rho_o)^2 + \rho_o \Delta^2] \end{aligned} \quad (4-6)$$

At grazing incidence, where the phase factor  $\Delta$  is zero, Equation 4-6 is expressed as:

$$A_o = A_{\text{REF}} (\Delta = 0) = -20 \log (1 - \rho_o) \quad (4-7)$$

The above formulation accounts for the space-wave part of the LOS field contribution. For frequencies below approximately 20 MHz where the wavelength is 15 meters or more, moderate terrain irregularities become less important and it is reasonable to approximate LOS propagation using the space- and surface-wave formulations described in the previous section for propagation over a spherical earth. This is done in TIREM by employing the spherical-earth algorithms exclusively for frequencies below 16 MHz and by combining the spherical-earth loss and reflection loss by linear interpolation for frequencies between 16 and 20 MHz.

The surface-wave field contribution is estimated through the field calculation based on a spherical earth (no simple method exists to derive the surface-wave field in the presence of terrain features) and is given by Equation 3-20. The surface-wave calculation is part of subroutine SEARTH (refer to paragraph 3.5 and Table 3-1), resulting in a loss relative to free space  $A_{\text{SELOSS}}$ , and depends on antenna heights, distance, and dielectric constant and conductivity of the terrain.

The LOS loss relative to free space is then estimated to be:

$$A_{\text{LOS}} = \begin{cases} \min (A_{\text{SELOSS}}, A_{\text{REF}}) & f_{\text{MHz}} < 16 \\ \min [\alpha A_{\text{SELOSS}} + (1-\alpha) A_{\text{REF}}, A_{\text{REF}}] & 16 \leq f_{\text{MHz}} \leq 20 \\ A_{\text{REF}} & f_{\text{MHz}} > 20 \end{cases} \quad (4-8)$$

where

$$\alpha = 5 - f_{\text{MHz}}/4 \quad (4-9)$$

#### 4.3.2 Diffracting Region

In the region where the radiation emitted by a source is diffracted by prominent terrain features such as hills, these features are modeled as ideal knife-edges. Reflection may also be present. Figure 4-2 shows the situation where the field is diffracted by  $k$  ridges. In this figure, the terminating points (transmitting and receiving antennas) are represented by darkened circles and the diffracting points by open circles. For  $k$  knife edges the field intensity  $E_{\text{DIF}}$  normalized to the free-space intensity is:

$$|E_{\text{DIF}}/E_0| = \alpha_{1,k} \left( \prod_k F_k \right) \alpha_{2,k} \quad (4-10)$$

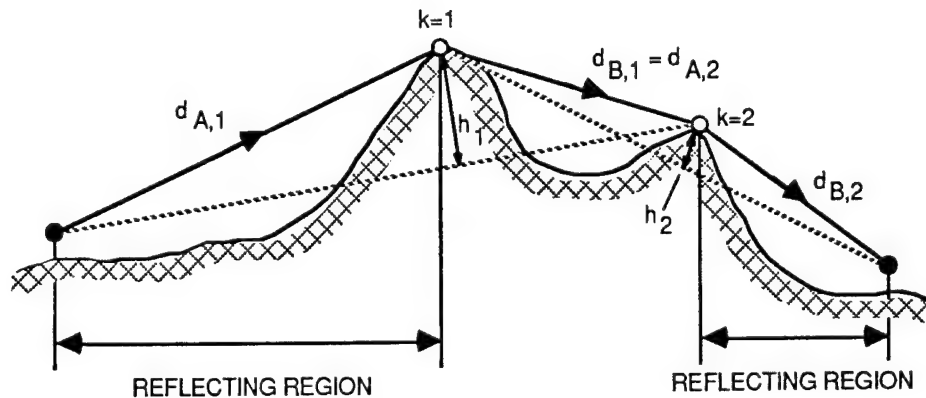


Figure 4-2. Diffraction Over Two Knife Edges, Epstein-Peterson Construction

The knife-edge diffraction term  $F_k$  for each knife edge is the magnitude of the Fresnel integral:

$$F_k = \left| \int_{\sqrt{2u_k}}^{\infty} e^{-j\pi u^2} du \right| = \begin{cases} \frac{1}{2} \exp(-\sqrt{2} u_k + 0.252 u_k^2) & 0 \leq u_k < 1.8 \\ \frac{1}{2\pi u_k} & u_k \geq 1.8 \end{cases} \quad (4-11)$$

The Fresnel integral in Equation 4-11 is approximated in subroutine SKEDIF by a convenient curve fit for values of  $u_k$  between 0 and 1.8 and by its asymptotic value for  $u_k \geq 1.8$ . The dimensionless parameter  $u_k$  is given by:

$$u_k = h_k / f_k \quad (4-12)$$

where  $h_k$  is the "height" of the  $k$ -th knife edge as shown in Figure 4-2 and:

$$f_k = \sqrt{\lambda \left( \frac{1}{d_{A,k}} + \frac{1}{d_{B,k}} \right)} \quad (4-13)$$

is the radius of the first Fresnel spheroid at the  $k$ -th knife edge, and  $d_{A,k}$  and  $d_{B,k}$  are the separation distances. The parameter  $u_k$  is related to the frequently used parameter  $v$  by  $v = \sqrt{2} u_k$  (Reference 1-4, p. 7-1).

For a single ridge where  $k = 1$ , Equation 4-10 reduces to an approximation for the four-ray expression given first by Bullington.<sup>4-4</sup> The diffracting ridge is treated as a knife edge, and reflection can occur in the reflecting regions between the transmitting point and the ridge and

---

<sup>4-4</sup>Radio Wave Propagation: Consolidated Summary Technical Report of the Committee on Propagation of the National Defense Research Committee, Academic Press, New York, NY, 1949, p. 69.

between the ridge and the receiving point.<sup>4-5</sup> For more than one ridge, Equation 4-10 incorporates the extended Epstein-Peterson method<sup>4-6</sup> wherein the first ridge is treated as the source illuminating the second ridge, etc. Terrain effects between the ridges are not taken into account; hence, only the region preceding the first peak and the region following the last peak are considered reflecting regions. The contributions  $\alpha_{1,k}$  and  $\alpha_{2,k}$  of the reflecting regions result from the phase shifts in the rays due to specular reflection and are expressed as in the LOS case, Equation 4-2b, by:

$$\alpha_{1,k} = \sqrt{(1 - \rho_k)^2 + \rho_k \Delta_1^2} \quad (4-14)$$

$$\alpha_{2,k} = \sqrt{(1 - \rho_k)^2 + \rho_k \Delta_2^2} \quad (4-15)$$

The phase factors  $\Delta_1$  and  $\Delta_2$  for the two reflecting regions are evaluated as in Equation 4-3b. The mean scattering coefficient  $\rho_k$  is empirically determined from measured propagation data and has the same wavelength dependence as in the LOS case. The coefficient  $\rho_k$  reduces to the LOS case, Equation 4-5, for  $k = 0$ , and is given by:

$$\rho_k = e^{-(k+1)\lambda_o/\lambda} \quad (4-16)$$

From an examination of the terrain profiles where diffraction takes place, and associated measured propagation data, it appears that the reflecting regions are not on, or near, the slopes leading to the point of diffraction. Hence, those terrain points within 5 percent of the distance from the ridge to the terminal point are excluded from the calculation of  $\Delta_1$  and  $\Delta_2$ . It is also evident that

<sup>4-5</sup>Crysdale, J. H., "Large Reduction of VHF Transmission Loss and Fading by the Presence of a Mountain Obstacle in Beyond-Line-of-Sight Paths," Proc. IRE, Vol. 43, No. 5, May 1955, p. 627.

<sup>4-6</sup>Epstein, J. and Peterson, D. W., "An Experimental Study of Wave Propagation at 850 MC," Proc. IRE, Vol. 41, No. 5, May 1953, pp. 595-611.

such a restriction is required. Otherwise,  $\alpha_{1,k}$  and  $\alpha_{2,k}$  would always be evaluated by their limiting value  $\Delta_1 = \Delta_2 = 0$  because points close to the ridge obstruct the clearance.

Extensive evaluation of predictions using Equation 4-10 versus measured propagation data showed that the best results were obtained by limiting the specular reflection to the one region for which the effect of the phase relations between  $\alpha_{1,k}$ ,  $\alpha_{2,k}$ , and  $F_k$  is to reduce the received field intensity the most. In the modeling, therefore, Equation 4-10 is replaced by:

$$|E_{DIF}/E_o| = \min(\alpha_{1,k}, \alpha_{2,k}) (\prod_k F_k) \quad (4-17)$$

It is noted that the above knife-edge diffraction equation is independent of the conductivity and dielectric constant of the terrain. The equation is applicable for frequencies greater than 20 MHz and is evaluated in subroutine DIF. The result is the knife-edge diffraction loss above free space  $A_{KNIFE}$ :

$$\begin{aligned} A_{KNIFE} &= -20 \log(|E_{DIF}/E_o|) \\ &= \max(A_{1,k}, A_{2,k}) + \sum_k A_{F,k} \end{aligned} \quad (4-18)$$

where

$$A_{1,k} = -20 \log \alpha_{1,k} \quad (4-19)$$

$$A_{2,k} = -20 \log \alpha_{2,k} \quad (4-20)$$

$$A_{F,k} = -20 \log F_k \quad (4-21)$$



At grazing incidence, where the phase factors  $\Delta_1$  or  $\Delta_2$  are zero, Equations 4-19 and 4-20 are identical, and using Equations 4-14 and 4-15 may be expressed as:

$$A_k = \alpha_{1,k} (\Delta_1 = 0) = \alpha_{2,k} (\Delta_2 = 0) = -20 \log (1 - \rho_k) \quad (4-22)$$

As in the LOS case, the excess loss defined above for grazing incidence  $A_k$  is required in paragraph 4.3 for land/sea propagation. Moreover for  $k = 0$ , this definition agrees with Equation 4-7.

The diffraction loss is as given by  $A_{\text{KNIFE}}$  except for terrain features approaching the smoothness of a spherical earth. The modeling in such a case would detect a knife edge at every terrain point resulting in unreasonable high-loss values, as every diffraction point would result in a loss of at least 6 dB. Consequently, if there are more than two knife edges, an average knife-edge loss value of  $\bar{A}_{\text{KE}}$  is calculated by:

$$\bar{A}_{\text{KE}} = \frac{1}{k} \Sigma A_{\text{F},k} \quad (4-23)$$

The diffraction loss for 20 MHz and above is given by:

$$A_{\text{DIF,VHF}} = \begin{cases} \min(A_{\text{SELOSS}}, A_{\text{KNIFE}}) & k \geq 3 \text{ and } \bar{A}_{\text{KE}} \leq 7\text{dB} \\ A_{\text{KNIFE}} & k < 3 \text{ or } \bar{A}_{\text{KE}} > 7\text{dB} \end{cases} \quad (4-24)$$

where  $\bar{A}_{\text{KE}} = 7$  dB is an empirically established transition value.  $A_{\text{SELOSS}}$  is the spherical-earth estimate of the surface-wave and diffracted-wave contribution and depends on the relative permittivity and conductivity of the terrain.  $A_{\text{SELOSS}}$  is evaluated in subroutine SEARTH (refer to paragraph 3.5 and Table 3-1). If there are fewer than three knife edges, the diffraction loss is simply  $A_{\text{KNIFE}}$ .

For frequencies less than 16 MHz, the diffraction loss can be estimated by the spherical-earth loss, as shown in the statistics in Chapter 5. Hence, for frequencies from 1 through 16 MHz:

$$A_{\text{DIF,HF}} = A_{\text{SELOSS}} \quad f_{\text{MHz}} \leq 16 \quad (4-25)$$

The loss for the intermediate frequency region  $16 < f_{\text{MHz}} \leq 20$  is calculated by a linear interpolation:

$$A_{\text{DIF},\alpha} = \alpha A_{\text{DIF,HF}} + (1 - \alpha) A_{\text{DIF,VHF}} \quad (4-26)$$

where  $\alpha$  is given by Equation 4-9.

#### 4.3.3 Summary of Land Propagation Formulas

The path loss predicted by TIREM consists of the appropriate loss terms defined in Chapter 2 and paragraph 4.3 of this handbook and depends on whether the path is LOS or BLOS. For a BLOS path, the total loss for both diffraction and troposcatter are calculated and the dominant coupling (minimum of the two path losses) is assumed to prevail. The total terrain-dependent propagation loss for LOS and BLOS paths is:

$$L_{\text{TIREM}} = \begin{cases} L_{\text{FS}} + A_{\text{LOS}} + A_{\text{ABSORB}} & \text{LOS} \\ \min (L_{\text{FS}} + A_{\text{DIF}} + A_{\text{ABSORB}}, L_{\text{TRO}} + A_{\text{ABSORB}}) & \text{BLOS} \end{cases} \quad (4-27)$$

The excess propagation loss as obtained from the normalized fields for LOS or diffraction is shown in Table 4-1.  $A_{\text{LOS}}$  is the appropriate excess loss for line-of-sight as determined by the frequency.  $A_{\text{DIF}}$  is the appropriate excess loss for the diffracting region.  $A_{\text{ABSORB}}$  is the molecular absorption loss calculated by Equation 2-14 as appropriate for each case shown in Figure 2-3. The

LOS, knife-edge-diffracted, and spherical-earth-diffracted propagation losses are calculated in subroutines TIRLOS, DIF, and SEARTH, respectively. The troposcatter loss  $L_{TRO}$  is calculated using Equation 2-15. The troposcatter loss is calculated in subroutine TROPSC.

Table 4-1. Summary of Terrain-Dependent Propagation Formulas for LOS or Diffraction

Region	Excess Propagation Loss	Limits	Equation in Text
Line-of-sight	$A_{LOS} = \begin{cases} \min (A_{SELOSS}, A_{REF}) \\ \min [\alpha A_{SELOSS} + (1-\alpha) A_{REF}, A_{REF}] \\ A_{REF} \end{cases}$	$f \text{ MHz} < 16$ $16 \leq f \text{ MHz} \leq 20$ $f \text{ MHz} > 20$	4-8
	$A_{REF} = -20 \log ( E_{SPW}/E_o )$	-	4-6
	$A_{SELOSS}$ from Table 3-1	-	-
Diffracting	$A_{DIF,HF} = A_{SELOSS}$	$f_{MHz} \leq 16$	4-25
	$A_{DIF,\alpha} = \alpha A_{DIF,HF} + (1 - \alpha) A_{DIF,VHF}$	$16 < f_{MHz} \leq 20$	4-26
	$A_{DIF,VHF} = \begin{cases} \min (A_{SELOSS}, A_{KNIFE}) \\ A_{KNIFE} \end{cases}$	$k \geq 3$ and $\bar{A}_{KE} \leq 7 \text{ dB}$ $f_{MHz} > 20$	4-24
		$k < 3$ or $\bar{A}_{KE} > 7 \text{ dB}$ $f_{MHz} > 20$	
	$A_{SELOSS}$ from Table 3-1	-	-
	$\alpha = -1/4 f_{MHz} + 5$	-	4-9
	$A_{KNIFE} = -20 \log ( E_{DIF}/E_o )$	-	4-18
	$\bar{A}_{KE} = 1/k \Sigma A_{F,k}$	-	4-23

The formulas pertaining to propagation loss estimates over terrain are semi-empirical and involve certain assumptions and approximations. The major empirical points are summarized here.

- The terrain-reflected energy is assumed to emanate from a region surrounding the terrain point for which the ratio of clearance to the radius of the first Fresnel zone ellipsoid is a minimum. Actually, the region formed by the intersection of the first Fresnel zone ellipsoid with the terrain plane contributes to the reflected energy. For low antennas, this region is virtually all the terrain between transmitting and receiving points, including terrain on both sides of the great circle plane. Such transverse terrain is not considered in TIREM.
- The mean scattering coefficient (Equations 4-5 and 4-16) is empirically determined from available measurements, regardless of the attributes of the terrain at the various measurement locations.
- When taken into account, the surface-wave contribution within LOS is derived from a flat earth.
- In the diffracted region, each peak is assumed to be a ridge and is treated as an ideal knife-edge, regardless of the appearance of the peak. For one knife-edge, the diffraction loss calculated is rigorous. For more than one knife-edge, the method where the first knife-edge is treated as a source illuminating the second knife-edge is an expedient approximation.<sup>4-7,4-8</sup> The case where the ridges are of equal elevation (as would be the situation for plain-like areas, where each terrain point acts as a ridge and contributes about 6 dB loss) is the worst situation. A more rigorous analysis shows that the loss contribution diminishes as the number of ridges increases.<sup>4-9</sup>

---

<sup>4-7</sup>Millington, G., Hewitt, R., and Immirzi, F. S., "Double Knife-Edge Diffraction in Field-Strength Predictions," IEE Monograph, No. 5073, March 1962, pp. 419-429.

<sup>4-8</sup>Pogorzelski, R. J., "A Note on Some Common Diffraction Link Loss Models," Radio Science, Vol. 17, No. 6, Nov. - Dec. 1982, pp. 1536-1540.

<sup>4-9</sup>Vogler, L. E., "An Attenuation Function for Multiple Knife-edge Diffraction," Radio Science, Vol. 17, No. 6, 1982, pp. 1541-1546.

- The loss at lower frequencies,  $\leq 16$  MHz, is derived from a spherical earth regardless of the terrain features.

#### 4.4 PROPAGATION OVER LAND/SEA

Although TIREM is intended primarily for evaluation of the path loss over rough earth surfaces, there may be situations where path loss estimates are needed for paths that consist of alternate segments of land and sea. For example, a path across a bay or along a chain of islands may require the calculation and combining of diffraction losses due to both knife-edge and spherical-earth diffraction.

Whenever any segment of a propagation path passes over sea water, the land/sea propagation loss is estimated. The land/sea loss calculation is an algorithm that provides a weighted combination of the rough-earth formulation, described in paragraph 4.3, with the spherical-earth method, taken from Chapter 3. The presence of sea water in the path profile is recognized during the profile examination process by observing that points having zero elevations are sea water. Although it is realized that occasional points with zero elevations may be present when a profile extends into regions of below-sea-level land, a sequence of profile points must represent at least 1 percent of the path before it is regarded as sea.

Propagation over land/sea implies that the propagation path traverses both irregular terrain over land and the spherical-earth surface representing the sea; antennas may be on land or at sea. Millington<sup>4-10</sup> formulated a semi-heuristic method based on modeling both land and sea as a spherical earth. Millington's method successfully predicts the so-called recovery effect that is observed when the received field strength increases as the antenna moves from land to sea. This effect is shown in Figure 4-3 by measurements for a land/sea path at a low frequency of 3.13 MHz. Measurements made over land are shown with the symbol + and over-sea measurements are shown as ○ or ×. For irregular terrain, Millington's technique does not apply and a practical field determination is

---

<sup>4-10</sup>Millington, M. A., and Isted, G. A., "Ground Wave Propagation Over An Inhomogeneous Smooth Earth, Part 2: Experimental Evidence and Practical Implications," Proc. IEE, Vol. 97, Part III, No. 48, July 1950, pp. 209-217.

made in TIREM using weighting factors. The use of weighting factors is described in paragraph 4.4.1. Both techniques predict a recovery effect and are compared in Figure 4-3 for Millington's measured data.

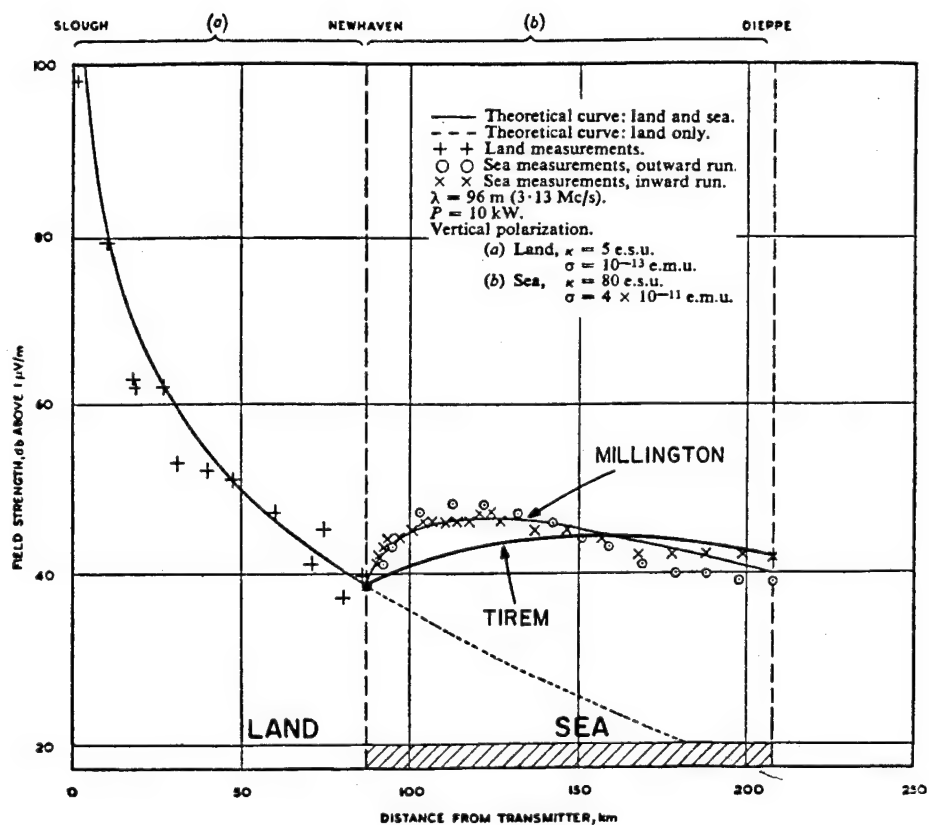


Figure 4-3. Comparison of Millington's Method and Results Derived Using Weighting Factors With Measurements (From Reference 4-10)

#### 4.4.1 Weighting Factors

Whenever any part of a propagation path passes over sea water, the land/sea propagation loss is estimated as a weighted combination of the propagation loss for the irregular terrain over land and the spherical-earth propagation loss for the sea. The propagation loss for land segments is calculated by the appropriate formula from Table 4-1, and the loss for sea segments is taken from Table 3-1. Land/sea paths are subdivided into three basic path segments as will be discussed in paragraphs 4.4.2.1, 4.4.2.2, and 4.4.2.3.

For each path segment, the land/sea weighting factors  $l$  and  $s$  are the ratios:

$$l = d_{\text{LAND}}/D \quad (4-28)$$

$$s = d_{\text{SEA}}/D \quad (4-29)$$

so that

$$s + l = 1 \quad (4-30)$$

and where  $d_{\text{LAND}}$  and  $d_{\text{SEA}}$  are the sums of the great-circle distances over land and sea, respectively, and  $d$  is the great-circle distance of the path segment.

The land/sea weighting factors for the total path consisting of all path segments are similarly defined, with  $L$ ,  $S$ ,  $D$ ,  $D_{\text{LAND}}$ , and  $D_{\text{SEA}}$  replacing  $l$ ,  $s$ ,  $d$ ,  $d_{\text{LAND}}$ , and  $d_{\text{SEA}}$ , respectively, in Equations 4-28 through 4-30.

Also required are weighting factors  $p$  and  $q$  for a transition from the sea-diffracted path section to a LOS path section, given as:

$$p = 1 - q \quad (4-31)$$

$$q = \frac{d_0}{2d - d_0} \quad (4-32)$$

where  $d_0$  is the great-circle distance of the sea-diffracted arc of the segment, and  $d$  is again the great-circle distance of the path segment. The coefficients,  $p$  and  $q$ , serve to impose a smooth transition between spherical-earth LOS and diffraction losses as the direct ray just grazes the surface of the sea.

#### 4.4.2 Propagation Formulas for Land/Sea Profiles

The land/sea losses are heuristically formulated and are expressed as excess propagation losses relative to free space. The presence of sea water in the terrain profile is recognized by zero elevations. Losses for path segments over sea water are calculated using the spherical-earth formulation discussed in Chapter 3. For BLOS propagation paths leading over islands with diffracting peaks, the losses are calculated in analogy to the Epstein-Peterson method in that the total loss is the sum of the partial diffracting losses. The partial losses are spherical-earth and knife-edge losses of a particular segment of a propagation path. For paths undergoing more than one diffraction, the spherical-earth propagation loss between the transmitting and receiving point is also calculated and compared with the loss derived from the extended Epstein-Peterson method to select the minimum path loss.

A number of frequently recurring quantities are required to describe the propagation formulations; they are defined in Table 4-2. The excess loss calculations for a given frequency are dependent on the elevation, antenna height, and distance. The land/sea loss representations are, for



example, of the form  $A_{SEA}(e, D)$ , implying that the spherical-earth propagation loss is evaluated with the dielectric constant and conductivity of sea water, with both antenna heights  $e$  (= elevation + actual antenna height) and with  $D$  (= distance) as parameters. The formulations for the over-sea cases are given below. These formulations are implemented in subroutine TIRLOS for LOS land/sea paths and in subroutine DIF for BLOS land/sea paths.

Table 4-2. Land/Sea Definitions

$A_{SELOSS}$ :	Spherical-earth loss above free space with given $\epsilon$ and $\sigma$ for land
$A_{SEA}$ :	Spherical-earth loss above free space with $\epsilon = 81, \sigma = 4 \text{ S/m}$
$A_k$ :	Reflection loss at grazing incidence (Equation 4-22)
$A_{F,k}$ :	Knife-edge diffraction loss only (Equation 4-21)
$A_{l,k}$ :	Reflection loss (Equation 4-19 for $k$ knife edges)
$h$ :	Antenna height
$e$ :	Elevation above MSL + antenna height
$d, D$ :	Great circle distances*
$\bar{d}, \bar{D}$ :	Linear distances*
$l, L$ :	Land weighting factors (Equation 4-28)*
$s, S$ :	Sea weighting factor (Equation 4-29)*
$p, q$ :	Weighting factors (Equations 4-31 and 4-32)
*Lower-case letters apply to path segments, capital letters apply to entire path.	

#### 4.4.2.1 Line-of-Sight Land/Sea Path

In the following figures, the terminating antennas are represented by darkened circles and the diffracting points are represented by open circles. For a LOS land/sea path (where the path segment represents the total path, Figure 4-4), the excess propagation loss  $A_{L/S,LOS}$  is a weighted combination of the spherical-earth loss over a smooth sea surface and the appropriate loss for propagation over the land.

$$A_{L/S,LOS} = S A_{SEA}(e,D) + L A_{LOS}(h,D) \quad (4-33)$$

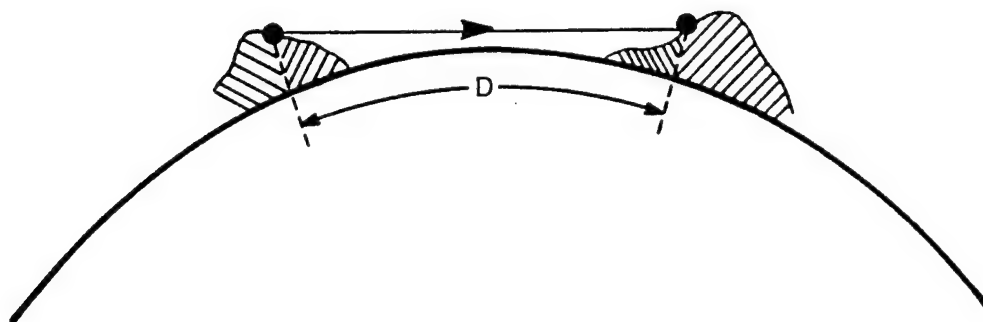


Figure 4-4. Line-of-Sight Land/Sea Path

If the frequency is below 16 MHz, the spherical-earth model is applicable for both the sea and land portions of the path. Therefore, in this case  $A_{L/S,LOS}$  is simply the weighted combination of spherical-earth losses for an all-sea and an all-land path. Ground constants appropriate for sea water and antenna heights above sea level are used when the loss is calculated for an all-sea path. However, the user-specified ground constants for land and antenna heights measured above ground level are used when the loss is calculated for an all-land path.

$$A_{L/S,LOS} = S A_{SEA}(e,D) + L A_{SELOSS}(h,D) \quad f < 16 \text{ MHz} \quad (4-34)$$

On the other hand, if the frequency is above 20 MHz, the over-land contribution is simply the reflection loss  $A_{REF}$  as calculated by Equation 4-6, and the LOS land/sea loss is:

$$A_{L/S,LOS} = S A_{SEA}(e,D) + L(h,D) \quad f > 20 \text{ MHz} \quad (4-35)$$

At grazing distance  $D = D_{GR}$ , where by Equation 4-7  $A_{REF} = A_o$ , the above equation becomes:

$$A_{L/S,LOS} = S A_{SEA}(e,D_{GR}) + L A_o \quad f > 20 \text{ MHz} \quad (4-36)$$

For frequencies between 16 and 20 MHz inclusive, the over-land loss is interpolated by frequency using the spherical-earth and reflection loss algorithms. The interpolation coefficient  $\alpha$  is calculated as in Equation 4-9.

$$A_{L/S,LOS} = S A_{SEA}(e,D) + L [\alpha A_{SELOSS}(h,D) + (1-\alpha) A_{REF}(h,D)] \quad (4-37)$$

$$16 \leq f \leq 20 \text{ MHz}$$

#### 4.4.2.2 Land/Sea Path Diffracted Over Sea Only

For a land/sea path with the diffracting part of the path over sea only (see Figure 4-5), the formulation is identical with Equation 4-34 when the frequency is below 16 MHz:

$$A_{L/S,SELOSS} = S A_{SEA}(e,D) + L A_{SELOSS}(h,D) \quad f < 16 \text{ MHz} \quad (4-38)$$

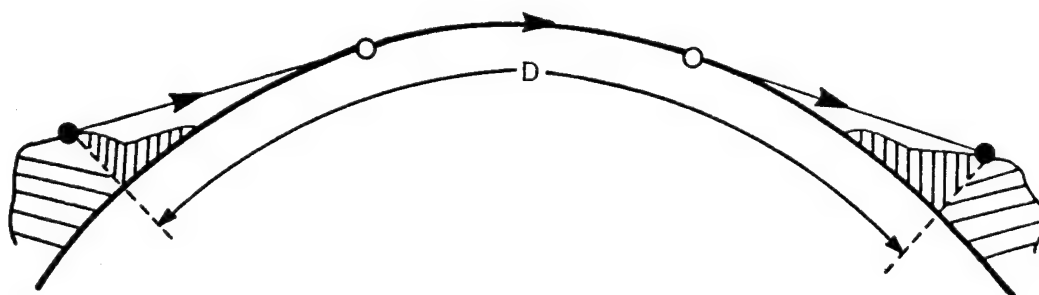


Figure 4-5. Land/Sea Path Diffracted Over Sea Only

If the frequency is above 20 MHz, the formulation is:

$$A_{L/S,SELOSS} = S A_{SEA}(e,D) + L [p A_o + q A_{SELOSS}(h,D)] \quad f > 20 \text{ MHz} \quad (4-39)$$

At grazing distance  $D = D_{GR}$ , where  $d_o = 0$  and hence  $p = 1$ ,  $q = 0$  the above equation becomes:

$$A_{L/S,SELOSS} = S A_{SEA}(e,D_{GR}) + L A_o \quad f > 20 \text{ MHz} \quad (4-40)$$

Equation 4-40 is identical with Equation 4-36, so that there is a smooth transition between LOS and diffraction.

For frequencies between 16 and 20 MHz inclusive, the over-land portion of the loss is interpolated by frequency using the spherical-earth and reflection loss algorithms. The interpolation coefficient  $\alpha$  is again calculated as in Equation 4-9.

$$A_{L/S,SELOSS} = A_{SEA}(e,D) + L [(p\alpha + q)A_{SELOSS}(h,D) + p(1-\alpha)A_o] \quad (4-41)$$

$$16 \leq f \leq 20 \text{ MHz}$$

Equation 4-37 also becomes identical to the above equation at grazing distance when  $p = 1$ ,  $q = 0$ , and  $A_{REF} = A_o$ . Furthermore, Equation 4-41 reverts to Equation 4-38 when  $f = 16 \text{ MHz}$  ( $\alpha = 1$ ) and to Equation 4-39 when  $f = 20 \text{ MHz}$  ( $\alpha = 0$ ). These methods assure a smooth loss transition between LOS and diffraction over sea and between appropriate loss algorithms in the transition frequency range.

#### 4.4.2.3 Land/Sea Path With Knife-Edge and Sea Diffraction

All other land/sea path configurations are obtained by cascading the path segments displayed in Figure 4-6 with land segments having no over-water diffraction in various combinations. These paths always consist of a sea-diffracted path segment followed (or preceded) by at least one knife-edge diffraction. The partial losses of these subpath segments are added in a manner analogous to the extended Epstein-Peterson method for knife edges over land. Let this excess loss (relative to free space) be designated  $A_{\text{MIXED}}$ . The total excess path loss is then expressed as:

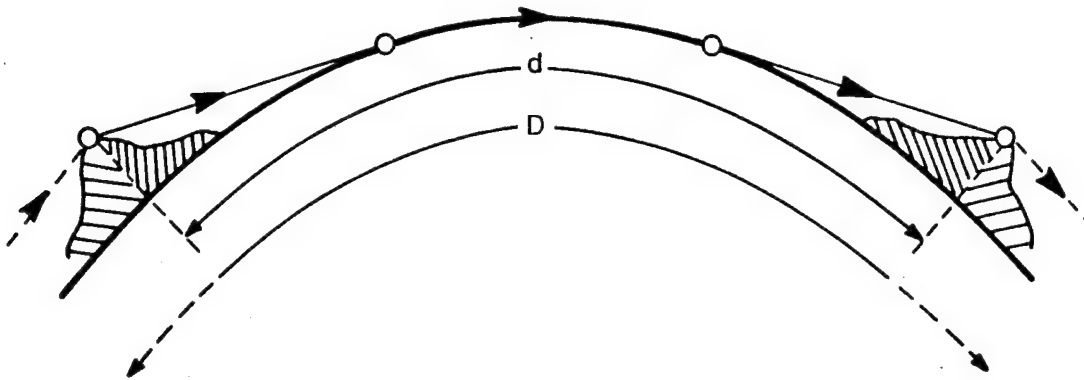
$$A_{L/S, \text{MIXED}} = \min \{ [S A_{\text{SEA}}(e, D) + L A_{\text{SELOSS}}(h, D)], A_{\text{MIXED}} \} \quad (4-42)$$

The term in the square brackets represents the estimated loss of the total path over a spherical earth, weighted by the ratios  $L$  and  $S$ . This term tends to predominate at HF frequencies and below, when the antennas are low to the ground, or the path passes predominately over sea.

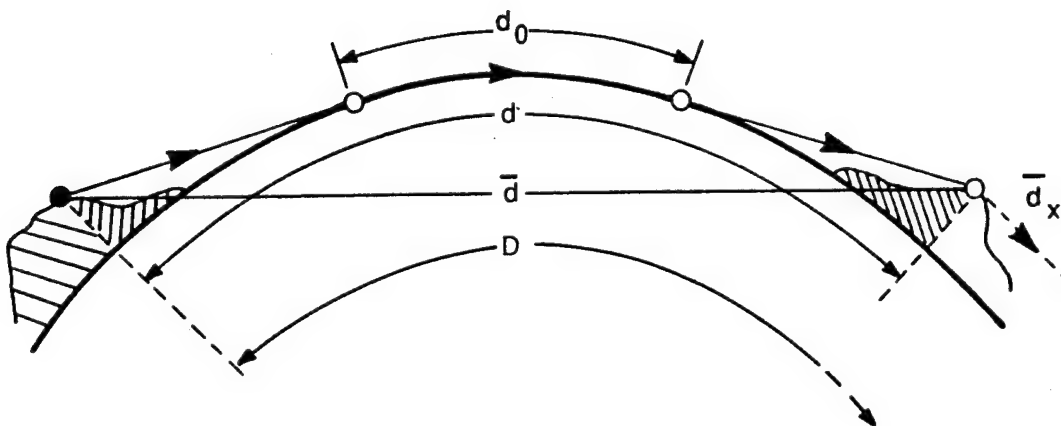
The term  $A_{\text{MIXED}}$  also estimates the loss for the total path but combines the losses attributable to a mixture of path segments where either knife-edge diffraction over land or spherical-earth diffraction over sea occurs. This mixed loss tends to predominate when the surface wave terms of the spherical-earth loss become negligible such as for high antennas, essentially over-land paths, or frequencies at VHF or above. The BLOS path is divided into segments, each of which includes either a single over-sea diffraction, or one or more land knife-edges not interrupted by over sea-diffraction. The end points for each segment are defined by the land knife edges adjacent to each arc of sea water where diffraction takes place (see Figure 4-6 for examples).

Three cases of paths involving over-sea diffraction are examined by TIREM. These are:

- Case 1 - both transmitter and the receiver horizons are land (both end segments are land)
- Case 2 - only one end-segment of the total path is diffracting over sea
- Case 3 - both end-segments of the total path are diffracting over sea.



(EXAMPLE A) SUBSEGMENT DIFFRACTING OVER SEA BETWEEN TWO DIFFRACTING PEAKS



(EXAMPLE B) END SEGMENT DIFFRACTING OVER SEA

Figure 4-6. Land/Sea Path Segments

The first case is simply an extension of the method described in paragraph 4.2.2 for diffraction over an all-land path with  $k$  knife edges. The method sums the individual losses for the  $k$  knife edges using the extended Epstein-Peterson method and accounts for the reflection losses in the foregrounds of the transmitting and receiving antennas by adding the greater of these two losses (Equation 4-18). This procedure is further extended for land/sea paths to incorporate any additional losses due to segments with spherical-earth diffraction that may be distributed among the knife edges. Each such subsegment is bounded by its adjacent knife edges and appears as in Figure 4-6, example A. The added loss for each such subsegment  $A_{SUB}$  is:

$$A_{SUB} = s A_{SEA}(e,D) + l A_{SELOSS}(h,D) \quad (4-43)$$

where the weighting coefficients  $s$  and  $l$  are the respective fractions of sea and land along the profile of each such subsegment.  $A_{MIXED}$  for this first case is then simply the combined knife-edge diffraction losses  $A_{KNIFE}$  plus the sum of the  $A_{SUB}$  losses:

$$A_{MIXED} = \max(A_{1,k}, A_{2,k}) + \sum_k A_{F,k} + \sum A_{SUB} \quad (4-44)$$

If one or both end segments involve diffraction over sea (cases 2 or 3), these end segments are treated much like the land/sea diffraction path discussed in paragraph 4.4.2.2. This treatment of the end segments having spherical-earth diffraction is necessary to ensure a smooth transition between LOS and diffraction, to employ an appropriate reflection term, and to define the geometry for the knife edge that bounds such a segment.

For example, if only one end segment is diffracting over sea (case 2),  $A_{MIXED}$  is given by the sum of the excess losses for knife-edge diffraction (including the first knife edge that defines the limit of the end segment), the sum of the  $A_{SUB}$  losses for any sea-diffracted subsegments along the path, and a term  $A_{ONE}$  that accounts for reflection and spherical-earth diffraction within the end segment.

$$A_{MIXED} = [A_{F,1}(\bar{d}, \bar{d}_x) + \sum_{k \geq 2} A_{F,k}] + A_{SUB} + A_{ONE} \quad (4-45)$$

In the above equation:

$$A_{\text{ONE}} = \min \{ [A_{1,k}(\bar{d}) + p A_k], A_k \} + q[s A_{\text{SEA}}(e,d) + l A_{\text{SELOSS}}(h,d)] \quad (4-46)$$

estimates the losses over the sea-diffracting end segment. The term in the square brackets of Equation 4-45 is the sum of all the knife-edge losses for the path. The first term, for the first knife edge, shows explicitly the distances  $\bar{d}$  and  $\bar{d}_x$  that are illustrated in Figure 4-6, example B. The distance  $\bar{d}_x$  can be the distance to the next knife edge or the distance to the terminating point. For grazing incidence, where  $p = 1$ ,  $q = 0$ ,  $A_{\text{ONE}}$  reduces to  $A_k$  so that:

$$A_{\text{MIXED}} = \sum_k A_{F,k} + A_k \quad (4-47)$$

The result is the same as that obtained when the over-sea path is considered as an all-land path at grazing. (When  $\bar{d}$  of Figure 4-6, example A, is above grazing, the configuration is evaluated as an all-land path with at least one knife-edge diffraction).

If both end segments are diffracting over sea (case 3),  $A_{\text{MIXED}}$  is given by:

$$A_{\text{MIXED}} = \sum_k A_{F,k} + \sum A_{\text{SUB}} + A_{\text{TWO}} \quad (4-48)$$



$A_{F,k}$  is again the diffracting loss due to the  $k$ -th knife edge, and  $A_{TWO}$  is:

$$\begin{aligned}
 A_{TWO} = & \min \{ (p_1 + p_2) A_k, A_k \} \\
 & + q_1 [s_1 A_{SEA}(e_1, d_1) + l_1 A_{SELOSS}(h_1, d_1)] \\
 & + q_2 [s_2 A_{SEA}(e_2, d_2) + l_2 A_{SELOSS}(h_2, d_2)]
 \end{aligned} \quad (4-49)$$

The indices 1 and 2 on  $p$ ,  $q$ ,  $s$ ,  $l$ ,  $e$  and  $d$  refer to the geometry of the two end segments each of the type displayed in Figure 4-6, example B.

The example shown in Figure 4-7 demonstrates the cascading of the subpath losses. Two diffracting peaks ( $k = 2$ ) are between two terminating over-sea diffracting paths. There is no over-sea diffraction between two diffracting knife edges (i.e.,  $\Sigma A_{SUB} = 0$ ). The sum of the partial loss is:

$$\begin{aligned}
 A_{MIXED} = & A_{F,1} + A_{F,2} + \min \{ (p_1 + p_2) A_2, A_2 \} \\
 & + q_1 [s_1 A_{SEA}(e_1, d_1) + l_1 A_{SELOSS}(h_1, d_1)] \\
 & + q_2 [s_2 A_{SEA}(e_2, d_2) + l_2 A_{SELOSS}(h_2, d_2)]
 \end{aligned} \quad (4-50)$$

If there were an over-sea diffraction between the two peaks shown in Figure 4-7, then the  $A_{SUB}$  term expressed by Equation 4-43 would be added to the above equation.

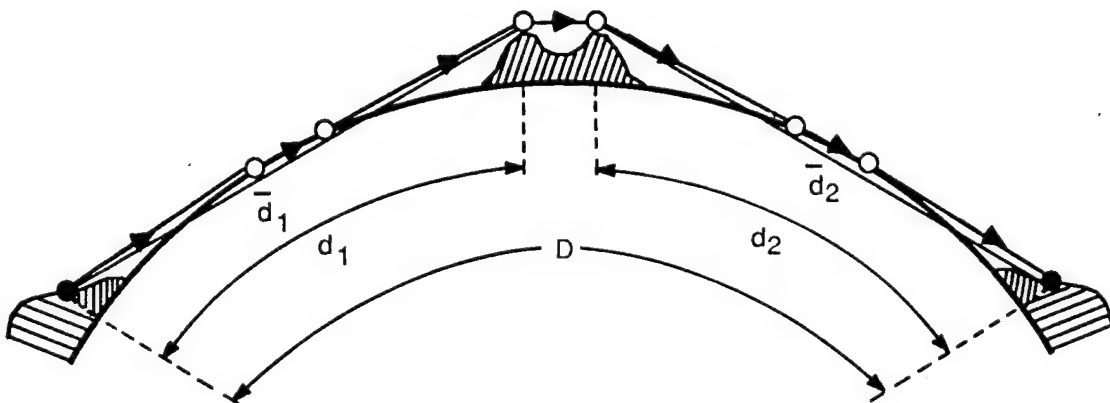


Figure 4-7. Cascading of Subpath Segments

## CHAPTER 5

# MODEL LIMITATIONS, STATISTICS, MEASUREMENT ERROR, AND REPEATABILITY STATISTICS

### 5.1 MODEL LIMITATIONS

Propagation models inevitably make certain assumptions and approximations that ignore or simplify the complex description of real-world variables. The SEM and TIREM models are intended for estimating path loss between antennas situated on a smooth spherical earth or an irregular earth, respectively. The effects of man-made or natural obstructions other than the terrain itself are not accounted for (unless the terrain profile has been adjusted to account for these features), nor are the effects of terrain not located along the great-circle path between the antennas.

The existence of an atmosphere whose refractivity gradient decreases linearly with height (Reference 1-4, p. 4-1) is assumed for heights below 3200 m and an exponentially decreasing refractivity is assumed above 3200 m (Reference 2-1, p. 1). For frequencies above 10 GHz, the atmospheric absorption due to molecular oxygen and water vapor is included and is estimated using the 1962 US Standard atmosphere (Reference 2-2) adjusted for the user-specified surface humidity.

None of the following factors that may affect path loss in practical situations are considered by either TIREM or SEM:

- Ionospheric effects
- Ducting phenomena
- Long-term path loss variability (although these effects may be incorporated within the driver program)
- Multipath effects (except in SEM when the theoretical loss option for spherical earth is selected)
- Absorption due to rain, foliage, or man-made obstructions.

## 5.2 SEM MODEL STATISTICS

Within ECAC, the standard of comparison for spherical-earth computations is the EFFSECC model because it uses exact methods for the loss calculations. Statistical results comparing propagation-loss values obtained with SEM and EFFSECC for 1069 LOS and BLOS paths are shown below. This subset was derived by stepping the frequency  $f_{\text{MHz}}$ , the antenna heights of transmitter  $h_{t,m}$  and receiver  $h_{r,m}$ , and distance  $d_{\text{km}}$  in approximately logarithmic steps as follows:

$$\begin{aligned} f_{\text{MHz}} &= 1, 10, 10^2, 10^3, 10^4 \\ h_{t,m}, h_{r,m} &= 1, 5, 10, 10^2, 5 \times 10^2, 10^3 \\ d_{\text{km}} &= 6, 12, 25, 50, 10^2, 2 \times 10^2, 4 \times 10^2, 8 \times 10^2, 10^3 \end{aligned}$$

The total set comprises 1620 paths, from which paths resulting in troposcatter were eliminated.

For each of the 1069 paths, the loss difference  $L_{\text{SEM}} - L_{\text{EFFSECC}}$  was computed. The statistics of the loss difference are:

$$\mu = -1.3 \text{ dB}, \sigma = 3.5 \text{ dB}$$

where  $\mu$  is the mean error, and  $\sigma$  is the standard deviation of error. The advantage of SEM is that the runtime is about 1/35 of the runtime of EFFSECC.

## 5.3 TIREM MODEL STATISTICS

TIREM model statistics were determined by comparing TIREM predictions with an extensive set of propagation data, collected in various propagation-measurement programs. Table 5-1 provides a summary of the different propagation-measurement programs including the location, the terrain characteristics, the frequencies, path length, etc. The data selected for comparison included data from each program (all available frequencies and distances are used, but not all available antenna heights and only data obtained using copolarized antennas).

Table 5-1. Summary of Terrain Characteristics

Location	Reference <sup>a</sup>	Description of Terrain
Worldwide	5-1	No foliage effects are included since the data comprise measurements obtained by monitoring reliable communications links over long (yearly) periods.  Path Length: 10 - 800 km Frequency: 40 - 4000 MHz
Flagstaff, Arizona	5-2	Area is characterized by extremely rough terrain interspaced with flat areas. Foliage varies from dense forest to widely spaced trees to sparsely covered land in flat areas. Transmitter and receiver sites are relocated.  Path Length: 1 - 30 km Frequency: 2, 4, 8, 16, 32, 64, 128, 256, 400, 512, 800 MHz
Colorado (Gunbarrel Hill)	5-3	Receiver site is near the summit of a hill in the open plains of the Rocky Mountain foothills. Ten of the 55 transmitter sites associated with this receiver site are located in the mountains and only one of these results in a line-of-sight path. Five transmitter sites are concealed by foliage.  Path Length: 1 - 120 km Frequency: 230, 400, 800, 1800, 4600, 9200 MHz
Colorado (North Table Mt.)	5-4	Receiver site is on a high mesa at the juncture between the mountains and plains and visible to most of its associated 59 transmitting sites.  Path Length: 1 - 120 km Frequency: 230, 400, 800, 1800, 4500, 9200 MHz
Colorado (Plains)	5-5	Transmitter site is on a plain. Area is composed of smoothly rolling hills east of transmitter. No vegetation or trees. Receiver sites at fixed semicircular distances, approximately 120 sites.  Path Length: 5 - 80 km Frequency: 20, 50, 100 MHz
Colorado (Mountains)	5-6	Same transmitter site as in plains. Area is very rugged mountains west of transmitter. Woods and trees present, approximately 40 sites.  Path Length: 5 - 50 km Frequency: 20, 50, 100 MHz
Ohio	5-7	Irregular and partly wooded terrain. Part of measurements taken with snow on ground. Receiver sites in approximate semicircles, with five peripheral transmitters. Approximately 250 sites.  Path Length: 5 - 50 km Frequency: 20, 50, 100 MHz
<sup>a</sup> References 5-1 through 5-7 are provided at the conclusion of Table 5-1.		

Table 5-1. Summary of Terrain Characteristics - Continued

## References

- 5-1. Longley, A. G., Reasoner, R. K. and Fuller, V. L., Measured and Predicted Long-term Distributions of Tropospheric Transmission Loss, OT/TRER 16, Institute for Telecommunication Sciences, Boulder, CO, July 1971.
- 5-2. Bell Aerosystems Co., Propagation Measurements Final Report, No. 280-2802, Vol. I, Sierra Vista, AZ, March 1965.
- 5-3. McQuate, P. L., et. al., Tabulations of Propagation Data Over Irregular Terrain in the 230-9200 MHz Frequency Range, Part I: Gunbarrel Hill Receiver Site, ESSA-TR-ERL-65-ITS 58, Institute for Telecommunication Sciences (ITS), Boulder, CO, March 1968.
- 5-4. McQuate, P. L., et. al., Tabulations of Propagation Data Over Irregular Terrain in the 230-9200 MHz Frequency Range, Part III: North Table Mountain-Golden, ESSA-TR-ERL-65-ITS 58-3, Institute for Telecommunication Sciences (ITS), Boulder, CO, July 1970.
- 5-5. Johnson, M. E., et. al., Tabulations of VHF Propagation Data Obtained Over Irregular Terrain at 20, 50, and 100 MHz, Part I: Colorado Plains Data, ESSA Technical Report IER-38-ITSA 38, Institute for Telecommunication Sciences and Aeronomy, Boulder, CO, May 1967.
- 5-6. Johnson, M. E., et. al., Tabulations of VHF Propagation Data Obtained Over Irregular Terrain at 20, 50, and 100 MHz, Part II: Colorado Mountain Data, ESSA Technical Report IER-38-ITSA 38-2, Institute for Telecommunication Sciences and Aeronomy, Boulder, CO, August 1967.
- 5-7. Johnson, M. E., et. al., Tabulations of VHF Propagation Data Obtained Over Irregular Terrain at 20, 50, and 100 MHz, Part III: Ohio Data, ESSA Technical Report IER-38-ITSA 38-3, Institute for Telecommunication Sciences and Aeronomy, Boulder, CO, December 1967.

The results of the comparison of TIREM-predicted losses with measurements are summarized in Table 5-2 for each of the propagation modes. The statistics shown in this table are the mean and the standard deviation of the loss difference,  $L_{\text{TIREM}} - L_{\text{Measurements}}$ . For all the modes, the overall loss difference had a mean of -0.6 and standard deviation of 10.5 dB.

In Table 5-2, mean and standard deviation for the spherical-earth propagation mode and for  $f_{\text{MHz}} \leq 16$  are displayed separately to demonstrate that, for lower frequencies, the spherical-earth approximation is good (all the measurements are in the Flagstaff area characterized by rough terrain).

Table 5-2. TIREM Statistical Summary

Propagation Mode	Nominal Frequency	Number of Measurements	Loss Difference	
			Mean dB	Standard Deviation dB
Spherical Earth	2, 4, 8, 16	102	-2.2	6.9
Line-of-sight	20, 32, 50, 64, 100, 230 400, 800, 1800 4600, 9200	1217	-2.8	8.9
Diffraction		2798	0.2	11.4
Troposcatter	60 - 4000	358	1.5	8.8
Total	2 - 9200	4475	-0.6	10.5

#### 5.4 ERROR ESTIMATES OF THE MEASUREMENTS

The Bell Aerosystem's report on propagation-loss measurements includes a detailed analysis of the instrumentation errors associated with transmitting and measuring systems. The reported accuracies of path-loss measurements as associated with instrumentation errors were shown to be within  $\pm 4.1$  dB for frequencies from 2 MHz to 32 MHz and within  $\pm 3.2$  dB for frequencies from 32 MHz to 900 MHz. This report clearly conveys the difficulties inherent in the error analysis of large-scale propagation-measurement programs, and is the only measurement analysis readily available.

## 5.5 STATISTICS CONCERNING REPEATED MEASUREMENTS

The Bell Aerosystem's report also contains, for each path, a series of repeated measurements. Measurement equipment was returned to the previous sites. For southern Arizona, repeated seasonal measurements were taken at approximately 3-month intervals. In northern Arizona, a series of measurements was taken every 5 weeks. Measurements of the seasonal variations were taken less frequently in southern Arizona because this region has just two temperature seasons per year, which vary only slightly; whereas, in northern Arizona the four seasons are more varied, with cool summer months and considerable snow in winter.

The results of the repeated measurement series for frequencies from 2 to 800 MHz are shown in Table 5-3. It shows that the repeatability is worse when the frequency increases.

Table 5-3. Results of Repeated Measurement Series

$f_{\text{MHz}}$	n	$\sigma$
2	1865	2.8
4	1831	3.0
8	1721	3.5
16	1593	3.3
32	1779	3.8
64	1754	5.8
128	1552	4.6
256	1350	4.5
400	1368	4.8
512	1278	5.0
800	353	6.7

## APPENDIX A

### INPUT PARAMETER RANGES

#### A.1 INPUT PARAMETER RANGES

The allowable ranges for the input parameters for TIREM are shown in Table A-1, and for SEM in Table A-2.

Table A-1. TIREM Input Parameter Ranges

Variable	Description	Valid Range
CONDOC	Conductivity of the earth surface	0.00001 to 100 S/m
EXTNSN	Profile indicator flag: .TRUE. - profile is an extension of the last path along a radial .FALSE.- new profile	.TRUE. or .FALSE.
HPRFL	Array of profile terrain heights above mean sea level	-450 to 9000 m
HUMID	Surface humidity at the transmitter site	0 to 50 g/m <sup>3</sup>
NPRFL	Total number of profile points for the entire path	≥ 3
PERMIT	Relative permittivity	1 to 100
POLARZ	Transmitter antenna polarization:  'V' - vertical 'H' - Horizontal	'V' or 'H'
PROPFQ	Transmitter frequency	1 to 20000 MHz
RANTHT	Receiver structural antenna height	>0 to 30000 m
REFRAC	Surface refractivity	200 to 450 N-units
TANTHT	Transmitter structural antenna height	>0 to 30000 m
XPRFL	Array of great-circle distances from the beginning of the profile point to each profile point.	≥ 0 m



Table A-2. SEM Input Parameter Range

Variable	Description	Valid Range
CONDUCT	Conductivity of the earth surface	0.00001 to 100 S/m
HUMID	Surface humidity at the transmitter site	0 to 50 g/m <sup>3</sup>
LANDHT	Average terrain elevation of the spherical earth above mean sea level	0 to 9000 m
PERMIT	Relative permittivity	1 to 100
POLARZ	Transmitter antenna polarization: 'V' - vertical 'H' - horizontal	'V' or 'H'
PROPFQ	Transmitter frequency	1 to 20000 MHz
PTHLEN	Great-circle distance from transmitter to receiver	≥ 0 m
RANTHT	Receiver structural antenna height	>0 to 30000 m
REFRAC	Surface refractivity	200 to 450 N-units
SEOPTN	Spherical-earth output option: 1 - free-space wave loss 2 - envelope of the field maxima (loss minima) 3 - envelope of the field minima (loss maxima) 4 - theoretical loss for spherical earth	1 to 4
TANTHT	Transmitter structural antenna height	>0 to 30000 m

## APPENDIX B

### TROPOSPHERIC SCATTER

#### B.1 GENERAL

The long-term, median, basic transmission loss for paths where forward scatter in the troposphere is the dominant coupling mechanism is given by Equation 2-15.

$$L_{\text{TRO}} = \max \{ [30 \log f - 20 \log D + F(D\theta) + 20 \log (r_o/D)], L_{\text{FS}} \} + H_o - F_o \quad (\text{B-1})$$

The empirical functions  $F(D\theta)$ ,  $H_o$ , and  $F_o$  are described in this appendix.

#### B.2 ATTENUATION FUNCTION $F(D\theta)$

The attenuation function  $F(D\theta)$  is an empirical function of the product of the mean sea level arc distance  $D$  and the scatter angle  $\theta_o$ . Figures B-1, B-2, B-3, and B-4 contain plots of the attenuation function  $F(D\theta)$  and the coefficients  $b_k$  for the values of  $N_s = 250, 301, 350$ , and  $400$ . The empirical curves are approximated by a fourth-order polynomial as:

$$F(D\theta) = \sum_{k=0}^4 b_k [\ln(D\theta_o/10)]^k \quad (\text{B-2})$$

Evaluation of  $F(D\theta)$  for intermediate values of  $N_s$  and  $s$  is by linear interpolation; for  $s > 1$  the value of  $s$  is replaced by  $1/s$ . The path asymmetry parameter is:

$$s = \alpha_{e,1}/\alpha_{e,2} \quad (\text{B-3})$$

$s$	$b_0$	$b_1$	$b_2$	$b_3$	$b_4$
0.01	172.1598	15.178922	0.673849	-0.02665	0.0065
0.02	172.0244	15.095866	0.748526	0.01245	0.0045
0.05	172.0847	15.610355	0.788888	-0.162934	0.0721
0.10	172.3286	16.509260	0.752966	-0.42048	0.1741
0.20	172.65585	16.661147	0.719552	-0.310936	0.2228
0.30	172.62052	16.116216	0.851304	+0.04552	0.1817
0.50	172.99412	16.805433	0.756862	-0.089631	0.2832
0.70	173.08063	17.334882	0.796767	-0.246248	0.3435
1.00	173.05149	17.192346	0.823508	-0.162147	0.3401

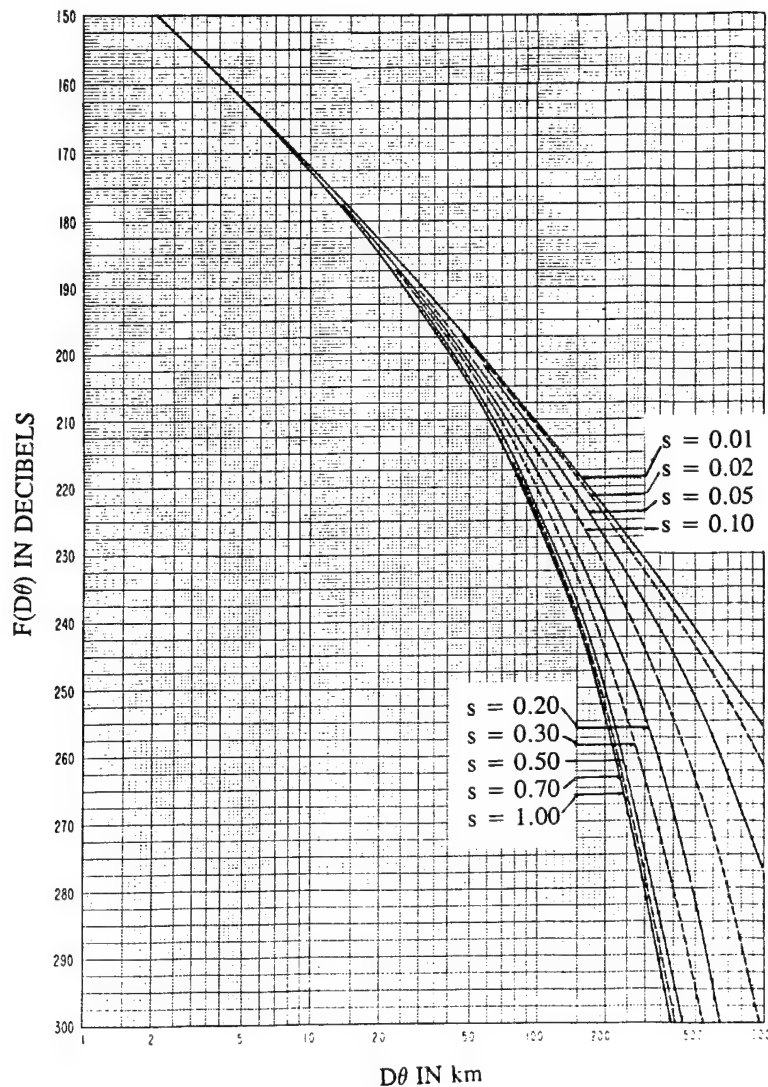


Figure B-1. Attenuation Function,  $F(D\theta)$ , and the Coefficients  $b_k$  for  $N_s = 250$

$s$	$b_0$	$b_1$	$b_2$	$b_3$	$b_4$
0.01	168.57	15.569	0.6467	-0.17929	0.04284668
0.02	168.61	15.285	0.5828	0.029297	0.0157242
0.05	168.37	15.557	1.01042	-0.069279	0.04924011
0.10	168.10	16.525	1.62945	-0.528870	0.1628723
0.20	168.39	17.253	1.7478	-0.6342316	0.2445526
0.30	168.70	17.938	1.8719	-0.693817	0.2944489
0.50	168.78	18.130	1.8984	-0.671310	0.3582764
0.70	168.85	18.543	1.9567	-0.837936	0.4245453
1.00	168.91	18.666	1.9751	-0.855865	0.4409485

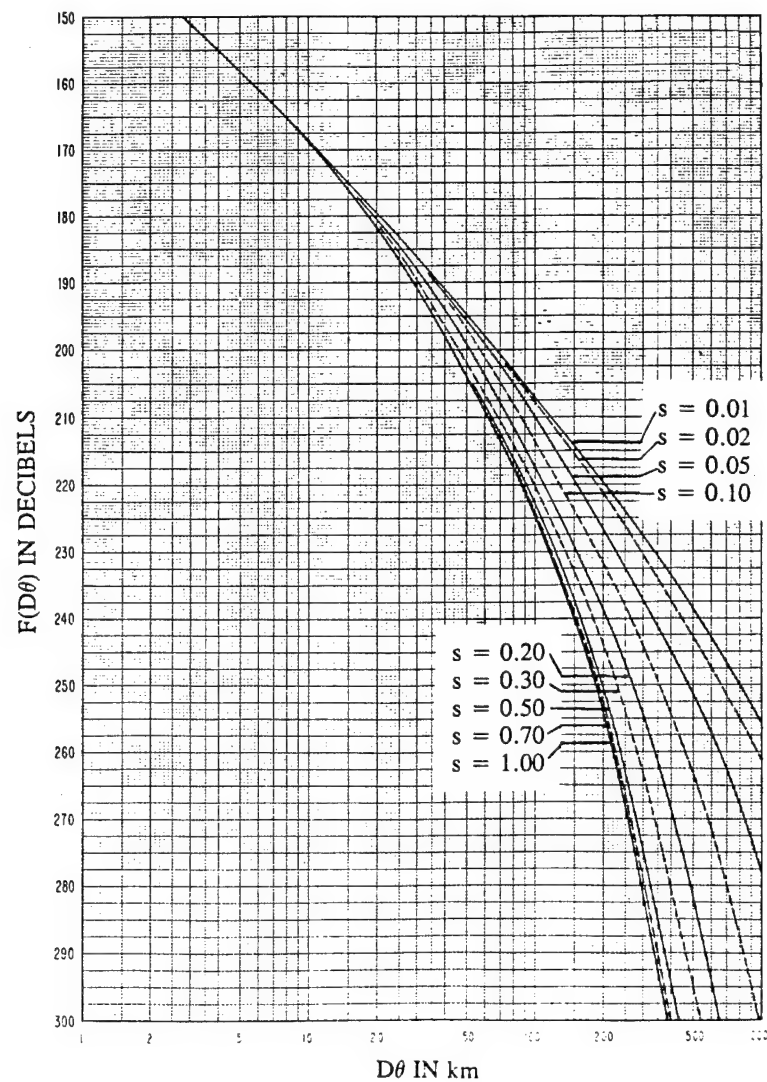


Figure B-2. Attenuation Function,  $F(D\theta)$ , and the Coefficients  $b_k$  for  $N_s = 301$

s	$b_0$	$b_1$	$b_2$	$b_3$	$b_4$
0.01	164.27	15.387	0.7816	-0.21782	0.0556259
0.02	164.37	15.139	0.5234	0.08553	0.017525
0.05	164.68	15.247	0.4200	0.3346	-0.000305
0.10	163.94	16.283	2.3161	-0.7292	0.18669
0.20	164.95	16.286	1.1963	0.42007	0.0368042
0.30	164.91	17.406	2.1280	-0.23667	0.182373
0.50	164.77	19.547	3.5410	-1.6774	0.500091
0.70	164.73	19.994	3.8334	-2.0837	0.619080
1.00	164.78	20.256	4.0000	-2.2122	0.648529

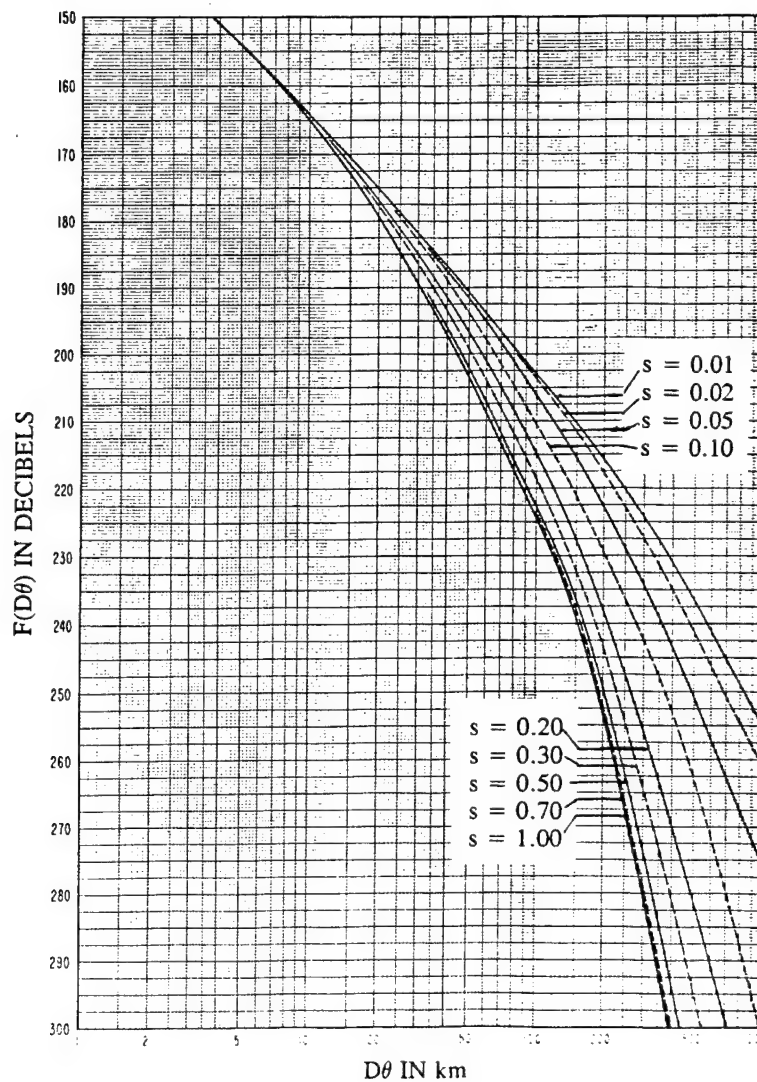


Figure B-3. Attenuation Function,  $F(D\theta)$ , and the Coefficients  $b_k$  for  $N_s = 350$

$s$	$b_0$	$b_1$	$b_2$	$b_3$	$b_4$
0.01	157.79	15.224	1.6914	-0.66772	0.1166382
0.02	158.51	16.141	-0.5607	0.46036	-0.010437
0.05	158.48	15.431	0.1686	0.774384	-0.0725098
0.10	157.93	14.722	3.3173	-0.283203	0.06176758
0.20	158.20	16.335	3.48969	-0.221252	0.0755615
0.30	158.47	17.583	4.47388	-1.15753	0.2868652
0.50	158.28	18.885	8.04977	-3.780518	0.7962647
0.70	158.35	19.216	8.33969	-3.815308	0.7985230
1.00	158.83	20.370	7.6408	-3.70209	0.807434

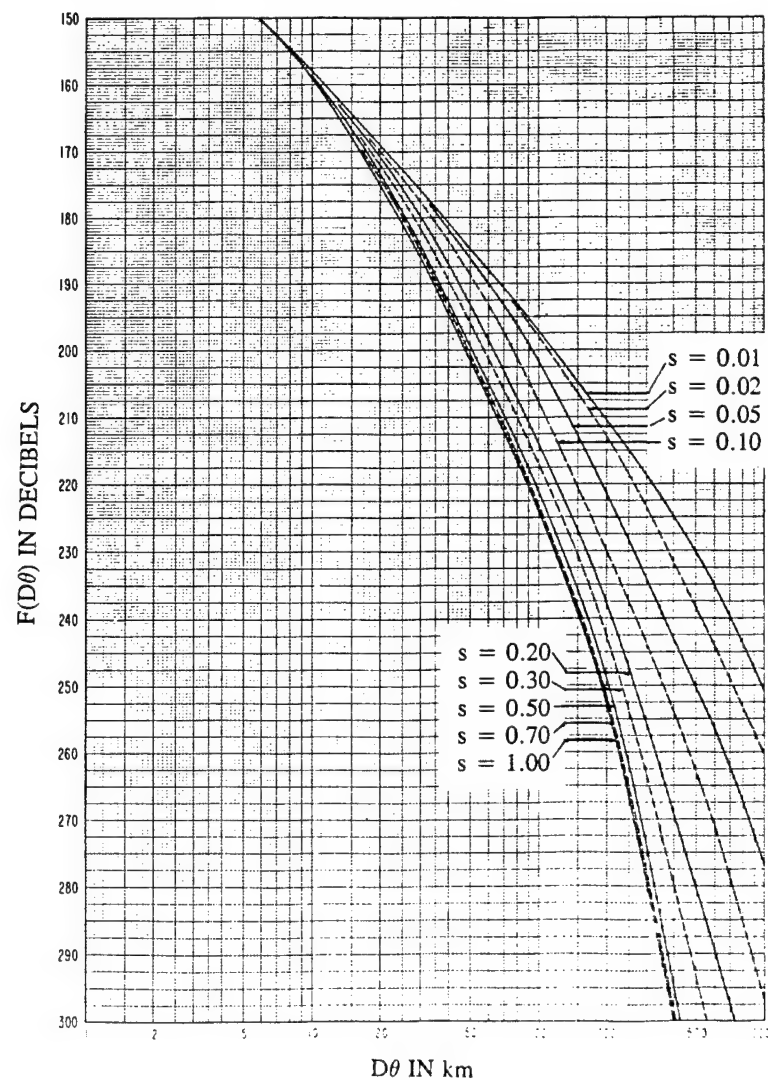


Figure B-4. Attenuation Function,  $F(D\theta)$ , and the Coefficients  $b_k$  for  $N_s = 400$

where

$$\alpha_{e,i} = \alpha_i + \Delta\alpha_i \quad (B-4)$$

The correction coefficient  $\Delta\alpha_i$  is required to account for the effects of a nonlinear refractivity gradient.  $\Delta\alpha_i$  is approximated for different ranges of  $\theta_{o,i}$  as follows:

Range:  $0 \leq \theta_{o,i} \leq 0.1$

$$\Delta\alpha_i = \max \{d_{C,i}(B + Cd_{C,i}) - A, 0\} \quad (B-5)$$

Where A, B, and C are empirical functions of  $\theta_{o,i}$  as plotted in Figure B-5 for  $N_s = 250, 301, 350, 400$ . (These plots are converted into tabular format, and intermediate values are retrieved by linear interpolation).

Range:  $\theta_{o,i} < 0$

The same format as Equation B-5 is used, replacing:

$$d_{C,i} \Rightarrow d_{C,i} - |a_e \theta_{o,i}| \quad (B-6)$$

and with A, B, and C evaluated at  $\theta_{o,i} = 0$

Range:  $0.1 < \theta_{o,i} < 0.9$

$$\Delta\alpha_i = \Delta\alpha_i(\theta_{o,i} = 0.1) + N_s(9.97 - \cot \theta_{o,i})[1 - \exp(0.05 d_{C,i})] \times 10^{-6} \quad (B-7)$$

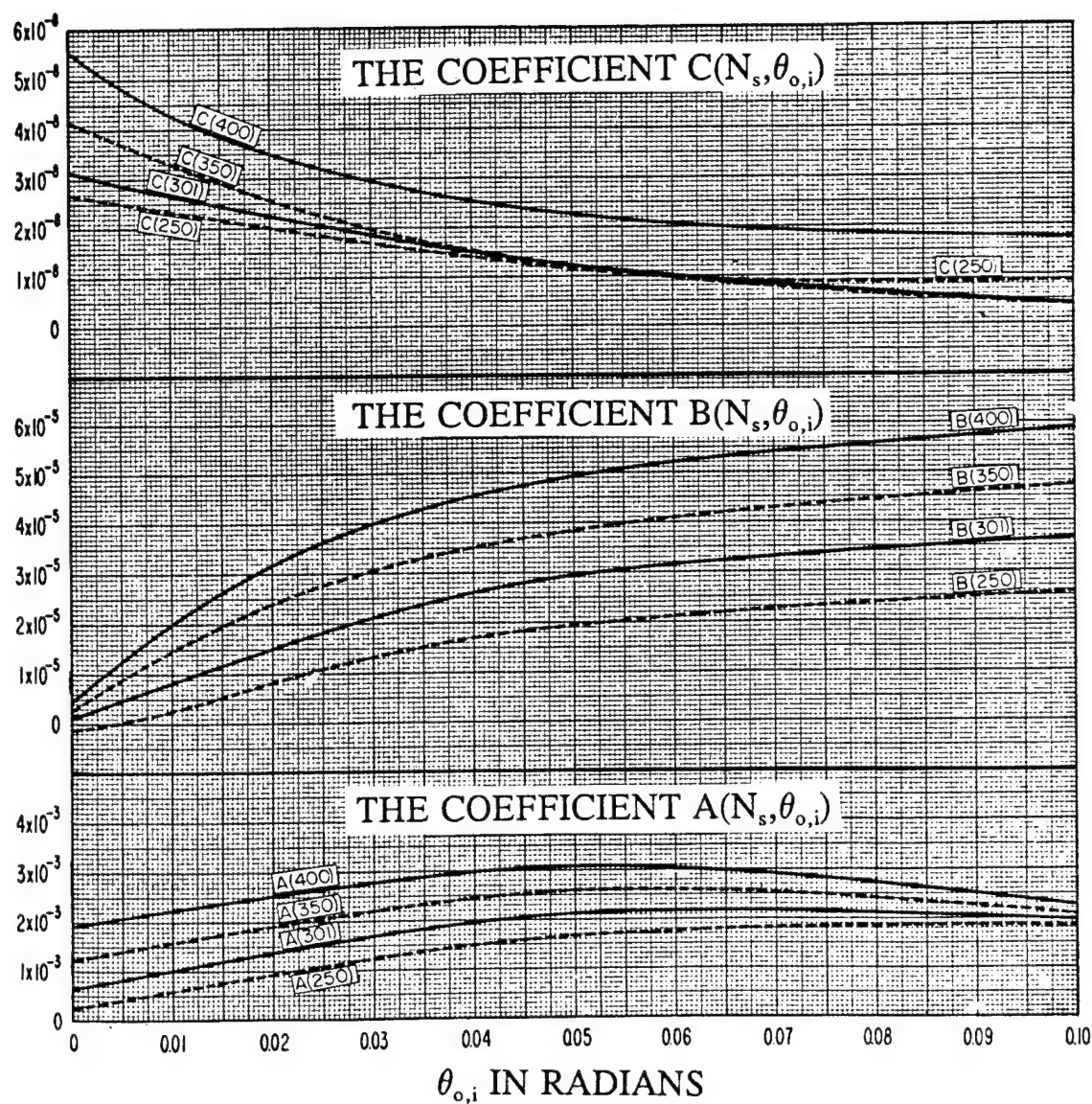


Figure B-5. Plots of the Functions A, B, and C



**B.3 SCATTERING EFFICIENCY CORRECTION  $F_o$** 

The scattering efficiency correction,  $F_o$ , which allows for the reduction of scattering efficiency at great heights in the atmosphere, is given by:

$$F_o = 1.086 (\eta_s/h_o) (h_o - h_d - h_{L,1} - h_{L,2}) \quad (B-8)$$

where

$$\eta_s = 0.5696 h_o [1 + (0.031 - 2.32 N_s \times 10^{-3} + 5.67 N_s^2 \times 10^{-6}) e^{-3.8 h_d^6 \times 10^{-6}}] \quad (B-9)$$

and

$$h_o = s D \theta / (1 + s)^2 \quad (B-10)$$

$$h_d = s d_s \theta / (1 + s)^2 \quad (B-11)$$

$$d_s = D - d_{L,1} - d_{L,2} \quad (B-12)$$

**B.4 FREQUENCY-GAIN FUNCTION  $H_o$** 

The frequency-gain function is a function of the path asymmetry parameter  $s$  (defined by Equation B-3),  $\eta_s$  (defined by Equation B-9) and the parameters  $V_i$  and  $q$ , where:

$$V_i = 4\pi h_i \alpha_{e,i} / \lambda \quad (B-13)$$

$$q = V_2 / V_1 \quad (B-14)$$

with  $h_i$  the structural antenna height of the transmitters and receivers, respectively, and  $\lambda$  is the wavelength.

Different methods are used to calculate  $H_o$  depending on  $\eta_s$ ,  $s$ , and  $q$ . The various methods are given below.

For  $\eta_s \geq 1$  and  $sq \neq 1$ ,  $H_o$  is given by:

$$H_o = [H_o(V_1) + H_o(V_2)]/2 + \Delta H_o, \quad (\text{B-15})$$

with

$$\Delta H_o = 6(0.6 - \log \eta_s) (\log s) (\log q), \quad (\text{B-16})$$

The empirical frequency-gain function  $H_o(V_i)$  is plotted in Figure B-6 for  $\eta_s = 1, 2, 4, 5, 10, 15, 20, 30, 50, 100$  and each plot is approximated by a fourth-order polynomial for intermediate values of  $V_i$  and by its asymptotes for very large or very small values of  $V_i$ .

$$H_o(V_i) = \begin{cases} 0, & V_i \geq V_u \\ \sum_{k=0}^4 d_k [\ln(V_i)]^k, & V_l < V_i < V_u \\ -40 \log V_i + a_1, & V_i \leq V_l \end{cases} \quad (\text{B-17})$$

$\eta_s$	$d_0$	$d_1$	$d_2$	$d_3$	$d_4$
1	9.74	- 8.97	2.181	0.0215	-0.03825
2	12.4629	-10.3134	2.2088	0.0634	-0.0406
4	16.1384	-12.1443	2.2196	0.1489	-0.0488
5	18.3623	-13.0333	2.1316	0.2148	-0.0547
10	23.9021	-15.1797	1.9291	0.3410	-0.0624
15	28.3813	-16.3590	1.6380	0.4097	-0.0611
20	32.5225	-17.1702	1.2061	0.5679	-0.0764
30	38.2910	-17.8950	0.6650	0.6906	-0.0831
50	45.9139	-18.0514	0.0310	0.6787	-0.0655
100	57.47	-17.65	-0.846	0.6286	-0.040778

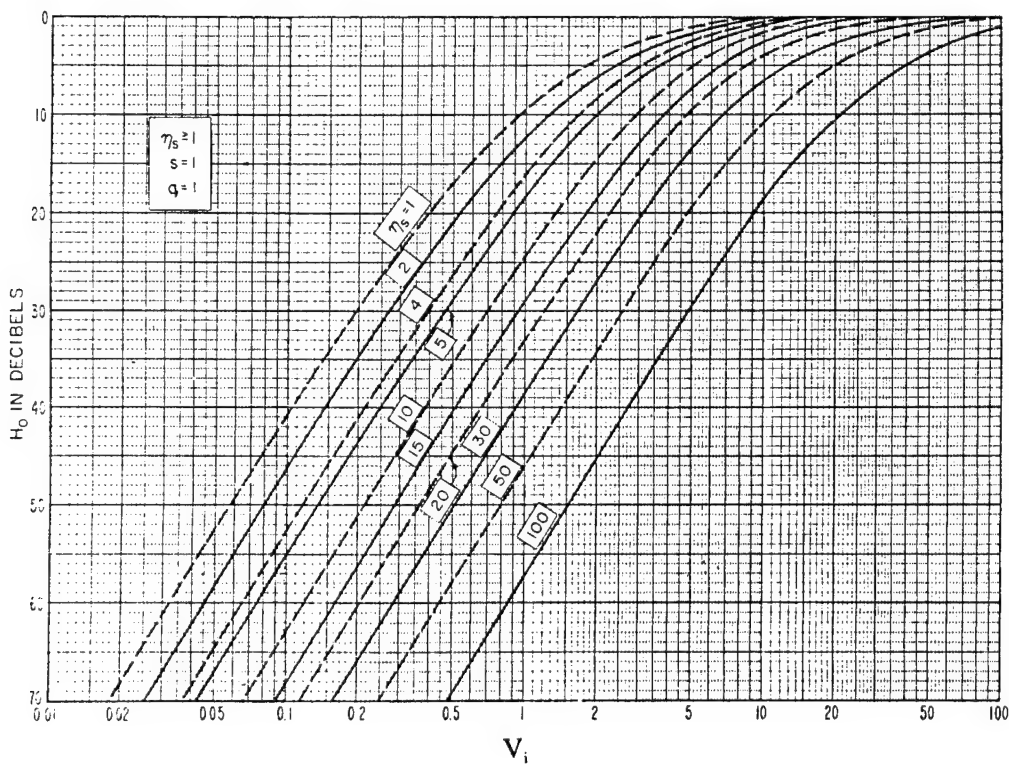


Figure B-6. Frequency-Gain Function,  $H_0$ , for  $sq \neq 1$

The coefficients  $d_k$  are tabulated as part of Figure B-6. The coefficients  $a_1$  and the upper and lower limits of  $V_i$  are tabulated in Table B-1. For intermediate values of  $\eta$ ,  $H_o(V_i)$  is linearly interpolated between the curves of Figure B-6.

Table B-1. Parameters for Calculating  $H_o$  For Very Large and Very Small Values of  $V_i$  Using Equation B-17

$\eta_s$	$a_1$	$V_l$	$V_u$
1	- 0.1705530256	0.018	9.0
2	5.8108634830	0.0255	10.0
4	11.9285966381	0.037	12.0
5	13.6631059879	0.042	13.0
10	21.9423214234	0.066	18.0
15	27.6657765715	0.09	25.0
20	30.3110521994	0.115	40.0
30	36.2956340498	0.16	70.0
50	44.8655247182	0.25	90.0
100	56.9580753795	0.48	100.0

The following constraints apply to Equation B-15:

1.  $s = \min(s, 10)$
2.  $q = \min(q, 10)$
3.  $s = \max(s, 0.1)$
4.  $q = \max(q, 0.1)$
5. If  $\Delta H_o > [H_o(V_1) + H_o(V_2)]/2$  and  $\Delta H_o \geq 0$ ,  
then  $H_o = H_o(V_1) + H_o(V_2)$
6. If  $|\Delta H_o| < [H_o(V_1) + H_o(V_2)]/2$  and  $\Delta H_o < 0$ ,  
then  $H_o = 0$

For  $\eta_s \geq 1$  and  $sq = 1$ , the functions  $H_o(V_i)$  are approximated by a fifth order polynomial for intermediate values of  $V_i$  and by its asymptotes for very large or small values of  $V_i$ .

$$H_o(V_i) = \begin{cases} 0, & V_i \geq V_u \\ \sum_{k=0}^5 d_k [\ln(V_i)]^k, & V_l < V_i < V_u \\ -40 \log V_i - a_2, & V_i \leq V_l \end{cases} \quad (B-18)$$

The plots of the function  $H_o(V_i)$  and the tabulation of the coefficient  $d_k$  for  $\eta_s = 1, 2, 4, 6, 10, 15$  each for  $s = 0.10, 0.25, 0.50, 0.75, 1.00$  are found in Figures B-7 through B-12.

For values  $V_i$  that are very large or very small,  $H_o(V_i)$  is evaluated by using the parameters tabulated in Tables B-2 and B-3 for the above  $\eta_s$  and  $s$  values. For intermediate values of  $\eta_s$  and  $s$ ,  $H_o(V_i)$  is derived by a linear interpolation for each variable.

For  $\eta_s < 1$  and  $sq \neq 1$ ,  $H_o$  is calculated by:

$$H_o(\eta_s < 1) = H_o(\eta_s = 0) + \eta_s[H_o(\eta_s = 1) - H_o(\eta_s = 0)] \quad (B-19)$$

where  $H_o(\eta_s = 1)$  is determined from Equation B-15 and where:

$$H_o(\eta_s = 0) = 10 \log \{2(1 - s^2 q^2)/[r_2^2(h(r_1) - h(r_2))]\} \quad (B-20)$$

with

$$r_1 = V_1(1 + 1/s) \quad (B-21)$$

$$r_2 = V_2(1 + s) = qsr_1 \quad (B-22)$$

s	d <sub>0</sub>	d <sub>1</sub>	d <sub>2</sub>	d <sub>3</sub>	d <sub>4</sub>	d <sub>5</sub>
0.10	1.60	-8.67118	12.75945	-4.10986	-2.31341	1.07634
0.25	4.20	-12.65708	11.83985	-2.57519	-1.46887	0.55132
0.50	6.65	-16.64002	12.76265	-1.2950	-2.16172	0.63291
0.75	8.2	-18.77319	13.55102	-0.75690	-2.81640	0.81096
1.0	9.35	-19.94592	15.20882	-1.02352	-3.98354	1.29045

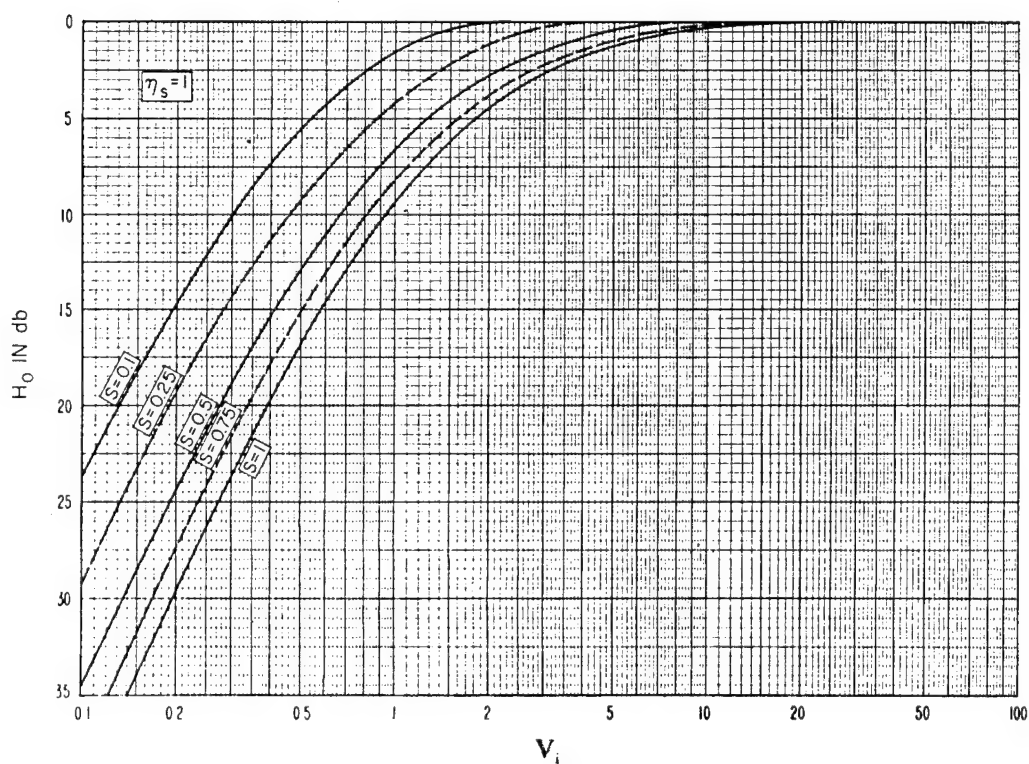


Figure B-7. Frequency-Gain Function,  $H_o$ , for  $s_q = 1$ ,  $\eta_s = 1$

s	d <sub>0</sub>	d <sub>1</sub>	d <sub>2</sub>	d <sub>3</sub>	d <sub>4</sub>	d <sub>5</sub>
0.10	5.20	-13.41458	10.59625	-1.66017	-1.23953	0.37910
0.25	6.85	-16.4377	12.1886	-1.4418	-1.6823	0.4826
0.50	9.00	-20.87493	13.37751	0.19556	-2.50718	0.54558
0.75	10.85	-22.44443	14.71246	0.29672	-3.87749	1.07771
1.0	12.25	-24.47169	15.00449	1.06392	-4.27598	1.13067

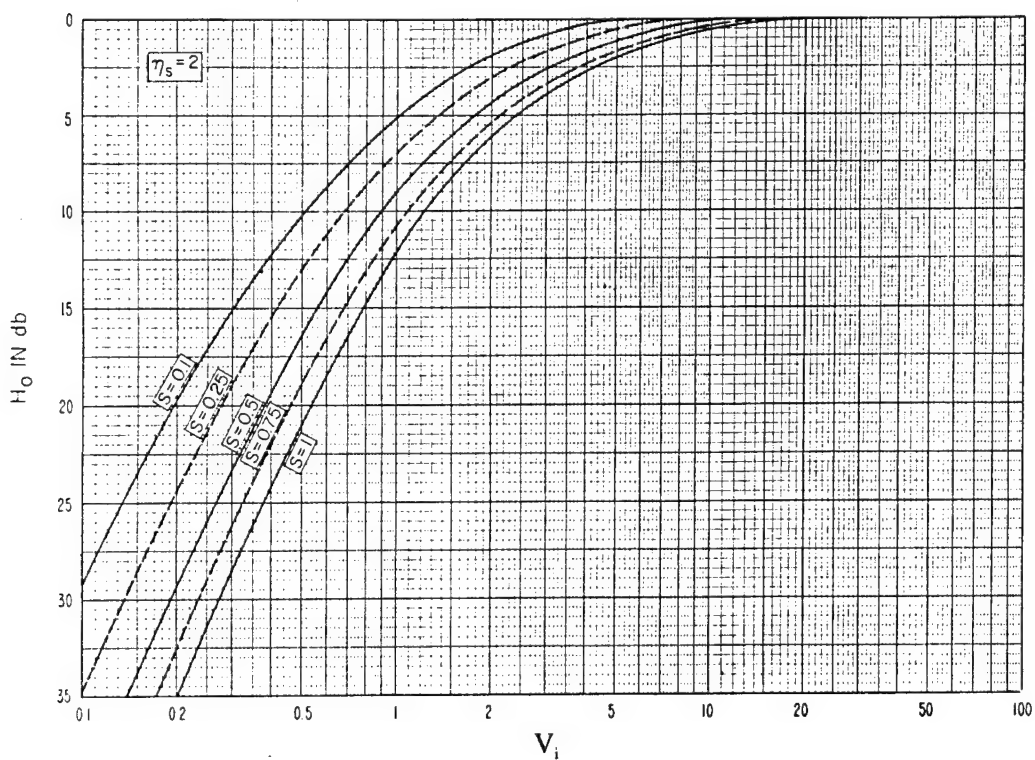


Figure B-8. Frequency-Gain Function,  $H_o$ , for  $sq = 1$ ,  $\eta_s = 2$

s	d <sub>0</sub>	d <sub>1</sub>	d <sub>2</sub>	d <sub>3</sub>	d <sub>4</sub>	d <sub>5</sub>
0.10	8.25	-16.85105	11.66699	-1.13846	-2.02690	0.62582
0.25	10.0	-20.53873	13.03909	-0.49841	-2.24447	0.57718
0.50	12.5	-24.56008	13.81639	0.96213	-2.99635	0.66226
0.75	14.65	-27.29517	13.44117	2.39064	-3.35508	0.63390
1.0	16.35	-29.41035	13.82817	3.16864	-3.98061	0.78180

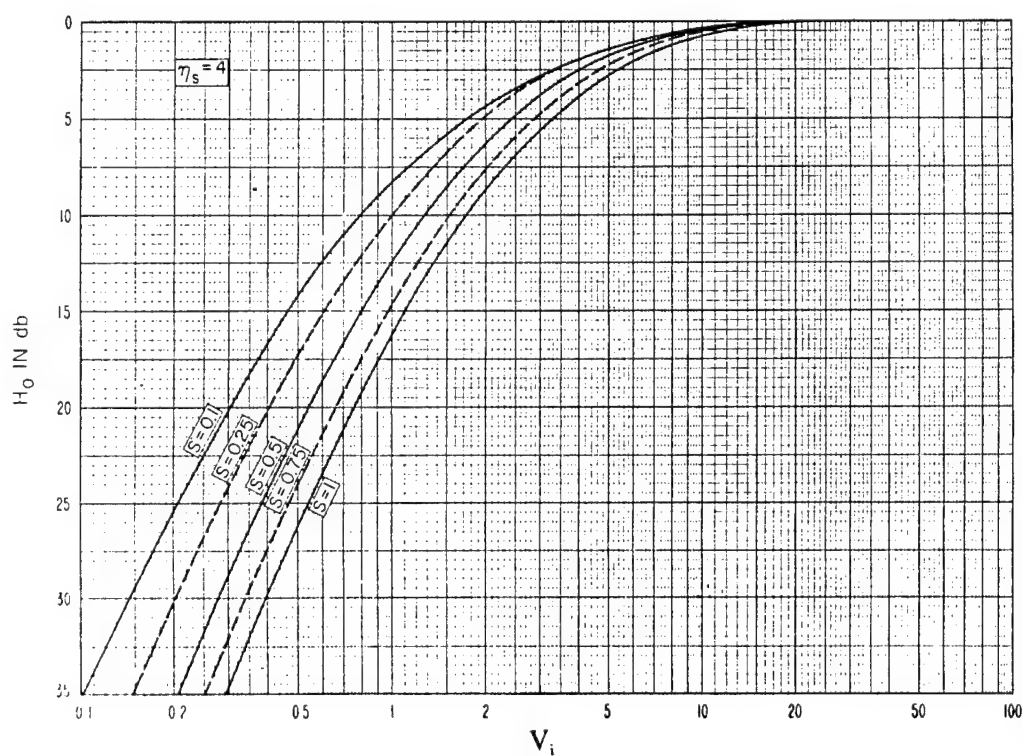


Figure B-9. Frequency-Gain Function,  $H_o$ , for  $sq = 1$ ,  $\eta_s = 4$



s	d <sub>0</sub>	d <sub>1</sub>	d <sub>2</sub>	d <sub>3</sub>	d <sub>4</sub>	d <sub>5</sub>
0.10	11.25	-18.99859	9.16108	-0.05206	-0.77583	0.08075
0.25	12.65	-23.28189	13.07615	-0.09284	-2.13960	0.50549
0.50	15.35	-27.78663	12.92337	2.43753	-2.89846	0.46697
0.75	17.75	-30.07131	11.50693	3.36909	-2.11519	0.08582
1.0	19.45	-32.12501	11.97889	4.05866	-2.77689	0.25943

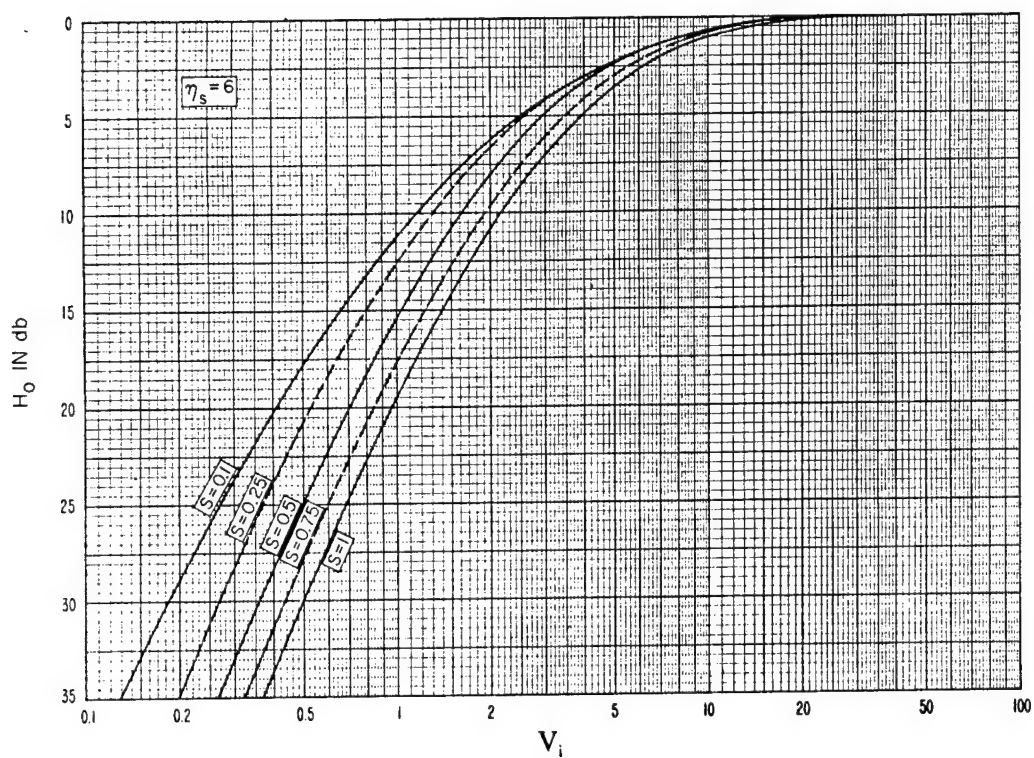


Figure B-10. Frequency-Gain Function,  $H_o$ , for  $sq = 1$ ,  $\eta_s = 6$

s	d <sub>0</sub>	d <sub>1</sub>	d <sub>2</sub>	d <sub>3</sub>	d <sub>4</sub>	d <sub>5</sub>
0.10	14.35	-22.14402	9.49536	1.04508	-1.74207	0.34566
0.25	16.6	-27.00765	11.37614	2.57663	-2.87428	0.52563
0.50	19.9	-31.90183	10.21261	4.15356	-1.50794	-0.20617
0.75	22.25	-34.66434	10.35173	4.54709	-1.29152	-0.33271
1.0	24.75	-35.71065	7.54665	5.56667	-0.05057	-0.87117

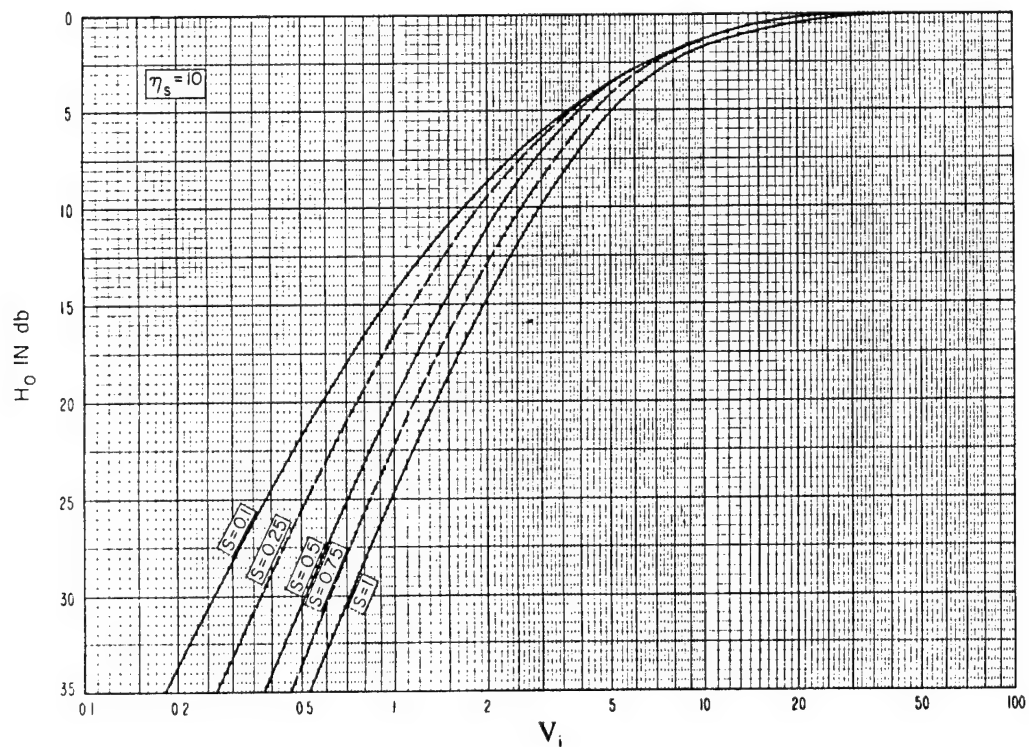


Figure B-11. Frequency-Gain Function,  $H_o$ , for  $sq = 1$ ,  $\eta_s = 10$

s	d <sub>0</sub>	d <sub>1</sub>	d <sub>2</sub>	d <sub>3</sub>	d <sub>4</sub>	d <sub>5</sub>
0.10	19.25	-26.67857	7.07404	2.76938	-0.33396	-0.35943
0.25	20.6	-30.84175	10.42451	3.90438	-2.47659	0.22601
0.50	24.25	-35.15910	7.79812	5.56981	-0.38235	-0.75589
0.75	26.75	-36.9974	6.85575	6.15626	-0.08357	-0.89875
1.0	29.25	-37.40957	3.43747	6.76033	1.63919	-1.53728

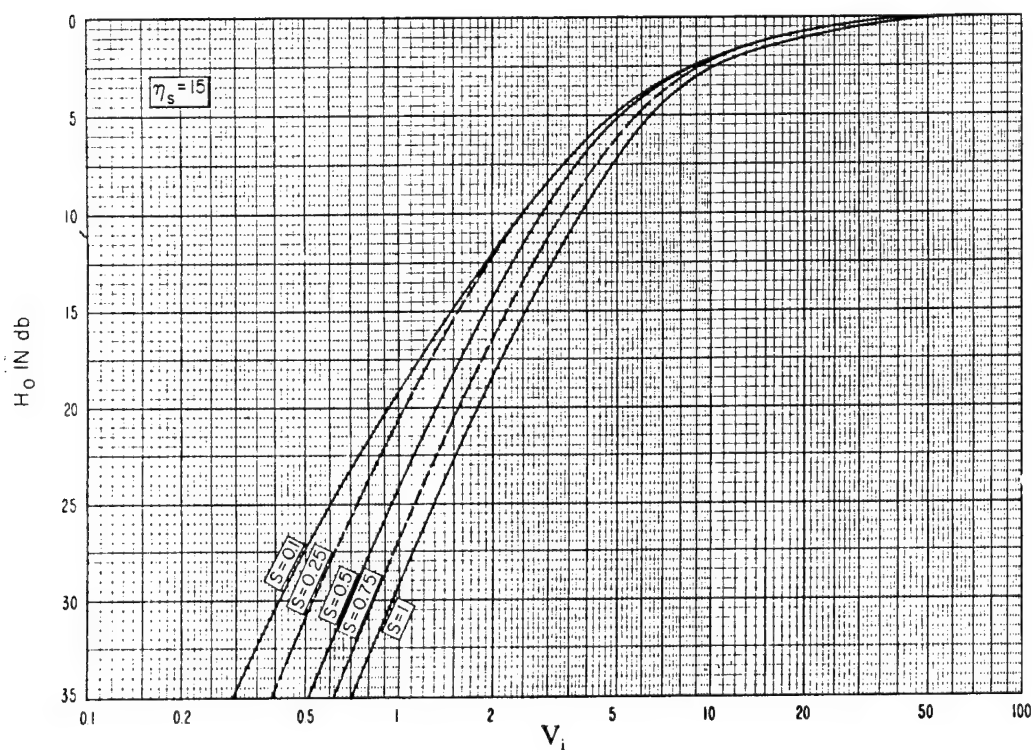


Figure B-12. Frequency-Gain Function,  $H_o$ , for  $sq = 1$ ,  $\eta_s = 15$

Table B-2. Upper Limit of  $V_i$  for Calculating  $H_0$  for Very Large Values of  $V_i$   
(Equation B-17 for  $s_q = 1$ )

$\eta_s$	$s = 0.1$ $V_u$	$s = 0.25$ $V_u$	$s = 0.50$ $V_u$	$s = 0.75$ $V_u$	$s = 1.0$ $V_u$
1	1.9	3.8	7.0	12.0	15.0
2	5.0	7.0	10.0	15.0	17.0
4	15.0	15.0	15.0	15.0	18.0
6	18.0	18.0	18.0	18.0	20.0
10	24.0	24.0	24.0	24.0	35.0

Table B-3. Lower Limit of  $V_i$  and Parameter  $a_2$  for Calculating  $H_0$  for Very Large  
Values of  $V_i$  (Equation B-17 for  $s_q = 1$ )

$\eta_s$	$s = 0.1$		$s = 0.25$		$s = 0.50$		$s = 0.75$		$s = 1.0$	
	$V_i$	$a_2$	$V_i$	$a_2$	$V_i$	$a_2$	$V_i$	$a_2$	$V_i$	$a_2$
1	0.1	16.25	0.1	10.75	0.1	5.45	0.122	1.78	0.14	1.25
2	0.1	10.75	0.1	5.25	0.14	7.20	0.172	4.29	0.2	7.15
4	0.1	4.75	0.149	1.83	0.209	7.35	0.25	10.86	0.295	18.80
6	0.13	6.52	0.20	6.79	0.265	11.79	0.32	15.12	0.37	17.86
10	0.18	5.27	0.27	12.08	0.38	17.95	0.46	21.44	0.53	24.03

The function  $h(r_i)$  is given in the form of a plot as shown in Figure B-13 and is approximated by:

$$h(r_i) = \begin{cases} 1.630637 r_i, & r_i < 0.001 \\ \exp(-0.47 + 0.445x - 0.1152x^2 - 0.007954x^3), & 0.001 \leq r_i < 0.6887 \\ \exp\{-\exp(v)/1000\}, & 0.6887 \leq r_i < 100 \\ \exp(-1.906295/r_i^2), & r_i \geq 100 \end{cases} \quad (B-23)$$

where

$$x = \ln(r_i) \quad (B-24)$$

$$v = 6.18705 - 0.892717x - 0.284649x^2 + 0.023584x^3 \quad (B-25)$$

For  $\eta_s < 1$ ,  $sq = 1$ , and  $s \leq 1$ ,  $H_o$  is calculated as in Equation B-19, except  $H_o(\eta_s = 0)$  is given by:

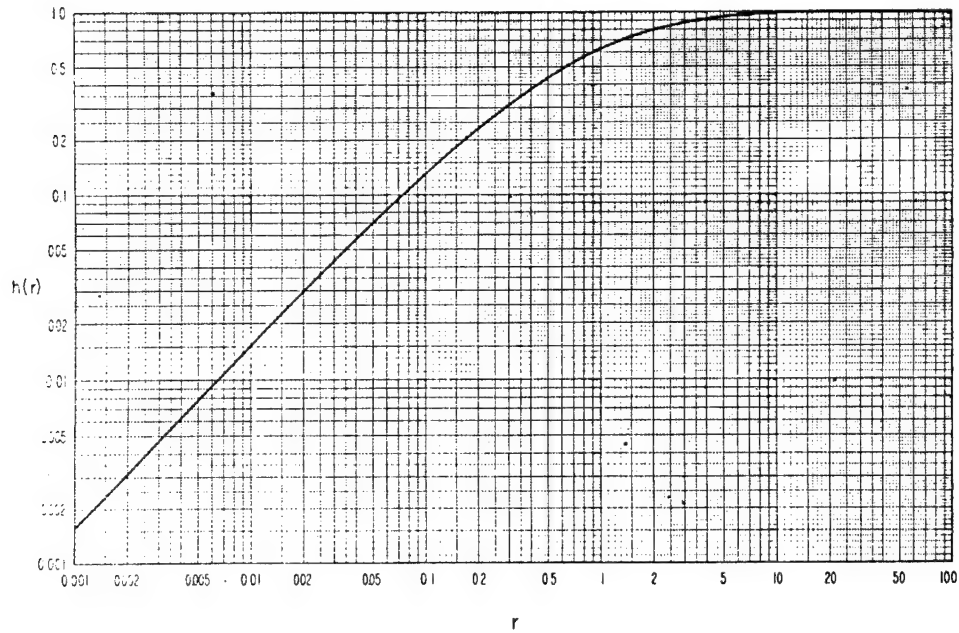
$$H_o(\eta_s = 0) = 11.68 - 7.792x + 1.310x^2 + 0.04222x^3 H_o(\eta_s) = -0.016545x^4 \quad (B-26)$$

where

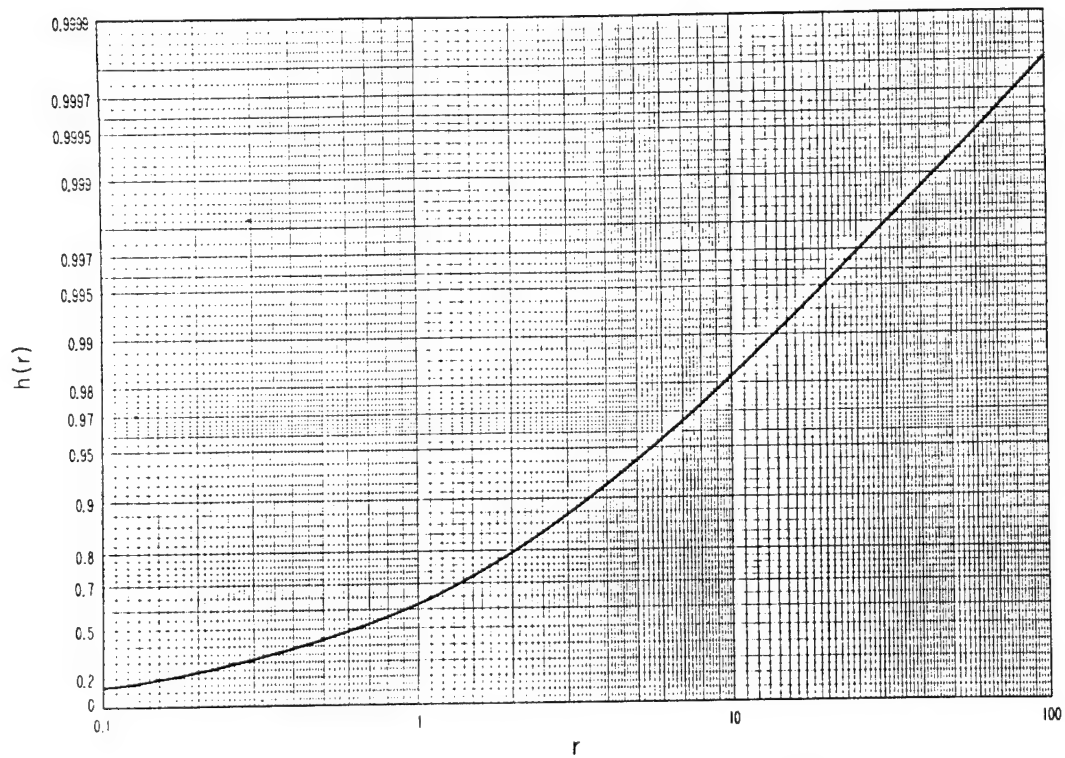
$$x = \ln(r_i) \quad (B-27)$$

For  $\eta_s < 1$ ,  $sq = 1$  and  $s > 1$ ,  $H_o$  is calculated as above in Equation B-26, with:

$$x = \ln(r_2) \quad (B-28)$$



VIEW A. THE FUNCTION  $h(r)$  FOR  $r < 0.6887$



VIEW B. THE FUNCTION  $h(r)$  FOR  $r > 0.6887$

Figure B-13. Function of  $h(r)$  for  $r > 0.6887$

## APPENDIX C

### SEM CRITICAL DISTANCES

#### C.1 GENERAL

Within LOS, the space wave, as given by Equation 3-1, oscillates with distance (see Figure 3-2). In SEM, there is an option (SEOPTN = 4) to calculate the path loss corresponding to the theoretical space-wave lobing structure  $E_{SPW}/E_o$  that results from alternate constructive and destructive interference between the direct and reflected waves within the LOS region over a perfectly smooth spherical earth.

When this option is chosen, Equation 3-1 is used to calculate  $E_{SPW}/E_o$  for any distance less than  $d_{SPW}$ . Alternative choices calculate losses corresponding to the envelope of the space-wave field maxima  $E_{MAX}/E_o$  (SEOPTN = 2) or the envelope of the space-wave field minima  $E_{MIN}/E_o$  (SEOPTN = 3).

With SEOPTN = 2, Equation 3-14 is used out to the distance  $d_{MAX}$  where the last field maximum occurs and Equation 3-1 is used between  $d_{MAX}$  and  $d_{SPW}$ .

With SEOPTN = 3, Equation 3-15 is used out to the distance  $d_{MIN}$  where the last field minimum occurs and Equation 3-1 is used between  $d_{MIN}$  and  $d_{SPW}$ .

A fourth option (SEOPTN = 1) permits use of a free-space approximation  $E_{FSW}/E_o$  to the oscillating space-wave field within the reflection region to a maximum distance,  $d_{ONE}$ , where the space-wave field last becomes equal to the free-space field. Equation 3-1 is again used beyond  $d_{ONE}$  to the distance  $d_{SPW}$ .

This appendix outlines the procedures for finding the maximum range at which the normalized space-wave electric field has a value of 1 ( $D = d_{ONE}$ ), the range of the last maximum ( $D = d_{MAX}$ ) of

the normalized field, and the range of its last minimum ( $D = d_{\text{MIN}}$ ). The distance  $d_{\text{MAX}}$  is also used in the calculation of  $d_{\text{SPW}}$ , given by Equation 3-17.

## C.2 QUARTIC EQUATION METHOD

This approximate method for finding  $d_{\text{MAX}}$  is sufficiently accurate for situations involving propagation over land and for frequencies generally above HF or for horizontal polarization. It is used wherever possible because the calculations are much faster than the more-accurate iterative method, which is required for propagation of vertically-polarized waves over sea at lower frequencies.

For antennas near the ground and for distances that are great compared to the antenna heights, such that  $r_1' \sim r_2'$ , the phase factor  $\Delta$  (Equation 3-4) may be approximated by:

$$\Delta = \frac{4 \pi h_1' h_2'}{\lambda D} \quad (\text{C-1})$$

where

$$h_1' = h_1 - \frac{d_1^2}{2 a_e} \quad (\text{C-2})$$

$$h_2' = h_2 - \frac{d_2^2}{2 a_e} \quad (\text{C-3})$$

$$d_{\text{MAX}} = d_1 + d_2 \quad (\text{C-4})$$

$$d_1/d_2 = h_1/h_2 \quad (\text{C-5})$$



From Equation 3-1 it is evident that, for plane earth and assuming a reflection coefficient of  $R = -1$ , the last oscillation maximum occurs at  $\Delta = \pi$ , so that:

$$\frac{4 \pi h_1' h_2'}{\lambda d_{\text{MAX}}} = \pi \quad (\text{C-6})$$

Using Equations C-2 through C-5, Equation C-6 can be brought into the form:

$$d_{\text{MAX}}^4 - 2 C d_{\text{MAX}}^2 - \frac{\lambda a_e (h_1 + h_2)}{h_1 h_2} C d_{\text{MAX}} + 4 a_e (h_1 + h_2) C = 0 \quad (\text{C-7})$$

where

$$C = \frac{a_e (h_1 + h_2)^3}{h_1 h_2} \quad (\text{C-8})$$

The Quartic Equation C-7 is then solved using Brown's method of biquadratic equations.<sup>C-1</sup> The solution of a quartic equation yields four (4) roots, of which all four (4) roots are complex, or two (2) roots are complex and two (2) roots are real, or all four (4) roots are real. Since the solution is a physical quantity (i.e. distance), it is assumed that real roots will always exist. Also the solution must be greater than zero but less than the radio horizon distance, therefore, the distance to the last oscillation peak is the largest real root less than the radio horizon distance. This has proved empirically correct.

---

<sup>C-1</sup>Brown, W. S., "Solution of Biquadratic Equations," Aircraft Engineering, January, 1944, page 14.

The last oscillation minimum occurs near  $\Delta = 2\pi$ , which yields the following quartic equation:

$$d_{MAX}^4 - 2 C d_{MAX}^2 - \frac{2 \lambda a_e (h_1 + h_2)}{h_1 h_2} C d_{MAX} + 4 a_e (h_1 + h_2) C = 0 \quad (C-9)$$

Since the distance to the last oscillation minimum must be greater than zero and less than the distance to the last oscillation maximum, the largest real root satisfying this condition is used.

### C.3 ITERATIVE METHOD

For some cases of propagation of vertically-polarized waves, the assumption that the specular reflection coefficient is -1 can be invalid. For these cases, the quartic solution can result in an erroneous estimate for  $d_{MAX}$ . Incorrect values of  $d_{MAX}$ , in turn, can cause the path loss predicted by SEM to exhibit inconsistent behavior. For these cases, an efficient, iterative algorithm is used to calculate the range parameters of interest. The algorithm requires more time resources than the quartic solution method, but yields the correct answer in all cases.

To minimize the number of times that the iterative method is used, the quartic solution method is first called to make an initial range estimate for all cases.

For vertical polarization, this range estimate is checked for consistency with the expected characteristics of the normalized space wave field at its last maximum (the magnitude of the last maximum  $> 1$  for example) and the iterative algorithm is called if a contradiction is detected.

First, a method to find the greatest range at which the normalized electric field has a value equal to 1,  $d_{ONE}$ , is described. Then this value is used to find the range to the last maximum,  $d_{MAX}$ , and the range to the last minimum,  $d_{MIN}$ .

### Last Range At Which $|E/E_0| = 1$

This section describes an iterative procedure for finding the greatest range,  $d_{\text{ONE}}$ , at which the normalized magnitude of the electric field is equal to 1. Using the normalized field values shown in Figure 3-2 as typical, it is recognized that  $d_{\text{ONE}}$  occurs at some distance less than the radio horizon given by Equation 3-18.

The following information is used to locate the relevant distance parameters.

- The field variation in the region between  $d_{\text{ONE}}$  and  $d_{\text{HOR}}$  is nearly linear on a linear/log scale
- The radian path length difference,  $2\pi(r_2' - r_1')/\lambda$ , monotonically decreases to zero at the horizon
- The phase of the reflection coefficient changes slowly as a function of distance in the vicinity of  $d_{\text{MAX}}$
- If the change of phase of the reflection coefficient between  $d_{\text{HOR}}$  and  $d_{\text{MIN}}$  is small, the radian path length difference between the radio horizon and  $d_{\text{MIN}}$  is about  $2\pi$

The distance,  $d_{\text{ONE}}$ , is found by iteratively decreasing the distance from the horizon until the normalized space-wave field  $|E_{\text{SPW}}/E_0|$  is 1. Because  $|E_{\text{SPW}}/E_0|$  oscillates through 1 many times, its derivative with respect to distance,  $D$ , and the phase difference  $\Delta$  between the estimated distance of  $d_{\text{ONE}}$  and  $d_{\text{HOR}}$  are kept within specified limits to ensure that  $d_{\text{ONE}}$  is the distance nearest the horizon where  $|E_{\text{SPW}}/E_0|$  last becomes 1.

The normalized space-wave field is calculated from Equation 3-1, but the effects of the path length ratio and divergence factor are ignored (the product  $(r_1'/r_2')D_c = 1$ ) since they affect only the magnitude of the field and not the range locations of interest.

To avoid problems with numerical precision in the estimation of the value of the derivative (with respect to distance) of the normalized field at  $d_{\text{HOR}}$ , a starting distance of:

$$d_{\text{START}} = \alpha d_{\text{HOR}} \quad (\text{C-10})$$

is used, where  $\alpha$  is initially 0.975. It is important that  $d_{\text{START}}$  be between  $d_{\text{ONE}}$  and  $d_{\text{HOR}}$ , and far enough from  $d_{\text{HOR}}$  that the iteration will converge. To this end, the value of  $\alpha$  is adjusted until the phase  $\Delta$  is between  $\pi/20$  and  $\pi/2$  and the normalized field is between 0.1 and 1.

Next, a range step  $dr$  is determined according to:

$$dr = d_{\text{START}} - 10^{\left[ \left( 1 - \left| \frac{E(d_{\text{START}})}{E_0} \right| \right) / \text{slope} + \log(d_{\text{START}}) \right]} \quad (\text{C-11})$$

where

$$\text{slope} = \frac{1}{\log(1 + 1/d_{\text{START}})} \left[ \frac{d}{dD} \left| \frac{E}{E_0} \right| \right]_{D = d_{\text{START}}} \quad (\text{C-12})$$

The estimated maximum distance  $d_{\text{IEST}}$  where the normalized space-wave field last becomes 1 within the horizon is then:

$$d_{\text{IEST}} = d_{\text{START}} - dr \quad (\text{C-13})$$

Equations C-11 and C-12 are derived assuming a linear variation in the normalized field with the log of distance between  $d_{HOR}$  and  $d_{ONE}$ . Because the field variation is not exactly linear, Equation C-13 will sometimes yield a distance less than the true value of  $d_{ONE}$ . This is because the variation of the field is not exactly as assumed.

To avoid overshooting the true value of  $d_{ONE}$ , a range step limit is calculated based upon the change of  $\Delta$  between  $d_{START}$  and  $d_{1EST}$ .

Assuming that the path length difference between the direct and reflected fields is the dominant factor influencing the change of phase of  $|E/E_0|$  near  $d_{ONE}$ , then the resultant field will increase to a value of 1 as distance decreases below  $d_{HOR}$  accompanied by a change in phase of less than  $\pi$ .

The total change of phase is defined as:

$$\Delta_T = \Delta(d_{1EST}) - \Delta(d_{HOR}) \quad (C-14)$$

where  $\Delta = 2\pi(r_2' - r_1')/\lambda$  as in Equation 3-4. The phase difference  $\Delta_T$  is not permitted to exceed  $\pi$ . To this end, if  $|\Delta_T| > \pi$  the range step is limited as follows:

$$dr \leq \frac{\pi}{\Delta_T} (d_{HOR} - d_{1EST}) \quad (C-15)$$

The range step is limited to the minimum of Equations C-11 and C-15. Of course, if the step is so limited then  $\Delta_T$  must be recalculated and checked that its value is less than  $\pi$ . Although the above limit on the range step may delay the achievement of convergence, it ensures that the distance  $d_{ONE}$  will not be bypassed.

The iteration proceeds by substituting the last, best estimate of  $d_{\text{ONE}}$  for  $d_{\text{START}}$  in Equation C-11 to find a range step, limit the step if necessary, and calculate the value of the normalized space-wave field as described above. The iteration stops when:

$$\left| \frac{E}{E_0} (d = d_{\text{TEST}}) - 1 \right| < 0.01 \quad (\text{C-16})$$

The above procedure is implemented in the FORTRAN routine R1CALC. This routine contains additional logic that is necessary to handle certain unique space-wave field distributions (limiting situations such as antenna heights equal to zero, frequency limits, etc.).

#### Range of Last Maximum

The last maximum of the normalized space-wave field  $|E_{\text{SPW}}/E_0|$  occurs at the distance  $d_{\text{MAX}}$  when the direct and reflected fields are in phase for the last time before the antennas become separated beyond the horizon. At  $d_{\text{MAX}}$ , the value of  $|E_{\text{SPW}}/E_0|$  lies between 1 and 2 (the maximum it could be if the earth were a perfect reflector). Also, at  $d_{\text{MAX}}$ , it is known that the first derivative of the field must change signs. Therefore, the search for  $d_{\text{MAX}}$  begins at  $d_{\text{ONE}}$  by stepping back in range (with an appropriate range step limit) until a change in the sign of the first derivative of the field is located. A bisection algorithm is used to refine the calculation of  $d_{\text{MAX}}$ . In this case, the starting point is:

$$d_{\text{START}} = d_{\text{ONE}} \quad (\text{C-17})$$

and the range step  $dr$  is:

$$dr = d_{\text{START}} - 10^{\left[ (2 - | \frac{E(d_{\text{START}})}{E_0} |) / \text{slope} + \log(d_{\text{START}}) \right]} \quad (\text{C-18})$$

and  $d_{\text{MEST}}$ ,

$$d_{\text{MEST}} = d_{\text{ONE}} - dr \quad (\text{C-19})$$

is an estimate of  $d_{\text{MAX}}$ .

A criterion is needed to determine if the range step is reasonable. Again, this criterion is determined from available information about the change in phase of the field over the range step:

$$\Delta_T = \Delta(d_{\text{MEST}}) - \Delta(d_{\text{ONE}}) \quad (\text{C-20})$$

where  $\Delta_T$  is the total phase change between  $d_{\text{ONE}}$  and the estimate for the range of the last maximum  $d_{\text{MEST}}$ . Examination of a typical space-wave field distribution, such as in Figure 3-2, shows that the difference between the phase of the field at  $d_{\text{ONE}}$  and  $d_{\text{MAX}}$  is less than or equal to  $\pi$ .

Therefore, a range step limit:

$$dr \leq \frac{\pi}{\Delta_T} (d_{\text{ONE}} - d_{\text{MEST}}) \quad (\text{C-21})$$

is imposed.

The approximation  $d_{\text{MEST}}$  is a reasonable estimate of the range of the last maximum  $d_{\text{MAX}}$ . To check the estimate, the value of the derivative of the field at the ranges  $d_{\text{MAX}}$  and  $d_{\text{ONE}}$  are calculated and compared for a sign difference. If there is a sign difference, then the location of the maximum has been successfully bracketed and a bisection algorithm can be used to resolve the location of  $d_{\text{MAX}}$  to any desired accuracy. If there is no sign difference between the values of the derivatives at the two range points, then it is assumed that another range step is necessary. Another range step is then calculated using Equations C-19, C-20, and C-21 with the current estimate of  $d_{\text{MEST}}$  substituted for

$d_{ONE}$  to obtain a new estimate, and the above procedure is repeated until a range bracket for  $d_{MAX}$  is found.

The calculation of the range of the last field maximum is implemented in the FORTRAN routine REXCAL. This routine also contains additional logic to handle exceptional cases.

### Range of Last Minimum

Using the same procedure that led to finding the range of the last field maximum, we may find the range of the last field minimum. To ensure that the search begins at a range point on the transmitter side of the last field maximum (which is necessary to use the same algorithm), begin the search at:

$$d_{START} = 0.9d_{MAX} \quad (C-22)$$

The minimum normalized field will never be less than 0 so a range step is calculated by:

$$dr = d_{START} - 10^{\left[ \left( 0 - \left| \frac{E(d_{MAX})}{E_0} \right| \right) / \text{slope} + \log(d_{MAX}) \right]} \quad (C-23)$$

The estimate of the distance to the last field minimum  $d_{mEST}$  is:

$$d_{mEST} = d_{START} - dr \quad (C-24)$$

and the range step is limited by:

$$dr \leq \frac{\pi}{\Delta_T} (d_{START} - d_{mEST}) \quad (C-25)$$



Using this new estimate for the range of the last field minimum, the derivative of the field is calculated. The derivative at the initial range ( $d_{\text{START}}$ ) is also calculated and the signs of the two derivatives are compared. If a sign change is detected, a bisection algorithm is used to refine the estimate. If no sign change is observed between the two values of the derivative, the above procedure is repeated until the required sign change indicating the field minimum is observed.

The calculation of the range of the last field minimum is implemented in the FORTRAN routine REXCAL. An argument is passed through the parameter list to indicate whether the range of the last maximum or the range of the last minimum is desired.

## APPENDIX D

### REFLECTION LOSS

#### D.1 PHASE FACTOR

The phase difference  $\delta$  between the direct wave and the wave reflected from a plane surface is (Figure D-1):

$$\delta = \frac{2\pi}{\lambda} [(r_2 + r_1) - (d_1 + d_2)] \quad (\text{radians}) \quad (\text{D-1})$$

where

$$d_1 + d_2 = d \quad (\text{D-2})$$

$$r_1 = \sqrt{d_1^2 + c^2} \sim d_1 + \frac{1}{2} \frac{c^2}{d_1}, \quad d_1 \gg c \quad (\text{D-3})$$

$$r_2 = \sqrt{d_2^2 + c^2} \sim d_2 + \frac{1}{2} \frac{c^2}{d_2}, \quad d_2 \gg c \quad (\text{D-4})$$

so that

$$\delta = \frac{\pi}{\lambda} c^2 \left[ \frac{1}{d_1} + \frac{1}{d_2} \right] \quad (\text{D-5})$$

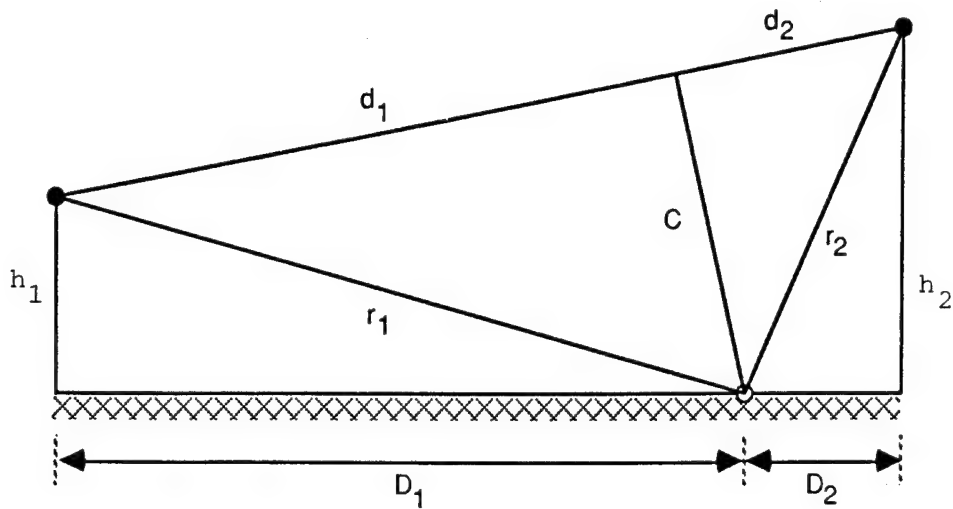


Figure D-1. Reflection by Plane Surface

The width  $f$  of the first Fresnel zone is defined as the ground clearance  $c$  for which the phase factor is  $\delta = \pi$ . Therefore, from Equation D-5.

$$f = \sqrt{\lambda \left[ \frac{1}{d_1} + \frac{1}{d_2} \right]} \quad (\text{D-6})$$

and the phase difference can be written in terms of the ratio of the clearance  $c$  of the direct ray above the reflecting point to the first Fresnel zone width  $f$ .

$$\delta = \pi(c/f)^2 \quad (\text{D-7})$$

For  $d_1 \gg h_1$  and  $d_2 \gg h_2$ , the distances  $d_1$  and  $d_2$  can be replaced by  $D_1$  and  $D_2$  (see Figure D-1), so that  $D_1 + D_2 = D$ . The clearance  $c$  and the width of the first Fresnel zone  $f$  can then be expressed as:

$$c = h_1 + \frac{h_2 - h_1}{D} D_1 \quad (\text{D-8})$$

$$f = \sqrt{\lambda \left( \frac{1}{D_1} + \frac{1}{D_2} \right)} \quad (\text{D-9})$$

The phase difference  $\delta$  has a minimum at  $\delta = \Delta$

$$\Delta = \pi \min(c/f)^2 \quad (\text{D-10})$$

for which

$$\frac{d\Delta}{dD_1} = 0 \quad (\text{D-11})$$

This condition results in the requirement that:

$$\frac{h_1}{D_1} = \frac{h_2}{D_2} \quad (\text{D-12})$$

This is the geometrical optical condition that reflection takes place when the angle of the incident ray equals the angle of the reflected ray. Equation D-10 is therefore the phase difference for interference of the direct and reflected ray.

## D.2 Plane-Earth Theory Space-Wave Reflection Loss

The effect of ground reflection is approximated in TIREM by assuming that a single dominant reflecting plane exists at a terrain profile point that has the smallest ratio of direct-path clearance to first Fresnel zone width,  $c/f$ . As shown above in D.1, the phase difference is:

$$\Delta = \pi \min(c/f)^2 \quad (D-13)$$

The resulting reflection loss  $A_{REF}$  is calculated using Equation 4-6 in which the normalized space-wave field  $|E_{SPW}/E_o|$  can be calculated using either Equation 4-2a or Equation 4-2b. When Equation 4-2a is used, the field oscillations that occur, as the clearance ratio  $c/f$  changes, become evident because of the  $\cos\Delta$  term in that equation. The reflection factor  $-A_{REF}$  is plotted from Equation 4-2a in Figure D-2 using dashed lines for  $\rho_o = 1$  and  $\rho_o = 0.2636$ . These values of  $\rho_o$  are the limiting values for frequencies of 1 MHz and 20 GHz, respectively, calculated with Equation 4-5. Note that the  $\rho_o = 1$  curve is identical with the plane-earth theory reflection factor curve for  $R = 1$  published by Bullington.<sup>D-1,D-2</sup>

Because the field oscillations that occur in real irregular terrain are not predictable with accuracy using plane-earth reflection theory, they should be eliminated. Elimination of these oscillations can be accomplished by substituting the free-space loss for cases where the clearance ratio exceeds  $\sqrt{1/3}$ . This value of  $c/f$  yields a phase difference  $\Delta$  of  $\pi/3$  which, when substituted in Equation 4-2a with  $\rho_o = 1$ , results in a normalized space-wave field of 1 (i.e., a free-space field). This

---

<sup>D-1</sup>Bullington, K., "Radio Propagation Fundamentals," The Bell System Technical Journal, Vol. 36, No. 3, May 1957, p. 608.

<sup>D-2</sup>Bullington, K., "Radio Propagation for Vehicular Communications," IEEE Transactions on Vehicular Technology, Vol. VT-26, No. 4, November 1977, p. 303.

substitution is indicated in Figure D-2 by the dark line extending to the right of  $c/f = 0.577$  (Fresnel zone 1/3) at the ordinate  $-A_{\text{REF}} = 0$ .

In TIREM, the free-space field is substituted for clearance ratios  $c/f \geq \sqrt{1/\pi} = 0.564$ . This value is used because the approximate Equation 4-2b is actually used in TIREM to estimate the reflection loss from free-space for low clearance ratios. Substitution of  $\sqrt{1/\pi}$  in Equation D-13 results in  $\Delta = 1$  and, with  $\rho_o = 1$ , Equation 4-2b then predicts that the normalized space wave field is equal to the free-space field. Figure D-2 shows curves of  $-A_{\text{REF}}$ , calculated using Equation 4-2b, for selected frequencies from 1 MHz to 20 GHz. These are the solid lines extending to the left of the point  $c/f = 0.564$ ,  $A_{\text{REF}} = 0$ . It is seen that TIREM includes  $A_{\text{REF}}$  only when the clearance ratio is less than  $\sqrt{1/\pi}$  and that the scattering coefficient  $\rho_o$  diminishes the effect of ground reflection as the frequency increases.

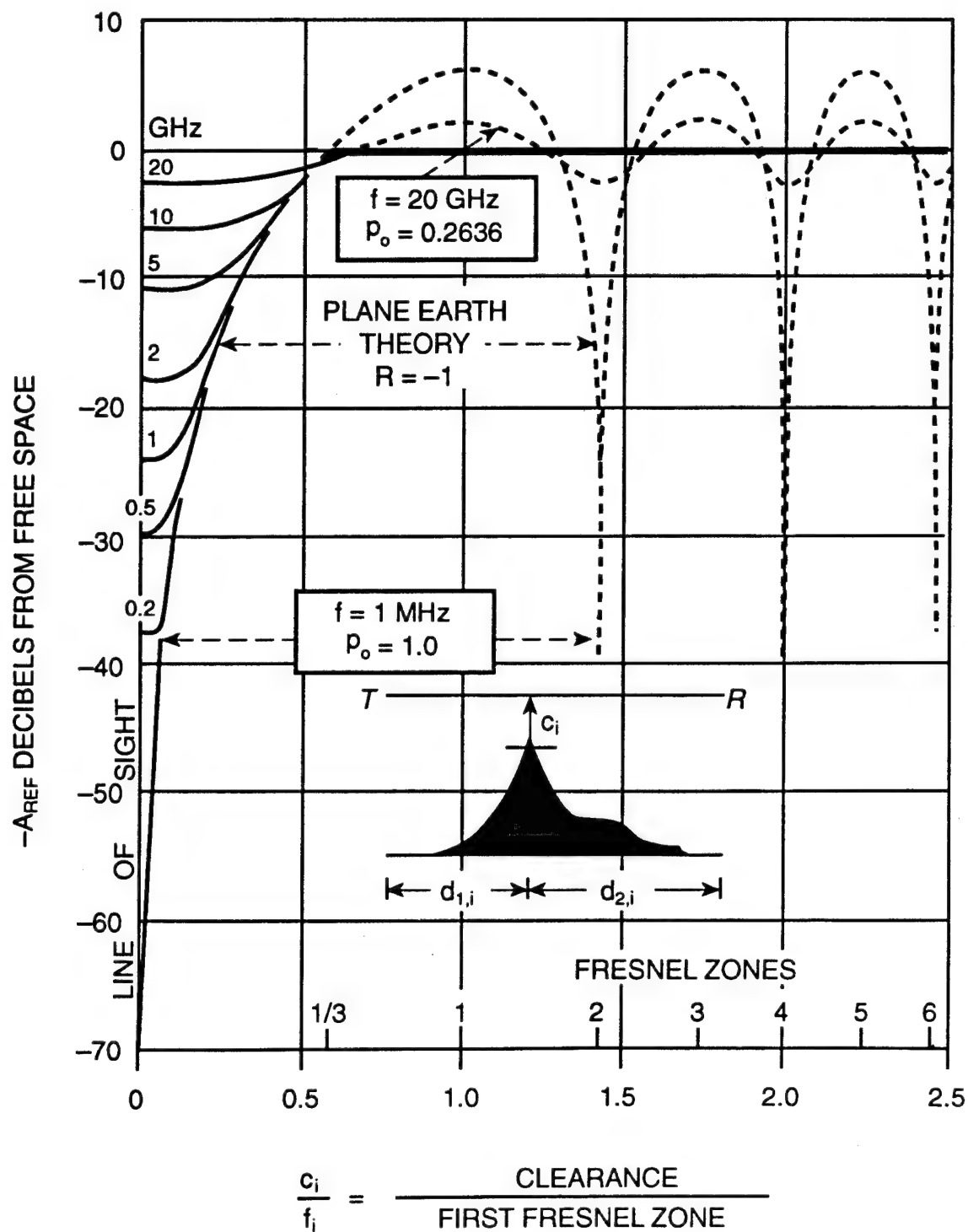


Figure D-2. Plane-Earth Theory Reflection Loss

DISTRIBUTION LIST FOR  
TIREM/SEM HANDBOOK  
ECAC-HDBK-93-076  
(Page 1 of 8)

<u>External</u>	<u>No. of Copies</u>
Commander Air Force Information Warfare Center SAV, (Attn: CAPT Doug Walters) 102 Hall Blvd, Ste 342 San Antonio, TX 78243-7020	1
Director DET1 AFREG/TWD (Attn: Kurt M. Krueger) P.O. Box 528 Mercury, Nevada 89023	1
Director Army Research Lab, SLAD/EWD (Attn: Bill Fuschetto) Evans Area, Bldg 9036D Ft Monmouth, NJ 07703-5602	1
Director CECOM Signals Warfare Directorate AMSEL-RD-SW-TRF (Attn: Michael Davis) Vint Hill Farm Station Warrenton, VA 22186-5100	1
Director USA CECOM Signals Warfare Directorate AMSEL-RD-IEW-TRF (Mark Fine) Vint Hill Farm Station Warrenton, VA 22186-5100	1
Director Central Intelligence Agency, OSD Washington, DC 20505	1



DISTRIBUTION LIST FOR  
TIREM/SEM HANDBOOK  
ECAC-HDBK-93-076  
(Page 2 of 8)

<u>External</u>	<u>No. of Copies</u>
Commander Joint Command and Control Warfare Center CAE (Attn: Larry Whatley) Ste 217, 2 Hall Blvd San Antonio, TX 78243-7008	1
Program Manager Joint Theater Missile Defense SFAE-SD-EAD (70) Huntsville, AL 35807-3801	1
Commander MCRDAC, C2CX (Attn: Major Bernal Allen) Quantico, VA 22134	1
Commander MCTSSA, Code CI-05 (Attn: Ken Wilson), Bldg 35 Camp Pendleton, CA 92055	1
National Security Agency Attn: G042/Dave Anderson 9800 Savage Road Fort George G. Meade, MD 20755-6000	1
National Security Agency Attn: G71/Maj Vermillion 9800 Savage Road Fort George G. Meade, MD 20755-6000	1
Director National Security Agency Attn: G423/Chet Teclaw 9800 Savage Road Fort George G. Meade, MD 20755-6000	1

DISTRIBUTION LIST FOR  
TIREM/SEM HANDBOOK  
ECAC-HDBK-93-076  
(Page 3 of 8)

<u>External</u>	<u>No. of Copies</u>
National Security Agency Attn: P0433/Kurt Wiebe 9800 Savage Road Fort George G. Meade, MD 20755-6000	1
National Security Agency Attn: K424/Jane Perry 9800 Savage Road Fort George G. Meade, MD 20755-6000	1
Director Naval Command Control and Ocean Surveillance Center Code 444 (Attn: Robert Fish) San Diego, CA 92152-5000	1
Director Naval Security Group Support Activity (30A) (Attn: LCDR Zmyslo) 3801 Nebraska Ave., NW Washington, DC 20393	1
Director NTIA (Attn: Bill Frazier) 179 Admiral Cochrane Drive Annapolis, MD 21401	1
Commander Headquarters Pacific Air Forces Hickam AFB, HI 96853-5001	1
US R and D Coordinator Shape Technical Centre (Attn: LTC Eric Snyder) OUDE Wallsdorperweg 61 2597 AK The Hague, Netherlands	1

DISTRIBUTION LIST FOR  
TIREM/SEM HANDBOOK  
ECAC-HDBK-93-076  
(Page 4 of 8)

<u>External</u>	<u>No. of Copies</u>
Director STRICOM, AMSTI-EE (Attn: Harold Spaulding) 12350 Research Parkway Orlando, FL 32826-3276	1
Commander USAEPG, STEEP-CT-E (Attn: LTC David A. McClung) Ft Huachuca, AZ 85613-7110	1
Commander US Army Material Systems Analysis Activity AMXSY-CT (Attn: Arthur S. Olsen) Aberdeen Proving Ground, MD 21005-5071	1
Commander US Army Missile Command AMSMI-JT Redstone Arsenal, AL 35898-8010	1
Commander US Army Signal Center ATZH-CDC/CPT (P) (Attn: Anthony Tabler) Ft Gordon, GA 30905	1
Commander US Army Signal Center ATZH-DCD (Attn: Tracey Wood) Fort Gordon, GA 30905	1
Commander US Army Space and Strategic Defense Command Attn: CSSD-SA-T (Attn: Dr. Nancy Wood) P.O. Box 1500 Huntsville AL 35807-3801	1

DISTRIBUTION LIST FOR  
TIREM/SEM HANDBOOK  
ECAC-HDBK-93-076  
(Page 5 of 8)

<u>External</u>	<u>No. of Copies</u>
Director U.S. Army Topographic Engineering Center CETEC-GL-AT (Attn: Joni Jarrett) Ft. Belvoir, VA 22060-5546	1
Industry and Science, Canada Communications Research Center Attn: James Whitteker 3701 Carling Avenue P.O. Box 11490, Station H Ottawa, Ontario K2H 8S2	1
Dr Arnold J. Tucker Assistant Director Applied Research Laboratories The University of Texas at Austin P.O. Box 8029 Austin, TX 78713-8029	1
CDR Gus K. Lott Naval Security Group 3801 Nebraska Avenue Washington, DC 20393	1
PEO CCS Attn: SFAE-CC-SEO (Attn: Bill Leonard) Fort Monmouth, NJ 07703	1
US Army Topographic Engineering Center Digital Concepts and Analysis Center Attn: CETEC-PD-DS (Attn: Juan Pérez) Alexandria, VA 22310-3864	1

DISTRIBUTION LIST FOR  
TIREM/SEM HANDBOOK  
ECAC-HDBK-93-076  
(Page 6 of 8)

<u>External</u>	<u>No. of Copies</u>
PEOTACAIR/PMA-233 Attn: Gary Yerace/RTM Study Crystal Gateway Two, Suite 413 1225 Jefferson Davis Hwy Arlington, VA 22202	1
Joint Command and Control Warfare Center (Attn: DT/William Swart) 2 Hall Blvd San Antonio, TX 78243-7008	1
ASC/YOE (Attn: Jim Carter) 102 W. D Avenue, Suite 300 Eglin AFB, FL 32542-6808	1
Central Intelligence Agency Attn: OSWR/SSD, 5Q32 NHB Washington, DC 20505	1
Central Intelligence Agency Attn: OS/ESG/EG/TCMB Washington, DC 20505	1
SAF/OR 1672 Air Force Pentagon Washington, DC 20330-1672	1

DISTRIBUTION LIST FOR  
TIREM/SEM HANDBOOK  
ECAC-HDBK-93-076  
(Page 7 of 8)

<u>Internal</u>	<u>No. of Copies</u>
CA	1
CA/D. O'Neill	1
CCN/T. Willey	1
CJ/R. Schneider	1
DC	1
DCA	1
DCA/B. Spressart	1
DCA/M. Makowski	1
DCB	1
DCB/J. Connor	1
DCB/L. Wilk	1
DCF	1
DCF/J. Head	1
DCF/M. Roberts	1
DCR	1
DCR/J. Dwyer	1
DCT	1
DCT/R. Sciandra	1
DF	1
DFA	1
DFJ	1
DFS	1
DL	1
DN	1
DNA	1
DNA/D. Kenney	1
DNN	1
DQ	1
DQT/G. Imhof	1
DR	1
DRA	1
DRA/M. Gruendl	1
DRC	1
DRD	2
DRD/D. Eppink	1
DRD/S. Leach	1

DISTRIBUTION LIST FOR  
TIREM/SEM HANDBOOK  
ECAC-HDBK-93-076  
(Page 8 of 8)

Internal

No. of Copies

DRD/G. Benoit  
DRD/J. Harbach  
DRD/L. Minor  
DRI  
DX  
DQL/G. Gildea  
DQL  
DQL

1  
1  
1  
1  
1  
1  
10

Camera-Ready Copy